Titre: Title:	Studies of HDPE and LLDPE extrudate distortions
Auteur: Author:	Xuhui Wang
Date:	1993
Type:	Mémoire ou thèse / Dissertation or Thesis
Référence: Citation:	Wang, X. (1993). Studies of HDPE and LLDPE extrudate distortions [Ph.D. thesis, École Polytechnique de Montréal]. PolyPublie. https://publications.polymtl.ca/54402/

UNIVERSITÉ DE MONTRÉAL

STUDIES OF HDPE AND LLDPE EXTRUDATE DISTORTIONS

par

Xuhui WANG

DÉPARTEMENT DE GÉNIE CHIMIQUE

ÉCOLE POLYTECHNIQUE

THÈSE PRESENTÉE EN VUE DE L'OBTENTION

DU GRADE DE PHILOSOPHIAE DOCTOR (Ph.D.)

(GÉNIE CHIMIQUE)

Août (1993)

ISBN 0-315-90030-X

Canada

lame XUHUI WANG

Dissertation Abstracts International is arranged by broad, general subject categories. Please select the one subject which most early describes the content of your dissertation. Enter the corresponding four-digit code in the spaces provided.

CHEMICAL ENGINEERING

SUBJECT TERM

0542

SUBJECT CODE

U·M·I

ubject Categories

'HE HUMANITIES AND SOCIAL SCIENCES

)MMUNICATIONS AND THE ARTS

rchitecture 0729
rt History 0377
inema 0900
ance 0378
ne Arts 0357
formation Science 0723
urnalism 0391
ibrary Science 0399
ass Communications 0708
usic 0413
peech Communication 0459
heater 0465

)UCATION

eneral 0515
dministration 0514
dult and Continuing 0516
gricultural 0517
rt 0273
lingual and Multicultural 0282
usiness 0688
ommunity College 0275
urriculum and Instruction 0727
arly Childhood 0518
lementary 0524
nance 0277
uidance and Counseling 0519
ealth 0680
igher 0745
istory of 0520
ome Economics 0278
dustrial 0521
nguage and Literature 0279
athematics 0280
usic 0522
hilosophy of 0998
hysical 0523

Psychology 0525
Reading 0535
Religious 0527
Sciences 0714
Secondary 0533
Social Sciences 0534
Sociology of 0340
Special 0529
Teacher Training 0530
Technology 0710
Tests and Measurements 0288
Vocational 0747

LANGUAGE, LITERATURE AND LINGUISTICS

Language
- General 0679
- Ancient 0289
- Linguistics 0290
- Modern 0291

Literature
- General 0401
- Classical 0294
- Comparative 0295
- Medieval 0297
- Modern 0298
- African 0316
- American 0591
- Asian 0305
- Canadian (English) 0352
- Canadian (French) 0355
- English 0593
- Germanic 0311
- Latin American 0312
- Middle Eastern 0315
- Romance 0313
- Slavic and East European 0314

PHILOSOPHY, RELIGION AND THEOLOGY

Philosophy 0422
Religion
- General 0318
- Biblical Studies 0321
- Clergy 0319
- History of 0320
- Philosophy of 0322

Theology 0469

SOCIAL SCIENCES

American Studies 0323
Anthropology
- Archaeology 0324
- Cultural 0326
- Physical 0327

Business Administration
- General 0310
- Accounting 0272
- Banking 0770
- Management 0454
- Marketing 0338

Canadian Studies 0385
Economics
- General 0501
- Agricultural 0503
- Commerce-Business 0505
- Finance 0508
- History 0509
- Labor 0510
- Theory 0511

Folklore 0358
Geography 0366
Gerontology 0351
History
- General 0578
- Ancient 0579
- Medieval 0581
- Modern 0582
- Black 0328
- African 0331
- Asia, Australia and Oceania 0332
- Canadian 0334
- European 0335
- Latin American 0336
- Middle Eastern 0333
- United States 0337

History of Science 0585
Law 0398
Political Science
- General 0615
- International Law and Relations 0616
- Public Administration 0617

Recreation 0814
Social Work 0452
Sociology
- General 0626
- Criminology and Penology ... 0627
- Demography 0938
- Ethnic and Racial Studies 0631
- Individual and Family Studies 0628
- Industrial and Labor Relations 0629
- Public and Social Welfare 0630
- Social Structure and Development 0700
- Theory and Methods 0344

Transportation 0709
Urban and Regional Planning 0999
Women's Studies 0453

'HE SCIENCES AND ENGINEERING

OLOGICAL SCIENCES

griculture
- General 0473
- Agronomy 0285
- Animal Culture and Nutrition 0475
- Animal Pathology 0476
- Food Science and Technology 0359
- Forestry and Wildlife 0478
- Plant Culture 0479
- Plant Pathology 0480
- Plant Physiology 0817
- Range Management 0777
- Wood Technology 0746

ology
- General 0306
- Anatomy 0287
- Biostatistics 0308
- Botany 0309
- Cell 0379
- Ecology 0329
- Entomology 0353
- Genetics 0369
- Limnology 0793
- Microbiology 0410
- Molecular 0307
- Neuroscience 0317
- Oceanography 0416
- Physiology 0433
- Radiation 0821
- Veterinary Science 0778
- Zoology 0472

ophysics
- General 0786
- Medical 0760

ARTH SCIENCES

ogeochemistry 0425
eochemistry 0996

Geodesy 0370
Geology 0372
Geophysics 0373
Hydrology 0388
Mineralogy 0411
Paleobotany 0345
Paleoecology 0426
Paleontology 0418
Paleozoology 0985
Palynology 0427
Physical Geography 0368
Physical Oceanography 0415

HEALTH AND ENVIRONMENTAL SCIENCES

Environmental Sciences 0768
Health Sciences
- General 0566
- Audiology 0300
- Chemotherapy 0992
- Dentistry 0567
- Education 0350
- Hospital Management 0769
- Human Development 0758
- Immunology 0982
- Medicine and Surgery 0564
- Mental Health 0347
- Nursing 0569
- Nutrition 0570
- Obstetrics and Gynecology .. 0380
- Occupational Health and Therapy 0354
- Ophthalmology 0381
- Pathology 0571
- Pharmacology 0419
- Pharmacy 0572
- Physical Therapy 0382
- Public Health 0573
- Radiology 0574
- Recreation 0575
- Speech Pathology 0460
- Toxicology 0383

Home Economics 0386

PHYSICAL SCIENCES

Pure Sciences

Chemistry
- General 0485
- Agricultural 0749
- Analytical 0486
- Biochemistry 0487
- Inorganic 0488
- Nuclear 0738
- Organic 0490
- Pharmaceutical 0491
- Physical 0494
- Polymer 0495
- Radiation 0754

Mathematics 0405
Physics
- General 0605
- Acoustics 0986
- Astronomy and Astrophysics 0606
- Atmospheric Science 0608
- Atomic 0748
- Electronics and Electricity 0607
- Elementary Particles and High Energy 0798
- Fluid and Plasma 0759
- Molecular 0609
- Nuclear 0610
- Optics 0752
- Radiation 0756
- Solid State 0611

Statistics 0463

Applied Sciences

Applied Mechanics 0346
Computer Science 0984

Engineering
- General 0537
- Aerospace 0538
- Agricultural 0539
- Automotive 0540
- Biomedical 0541
- Chemical 0542
- Civil 0543
- Electronics and Electrical 0544
- Heat and Thermodynamics ... 0348
- Hydraulic 0545
- Industrial 0546
- Marine 0547
- Materials Science 0794
- Mechanical 0548
- Metallurgy 0743
- Mining 0551
- Nuclear 0552
- Packaging 0549
- Petroleum 0765
- Sanitary and Municipal 0554
- System Science 0790

Geotechnology 0428
Operations Research 0796
Plastics Technology 0795
Textile Technology 0994

PSYCHOLOGY

General 0621
Behavioral 0384
Clinical 0622
Developmental 0620
Experimental 0623
Industrial 0624
Personality 0625
Physiological 0989
Psychobiology 0349
Psychometrics 0632
Social 0451

Nom _____

Dissertation Abstracts International est organisé en catégories de sujets. Veuillez s.v.p. choisir le sujet qui décrit le mieux votre thèse et inscrivez le code numérique approprié dans l'espace réservé ci-dessous.

_____ ☐☐☐ U·M·

SUJET CODE DE SUJET

Catégories par sujets

HUMANITÉS ET SCIENCES SOCIALES

COMMUNICATIONS ET LES ARTS

Architecture 0729
Beaux-arts 0357
Bibliothéconomie 0399
Cinéma 0900
Communication verbale 0459
Communications 0708
Danse 0378
Histoire de l'art 0377
Journalisme 0391
Musique 0413
Sciences de l'information 0723
Théâtre 0465

ÉDUCATION

Généralités 515
Administration 0514
Art 0273
Collèges communautaires 0275
Commerce 0688
Économie domestique 0278
Éducation permanente 0516
Éducation préscolaire 0518
Éducation sanitaire 0680
Enseignement agricole 0517
Enseignement bilingue et multiculturel 0282
Enseignement industriel 0521
Enseignement primaire. 0524
Enseignement professionnel 0747
Enseignement religieux 0527
Enseignement secondaire 0533
Enseignement spécial 0529
Enseignement supérieur 0745
Évaluation 0288
Finances 0277
Formation des enseignants 0530
Histoire de l'éducation 0520
Langues et littérature 0279
Lecture 0535
Mathématiques 0280
Musique 0522
Orientation et consultation 0519
Philosophie de l'éducation 0998
Physique 0523
Programmes d'études et enseignement 0727
Psychologie 0525
Sciences 0714
Sciences sociales 0534
Sociologie de l'éducation 0340
Technologie 0710

LANGUE, LITTÉRATURE ET LINGUISTIQUE

Langues
- Généralités 0679
- Anciennes 0289
- Linguistique 0290
- Modernes 0291

Littérature
- Généralités 0401
- Anciennes 0294
- Comparée 0295
- Médiévale 0297
- Moderne 0298
- Africaine 0316
- Américaine 0591
- Anglaise 0593
- Asiatique 0305
- Canadienne (Anglaise) 0352
- Canadienne (Française) 0355
- Germanique 0311
- Latino-américaine 0312
- Moyen-orientale 0315
- Romane 0313
- Slave et est-européenne 0314

PHILOSOPHIE, RELIGION ET THÉOLOGIE

Philosophie 0422
Religion
- Généralités 0318
- Clergé 0319
- Études bibliques 0321
- Histoire des religions 0320
- Philosophie de la religion 0322

Théologie 0469

SCIENCES SOCIALES

Anthropologie
- Archéologie 0324
- Culturelle 0326
- Physique 0327

Droit 0398
Économie
- Généralités 0501
- Commerce-Affaires 0505
- Économie agricole 0503
- Économie du travail 0510
- Finances 0508
- Histoire 0509
- Théorie 0511

Études américaines 0323
Études canadiennes 0385
Études féministes 0453
Folklore 0358
Géographie 0366
Gérontologie 0351
Gestion des affaires
- Généralités 0310
- Administration 0454
- Banques 0770
- Comptabilité 0272
- Marketing 0338

Histoire
- Histoire générale 0578
- Ancienne 05
- Médiévale 05
- Moderne 05
- Histoire des noirs 03
- Africaine 03
- Canadienne 03
- États-Unis 03
- Européenne 03
- Moyen-orientale 03
- Latino-américaine 03
- Asie, Australie et Océanie 03

Histoire des sciences 05
Loisirs 08
Planification urbaine et régionale 09
Science politique
- Généralités 06
- Administration publique 06
- Droit et relations internationales 06

Sociologie
- Généralités 06
- Aide et bien-àtre social 06
- Criminologie et établissements pénitentiaires 06
- Démographie 09
- Études de l' individu et de la famille 06
- Études des relations interethniques et des relations raciales 06
- Structure et développement social 07
- Théorie et méthodes. 03
- Travail et relations industrielles 06

Transports 07
Travail social 04

SCIENCES ET INGÉNIERIE

SCIENCES BIOLOGIQUES

Agriculture
- Généralités 0473
- Agronomie. 0285
- Alimentation et technologie alimentaire 0359
- Culture 0479
- Élevage et alimentation 0475
- Exploitation des pâturages 0777
- Pathologie animale 0476
- Pathologie végétale 0480
- Physiologie végétale 0817
- Sylviculture et faune 0478
- Technologie du bois 0746

Biologie
- Généralités 0306
- Anatomie 0287
- Biologie (Statistiques) 0308
- Biologie moléculaire 0307
- Botanique 0309
- Cellule 0379
- Écologie 0329
- Entomologie 0353
- Génétique 0369
- Limnologie 0793
- Microbiologie 0410
- Neurologie 0317
- Océanographie 0416
- Physiologie 0433
- Radiation 0821
- Science vétérinaire 0778
- Zoologie 0472

Biophysique
- Généralités 0786
- Medicale 0760

SCIENCES DE LA TERRE

Biogéochimie 0425
Géochimie 0996
Géodésie 0370
Géographie physique 0368
Géologie 0372
Géophysique 0373
Hydrologie 0388
Minéralogie 0411
Océanographie physique 0415
Paléobotanique 0345
Paléoécologie 0426
Paléontologie 0418
Paléozoologie 0985
Palynologie 0427

SCIENCES DE LA SANTÉ ET DE L'ENVIRONNEMENT

Économie domestique 0386
Sciences de l'environnement 0768
Sciences de la santé
- Généralités 0566
- Administration des hôpitaux 0769
- Alimentation et nutrition 0570
- Audiologie 0300
- Chimiothérapie 0992
- Dentisterie 0567
- Développement humain 0758
- Enseignement 0350
- Immunologie 0982
- Loisirs 0575
- Médecine du travail et thérapie 0354
- Médecine et chirurgie 0564
- Obstétrique et gynécologie 0380
- Ophtalmologie 0381
- Orthophonie 0460
- Pathologie 0571
- Pharmacie 0572
- Pharmacologie 0419
- Physiothérapie 0382
- Radiologie 0574
- Santé mentale 0347
- Santé publique 0573
- Soins infirmiers 0569
- Toxicologie 0383

SCIENCES PHYSIQUES

Sciences Pures

Chimie
- Généralités 0485
- Biochimie 487
- Chimie agricole 0749
- Chimie analytique 0486
- Chimie minérale 0488
- Chimie nucléaire 0738
- Chimie organique 0490
- Chimie pharmaceutique 0491
- Physique 0494
- PolymÇres 0495
- Radiation 0754

Mathématiques 0405
Physique
- Généralités 0605
- Acoustique 0986
- Astronomie et astrophysique 0606
- Electronique et électricité 0607
- Fluides et plasma 0759
- Météorologie 0608
- Optique 0752
- Particules (Physique nucléaire) 0798
- Physique atomique 0748
- Physique de l'état solide 0611
- Physique moléculaire 0609
- Physique nucléaire 0610
- Radiation 0756

Statistiques 0463

Sciences Appliqués Et Technologie

Informatique 0984
Ingénierie
- Généralités 0537
- Agricole 0539
- Automobile 0540
- Biomédicale 05
- Chaleur et ther modynamique 03
- Conditionnement (Emballage) 05
- Génie aérospatial 05
- Génie chimique 05
- Génie civil 05
- Génie électronique et électrique 05
- Génie industriel 05
- Génie mécanique 05
- Génie nucléaire 05
- Ingénierie des systämes 07
- Mécanique navale 05
- Métallurgie 07
- Science des matériaux 07
- Technique du pétrole 07
- Technique minière 05
- Techniques sanitaires et municipales 05
- Technologie hydraulique 0

Mécanique appliquée 0
Géotechnologie 0
Matières plastiques (Technologie) 0
Recherche opérationnelle 0
Textiles et tissus (Technologie) 0

PSYCHOLOGIE

Généralités 0
Personnalité 0
Psychobiologie 0
Psychologie clinique 0
Psychologie du comportement 0
Psychologie du développement 0
Psychologie expérimentale 0
Psychologie industrielle 0
Psychologie physiologique 0
Psychologie sociale 0
Psychométrie 0

UNIVERSITÉ DE MONTRÉAL

ÉCOLE POLYTECHNIQUE

Cette thèse intitulée:

STUDIES OF HDPE AND LLDPE EXTRUDATE DISTORTIONS

Présentée par: Xuhui WANG

en vue de l'obtention du grade de: Philosophiae Doctor (Ph.D.)

a été dûment acceptée par le jury d'examen constitué de:

M. KLVANA, Danilo, Ph.D., président

M. CARREAU, Pierre, Ph.D., membre et directeur de recherche

M. LAFLEUR, Pierre, Ph.D., membre et directeur de recherche

M. DEALY, John, Ph.D., membre

M. CLÉMENT, Bernard, Ph.D., membre

ABSTRACT

As the consumption of linear polyethylenes (HDPE and LLDPE) has increased rapidly (especially since LLDPE was introduced), the study of extrudate distortions of the polymers has become more and more important. There are many parameters affecting the extrudate appearances and the analysis of these parameters simultaneously will require a large amount of experimental work. No such complete investigation has been done before. The cause of the extrudate distortion remains unclear and many questions are not fully answered yet, although the subject has been studied for years. More recently, the mechanism for wall slip has been frequently discussed, but there is still no general agreement.

In this work, we examined several parameters affecting extrudate distortions of HDPE and LLDPE, using a statistical method, called "screening design". The method minimizes the amount of experimental work and allows us to find out the most important parameters affecting extrudate roughness. Further, we studied the mechanisms of extrudate distortions, especially the effect of slip, using a two-hole die and a slit die setups. The two-hole die has two channels and enables us to observe wall slip and related extrudate distortions by comparing the extrudates from the two channels. We have also used the slit die to observe the pressure variations along the die when distortions occur and relate wall slip to the sudden

pressure changes.

The results of the "screening design" suggest that shear stress is the most important factor affecting the extrudate roughness, followed by the polymer molecular weight. The use of high molecular weight polymer leads to more severe extrudate roughness. The relative importance of the other studied parameters cannot be concluded generally. For HDPE polymers, shear stress, molecular weight and entrance effect are the active parameters while the others are inert. For LLDPE polymers, there are no distinct active and inert groups of parameters, although shear stress and molecular weight are still the first two most important parameters. We also found that the two-parameter interactions from two active parameters had the same effect as that from the main effects. The interaction between one active and one inert parameters is less strong as well as those between two inert parameters.

In the two-hole die experiments, wall slip is clearly observed by a sudden jump of the apparent shear rate in one channel but not in the other, under the same reservoir pressure. The wall slip is also accompanied by extrudate roughness. However, presence of roughness doesn't necessarily assure the existence of wall slip. This is shown by early roughness in one LLDPE, for which there is no obvious wall slip. In other words, roughness is affected by wall slip but

not always caused by wall slip.

The slit die was used to obtain slip data along the die land so as to understand where slip is initiated. This is accomplished mainly by observing the spurting phenomenon. Using a fast data acquisition system, we could detect rapid changes in the pressure profiles and those indicate that slip starts upstream and propagates very rapidly downstream. The pressure profiles remain linear through the slit die, even when slip occurs. It indicates constant slip velocity along the die land. We also found that the entrance pressure loss was related to the extrudate roughness: higher entrance pressure was associated with more severe extrudate roughness. This is mostly observed for HDPEs; in the case of LLDPEs, we could not observe the similar phenomenon due to pressure limitations of the equipment.

In summary, for the first time, using a screening design, we have evaluated the relative importance of key parameters affecting extrudate roughness for a variety of HDPEs and LLDPEs. The two-hole die experiment showed obvious wall slip accompanied by changes of extrudate appearances. It is also the first time that wall slip during the spurting phenomenon is observed using a slit die. Slip is found to be initiated upstream.

RÉSUMÉ

Comme la consommation des polyéthylènes linéaires (de haute et basse densités HDPE et LLDPE) a augmenté rapidement (surtout depuis que LLDPE a été introduit), l'étude des distorsions d'extrudat des polymères est devenue de plus en plus importante. Il existe beaucoup de paramètres qui affectent les défauts d'extrusion et l'analyse simultanée de ces paramètres requerrait beaucoup d'expérimentation. Une étude exhaustive de ce sujet n'a pas été faite à date. La cause des distorsions d'extrudat demeure obscure et beaucoup de questions sont encore sans réponse complète, bien que le sujet a été étudié depuis des années. Récemment, le mécanisme du glissement à la paroi de la filière a été discuté souvent, mais il n'existe pas encore de concensus.

Dans cette étude, on examine plusieurs paramètres affectant simultanément les distorsions d'extrudat des HDPE et LLDPE, en utilisant une méthode statistique appelée "screening design". Cette méthode minimise la quantité de travaux expérimentaux et permet de déterminer les paramètres les plus importants qui affectent les défauts d'extrusion. De plus, on étudiera le mécanisme des distorsions d'extrudat, particulièrement l'effet du glissement, en utilisant une filière à deux orifices et une filière à fente. La filière à deux orifices (capillaires) permet d'observer le glissement à la paroi et les distorsions

d'extrudat résultantes. On a aussi utilisé la filière à fente pour observer les variations de pression le long de la matrice quand les distorsions se manifestent et on a relié le glissement à la paroi aux soudains changements de pression.

Les résultats de la méthode statistique suggèrent que la contrainte de cisaillement est le facteur le plus important qui affecte la rugosité de l'extrudat, suivi par la masse moléculaire du polymère. L'utilisation d'un polymère ayant une forte masse moléculaire cause les plus sévères distorsions. On ne peut pas conclure de façon générale sur l'importance relative des autres paramètres étudiés. Pour les polymères HDPE, la contrainte de cisaillement, la masse moléculaire et l'effet d'entrée sont des paramètres actifs alors que les autres sont inertes. Pour les polymères LLDPE, il existe peu de distinction entre le groupe de paramètres actifs et les inertes, même si la contrainte de cisaillement et la masse moléculaire sont les deux plus importants paramètres. On a également découvert que les interactions entre deux paramètres actifs ont le même effet que ceux des paramètres principaux. L'interaction entre un paramètre actif et un paramètre inerte est moins forte, de même que celle entre deux paramètres inertes.

Dans l'expérience de la filière à deux orifices, le

glissement à la paroi est clairement observé par un soudain saut de la contrainte de cisaillement apparente dans un capillaire mais pas dans l'autre, sous la même pression dans le réservoir. Le glissement est aussi accompagné de défauts d'extrusion. Cependant, la présence de défauts n'assure pas nécessairement l'existence du glissement. Ceci est démontré par des défauts observés pour un LLDPE, pour lequel il n'existe pas de glissement évident. En d'autres mots, les défauts sont affectés par le glissement à la paroi, mais pas toujours causés par celui-ci.

La filière à fente a été utilisée pour obtenir des données de glissement instantanément le long de la filière de façon à déterminer à quel endroit le glissement est initialisé. Ceci est accompli principalement en observant le phémomène de jaillissement (spurting). En utilisant un système rapide d'acquisition de données, on pouvait détecter des changements rapides dans les profils de pression et ceux-ci indiquent que le glissenment commence en amont et se propage très rapidement en aval de la filière. Les profils de pression demeurent linéaires à travers la longueur de la filière, même quand le glissement a eu lieu. Ceci indique une vitesse de glissement constante le long de la filière. On a également trouvé que l'excés de perte de pression à l'entrée était relié aux défauts d'extrusion: une plus haute presssion d'entrée était

associée avec une rugosité plus marquée. Ceci est observé surtout pour les HDPE; dans le cas des LLDPE, on ne peut pas observer un phénomène similaire étant donné les limites de pression de l'équipement.

En résumé, pour la première fois, en utilisant une méthode statistique ("screening design"), on a évalué l'importance relative des paramètres clés affectant les défauts d'extrusion pour une variété de HDPE et LLDPE. L'expérience avec la filière à deux orifices a montré un glissement à la paroi évident accompagné de défauts d'extrusion. C'est aussi la première fois que le glissement est observé pendant le phénomène de jaillissement (spurting) en utilisant une filière à fente. On conclut que le glissement est initialisé en amont près de l'entrée de la filière.

ACKNOWLEDGEMENTS

The author wishes likes to thank Professor P. Carreau and Professor P. Lafleur for their instructions and sincere helps throughout this work.

Many thanks to Professor B. Clément for his valuable help in statistical analyses.

The author sincerely appreciates Mr. L. Parent's work in preparing the data acquisition system and many friendly helps for the laboratory experiments.

TABLE OF CONTENTS

LIST OF FIGURES

LIST OF TABLES

NOMENCLATURE

e	Bagley correction factor
F_R	roughness parameter
G" (MPa)	loss modulus
h (cm)	gap of slit die channel
L (cm)	length of capillary and slit die channel
Mc (g/mole)	critical molucular weight
Mn (g/mole)	number average molecular weight
Mw (g/mole)	weight average molecular weight
Mz (g/mole)	z average molecular weight
m ($Pa \cdot s^n$)	consistency index in power law model
N_{DEB}	Deborah number
n	shear thinning index in power law model
P (MPa)	pressure in reservoir or along die
Q (mL/s)	volumetric flow rate
Q_{shear} (mL/s)	flow rate contributed by shear flow
Q_{slip} (mL/s)	flow rate contributed by slip flow
R (cm)	radius of capillary
S_R	elastic strain
S_{RC}	critical elastic strain
T (K)	temperature
u(w) (cm/s)	slip velocity
W (cm)	width of slit die
η (Pa·s)	viscosity
$\dot{\gamma}_A$ (1/s)	apparent shear rate

$\dot{\gamma}_c$ (1/s)	corrected apparent shear rate
$\dot{\gamma}_n$ (1/s)	shear rate of Newtonian fluid
$\dot{\gamma}_p$ (1/s)	shear rate of power law fluid
μ (MPa)	shear modulus of elasticity
ρ (g/mL)	density
σ (MPa)	shear stress
σ_c (MPa)	critical shear stress
σ_w (MPa)	shear stress at die wall

CHAPTER 1

INTRODUCTION AND OBJECTIVES

Although the first plastic, cellulose nitrate, was invented in the 1860's, the real impact of plastic products on our lives has started only since World War II. Since then, the growth has been very rapid, featuring numerous new types of plastics. Among many others, polyethylene (PE) is a widely used one. By the year 1995 PE will take about 36% of total thermoplastic market world wide. Because of the unique role of PE played in total plastic industry, the research on the nature and processing behaviour of PE has also been done for some 30 years. Among many topics, the instabilities during extrusion of linear polyethylenes (high density polyethylene, HDPE and linear low density polyethylene, LLDPE) have drawn more and more attention since decades ago, because those phenomena affect the quality of extrudate and limit extrusion to moderate production rates.

Although the subject has been studied for many years, there are still number of controversial points needed to be clarified, such as the relation between wall slip and extrudate distortion. On the other hand, since analyzing many parameters simultaneously will cause large amount of

experimental work, most of the previous research work focused on one individual parameter. Therefore the results from each researcher reflect a special restricted situation. For example, (see Chapter 2) some researchers reported that the dimension of the die affected the extrudate quality, while some other researchers reported the effects of temperature of the die and the melt were also important. Therefore it is quite interesting to know which parameter is more important than the others. For number of parameters affecting the quality of extrudate, which parameters are the most important or most active ones. It is also interesting to know how those parameters interact with each other when many parameters are acting together.

The objectives of this work are

(1) to determine the key parameters affecting extrudate distortions of high density polyethylene, HDPE, and linear low density polyethylene, LLDPE;

(2) to understand the relative importance of these key parameters;

(3) to obtain the interactions between the parameters and their relative importance to the individual effect;

(4) to better understand the mechanisms of extrudate distortions, such as the role of wall slip to extrudate appearance.

CHAPTER 2

REVIEW OF PREVIOUS WORK

There are many factors affecting the extrusion of linear polyethylenes. It would be quite instructive to do a systematic review over the research work in this field. Five aspects will be examined: Extrudate Distortions; Flow Visualization; Flow Curves; Parameters Affecting Extrudate Distortions; and Explanation of Extrudate Distortions.

2.1 EXTRUDATE DISTORTIONS

2.1.1 Observations of Extrudate Distortions and Nomenclature

During the extrusion of polymer melts, below certain flow rates the emerging filament is smooth exhibiting normal extrudate swelling. At higher rates the extrudate becomes irregular but the appearance varies form polymer to polymer.

Almost half a century ago, Nason (1945) described a gas driven rheometer used in laboratory scale extrusion experiments on thermoplastics. He extruded polystyrene, cellulose acetate and polyvinyl resin plastics through a flat entry die. At low shear rates he observed smooth extrudates, but at higher rates the extrudates became rough and wavy and the roughness and waviness increased as he increased the pressure. Possibly the first serious and systematic study of

extrudate distortions was carried out by Spencer and Dillon (1949). They investigated the flow of molten polystyrene through capillary dies of length to radius ratio ranging from 20 to 40. At low shear stresses the extrudate surface was smooth and normal die swell was observed. At higher shear stresses a regular spiralled extrudate with some surface roughness was produced, and at higher stresses still, the surface roughness disappeared but the extrudate was grossly distorted.

After 1949, many researchers started to investigate extrudate distortions. Many terms have been given in the literature to describe different phenomena. These include ''melt fracture'', ''elastic turbulence'', ''waviness'', ''ripple'', ''bamboo effect'', ''sausage link'', ''sharkskin'', ''matte'', and ''orange peel'' (Boudreaux and Cuculo, 1977-1978). The most widely studied polymer was branched or low density polyethylene, LDPE. However there were also studies of linear high density polyethylene, HDPE, such as White's (1973) work. He reported that HDPE showed a characteristic helical screw thread appearance. Bagley et al. (1958) found the discontinuity of HDPE flow curve and the corresponding surface distortions: changing from smooth to wavy before the flowrate jump; to rough after the flowrate jump. Schreiber et al. (1960) observed that if the shear rate

was increased further past the point of gross extrudate distortion, a second stable flow regime could be encountered in which the emerging extrudate would again become smooth. Tordella (1963) found a similar behavior for linear polyethylenes. The most systematic reviews on the polymer extrusion of the published work up to 70's were made by Petrie and Denn (1976) and Boudreaux and Cuculo (1977-1978). These reviews feature the end of first epoch of such studies.

Linear low density polyethylenes, LLDPE, joined the polyethylene family in the 1970's. Certain extrusion difficulties encountered during its processing, and the study of polyethylene extrudate distortion once again has become an active research field. Ramamurthy (1986) and Kalika and Denn (1987) studied LLDPE extrusion and reported sharkskin and gross fracture extrudate distortions as the extrusion rate increased. Kalika and Denn (1987) also observed pressure oscillations before the occurrence of gross fracture. Beaufils et al. (1989) studied carefully the development of sharkskin of LLDPE resin and observed the increase of distortions with extrusion rate from very small magnitude (0.1 micron) to visible scale. For the first time, a surface roughness parameter was defined to measure the surface distortion quantitatively. Becker et al. (1991) studied the extrusion of HDPE resin by using frequency analysis. They reported various

distortions as ''sharkskin'', ''wavy'', ''spurt defect'', ''spiral defect'', ''oscillation'', and ''chaotic''.

2.1.2 Summary

Based on many decades of observation in extrusion studies, the main three different forms of extrudate distortions for polyethylenes (Utracki and Gendron, 1984) are: surface roughness, melt fracture and the fracture during the pressure oscillation of ''spurting''. The first two are observed for all polymers, while the third is the typical phenomenon for linear polyethylenes and other linear polymers such as polybutadiene (Vinogradov, 1972, 1981).

Surface roughness refers to the high frequency, small amplitude helical pattern appearing on the surface of extrudate. The amplitude of the distortions are much smaller than the dimension (such as diameter) of the extrudate. This has been reported by different authors usually as ''sharkskin'', ''matte'', ''wavy'', and so on. However ''sharkskin'' is the most frequently used term. Recently, El Kissi and Piau (1992) have made some important comments on the definition of sharkskin. They pointed out that based on the observation of the extrudate made too downstream of the exit section was not suitable for describing the physical mechanisms which created the sharkskin defect. Because of

''too far downstream of the exit section'', the sharkskin cracks close and give the extrudate the rough appearance which results from the relaxation of stresses in the exit zone. On the other hand, the appearance is greatly affected by the characteristic time of the polymer system. If the relaxation time is very long (for the high molecular entangled polymer system), the cracks remain open and the extrudate downstream will not show simple sharkskin. Based on aforesaid reasons, they suggested sharkskin should based on visualization at the exit section of the die in the observation field (Piau et al., 1990).

Melt fracture refers to large magnitude of deformation of extrudate. The extrudate may lose its original shape (shaped by the solid flow channel) or even deform into broken pieces. Tordella (1958) found the deformation of emerging polymer stream with an increase of extrusion rate, and first used the term ''melt fracture'' to define serious defect of extrudate. The distortion in this category has been described by various researchers as ''gross fracture'', ''chaotic flow'', ''melt fracture'' and so on.

Spurting phenomenon features pressure oscillations (from constant-flowrate rheometer) or flowrate oscillations (from constant-pressure rheometer). In extruder extrusion, the

flowrate is controlled, (not as precisely as that in constant flowrate rheometer) by RPM of the extruder. One can observe both pressure and flowrate oscillations at a RPM of the extruder during the spurting. The oscillation period of the pressure has been observed constant with time through extruder extrusion, which usually can not be observed by the (piston driven) rheometers. This is because that the period of pressure oscillation is affected by amount of the polymer melt in the reservoir, which decreases with time in case of using rheometers. Therefore, it is an advantage of using extruder to obtain time-independent pressure oscillation data for spurting. During the spurting extrusion, the extrudate usually shows inconsistent extrudate distortions. The extrudates show different appearances during increasing and decreasing periods of the pressure oscillation. Vinogradov et al. (1972, 1981 and 1984) made the most impressive studies in this area with polybutadienes. They proposed that this phenomenon was caused by the polymer changing from the fluid state to the elastic one. Ramamurthy (1986) and Kalika and Denn (1987) also reported such phenomenon with HDPE and LLDPE. El Kissi and Piau (1990) observed similar phenomenon and called this ''cork flow''.

Figure 2.1 shows different extrudate distortions (Agassant et al. 1991): a) and b) are typical surface roughness from

extrusion of LLDPE and HDPE respectively; c) is a extrudate from spurting extrusion, the differences between the smooth and rough parts are quite obvious. d) depicts an extrudate of second stable flow regime. The extrudate distortion is less severe but not virtually smooth. e), f), and g) are different gross fracture examples with increasing of flowrate.

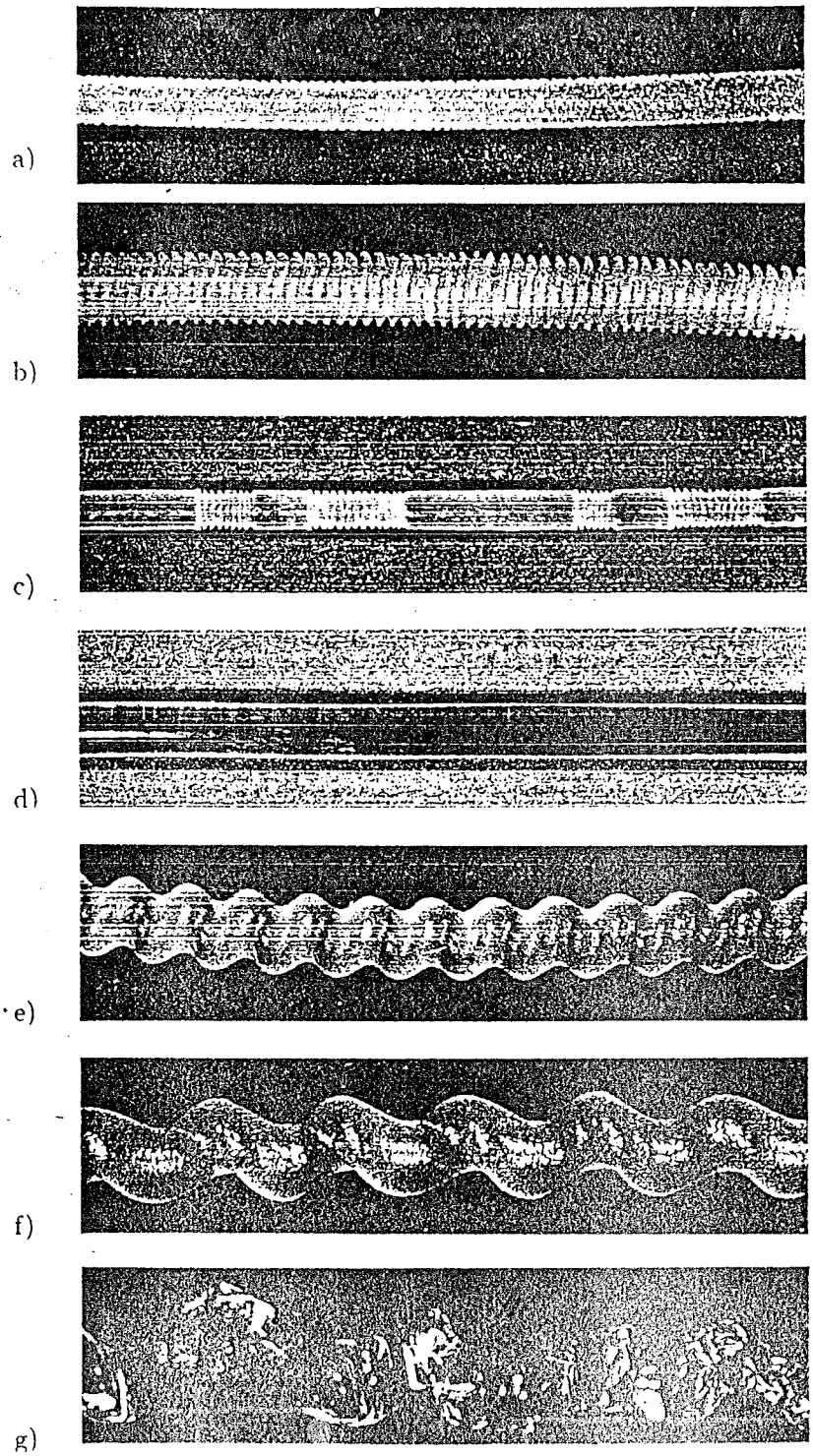

Figure 2.1. Various Extrudate Distortions (Agassant et al. 1991)

2.2 FLOW VISUALIZATION

2.2.1 Flow in Channel Entrance

In order to understand the flow situation inside the reservoir and channel, many approaches have been used by different authors to visualize and locate the flow instability. In a first study, Bond (1925) observed the flow patterns of glycerine and aqueous solutions of glycerine moving through a flat entry contraction under the force of gravity. He was able to visualize the streamlines by following the motion of air bubbles in the solutions. He found streamlines moving radially into the orifice. Ballenger and White (1970) and Ballenger et al. (1971) have observed the flow of the same solutions into flat entry dies, and they also reported streamlines moving radially into the orifice. This radial flow before the onset of Reynolds turbulence seems to be a characteristic of Newtonian flow. Bond also discovered the anomalous flow behavior: vortices in the corner of the reservoir which were not predicted by theory. Tordella (1956) studied the extrudate distortion that occurred when branched polyethylene, polymethyl methacrylate, and polytetrafluoroethylene were extruded through a flat entry capillary die at high flow rates. He suggested that the extrudate distortion originated in the reservoir. In companion studies, he (Tordella, 1957, 1958) observed the flow of

branched polyethylene by following the motion of hard and soft tracer particles made by mixing carbon black with high and low viscosity polyethylene. He observed at low flowrates, radial flow of the particles at the center of the reservoir above the die inlet, moving faster than those near the edge of the reservoir. At higher flowrates, the particles in the center converged toward the orifice whereas those in the corners of the reservoir appeared to be trapped. He found conical streamlines surrounded by circulating stagnant regions in the corners. At a critical flow rate the center streamlines break up or fractured and allow material from the stagnant area to flow through the orifice. When the stagnant area was depleted, the center streamlines reformed and new stagnant regions developed. The distorted extrudate was composed of alternate material from the central streamlines and the stagnant material in the corners. Similar behavior for branched polyethylene was reported by Clegg (1957). He observed the flow by extruding alternate layers of clear and pigmented polymer. At low flowrates a uniform extrudate with a pigmented core emerged from the die. At higher flowrates a rotary motion developed and a waviness occurred with a process of core, then no core indicating a breakdown of the flow lines. Since Clegg's work, many other investigators, Den Otter (1970), Ballenger et al. (1971), Ballenger and White (1971), have studied branched polyethylene, and its behavior has become

accurately characterized: at low flowrates, the streamlines move radially into the orifice in the manner similar to Newtonian fluids. At higher rates a trumpet or wine glass stem shaped funnel develops and secondary circulating stagnant areas. As the flowrate increases, the stagnant areas become larger and the angle of convergence of the funnel decreases. At the critical flowrate the funnel develops a swirling rotary motion similar to a vortex. Ballenger and White (1971) suggested that the vortex motion produces the periodic regularity of the distorted extrudate. With increasing rates the funnel fractures and the remaining flow is characterized by the alternate flow of material from the funnel and the stagnant areas. With further increases of the flow rate, the fracture of the center streamlines occurs more frequently and the alternation of the material from the two flow regions increases in frequency. The fracture is accompanied by gross extrudate distortion. With conical entry dies the flow behavior is essentially the same except that the corners of the reservoir are diminished and, therefore, there are no stagnant areas. Although the various flow patterns still occur at the same stresses, the visible evidence of extrudate distortion is delayed to higher rate because the flow is characterized by alternation of material which has similar deformation histories.

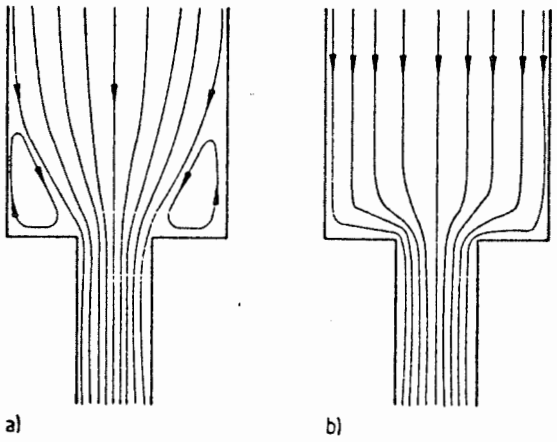

Figure 2.2. Flow patterns at entry of flow channel. a) Branched polyethylene; b) Linear polyethylene (Agassant et al. 1991).

The more interesting study came as the comparison between branched polyethylene (LDPE) and linear polyethylene (HDPE and LLDPE). In 1960, Bagley and Birks (1960) first investigated the flow patterns of linear polyethylene. Since then other researchers, Ballenger et al. (1971), Den Otter (1970, 1971), Ballenger and White (1970) have also examined the flow of linear polyethylene. In flat entry dies and at all flow rates, the streamlines move radially into the capillary with either very small or no dead spaces at the corners of the reservoir. At a critical flowrate the swirling motion of the flow lines which characterized branched polyethylene is not observed and above the critical flowrate the alternating flow typical of branched polyethylene is also not observed. As a result, the conical entry dies do not change the flow patterns

appreciably, nor alter the critical shear stress. The flow patterns of branched and linear polyethylenes at the entry of the flow channel are shown in the Figure 2.2, where, a) represents a branched polyethylene featuring vortex in the reservoir corners in addition to radial flow; b) represents the flow of linear polyethylene without stagnant zones.

2.2.2 Flow Inside the Channel

Compared to the entrance flow pattern study, very few researchers have worked on visualization inside the flow channel. This might be attributed to the difficulty of such measurement, and the very high velocity gradients at the wall that may lead to wrong conclusion about slip due to inaccuracy in the measurement. Bartos and Holomek (1971) appeared to be the first to make an impressive effort in this field. They used the cine film technique to study the flow pattern inside capillary dies. They observed no flow pattern change with surface roughness, but at the spurting, they found obvious slip at the die wall. Figure 2.3 shows the velocity profile during spurting extrusion. The top curve depicts the phase of flow corresponding to the sudden increase of flowrate. The bottom curve represents that of relatively constant flowrate. The top curve shows obvious slip at die wall while bottom curve gives no sign of slip. Vinogradov (1972) also showed the stick-slip phenomenon inside the die land using birefringence

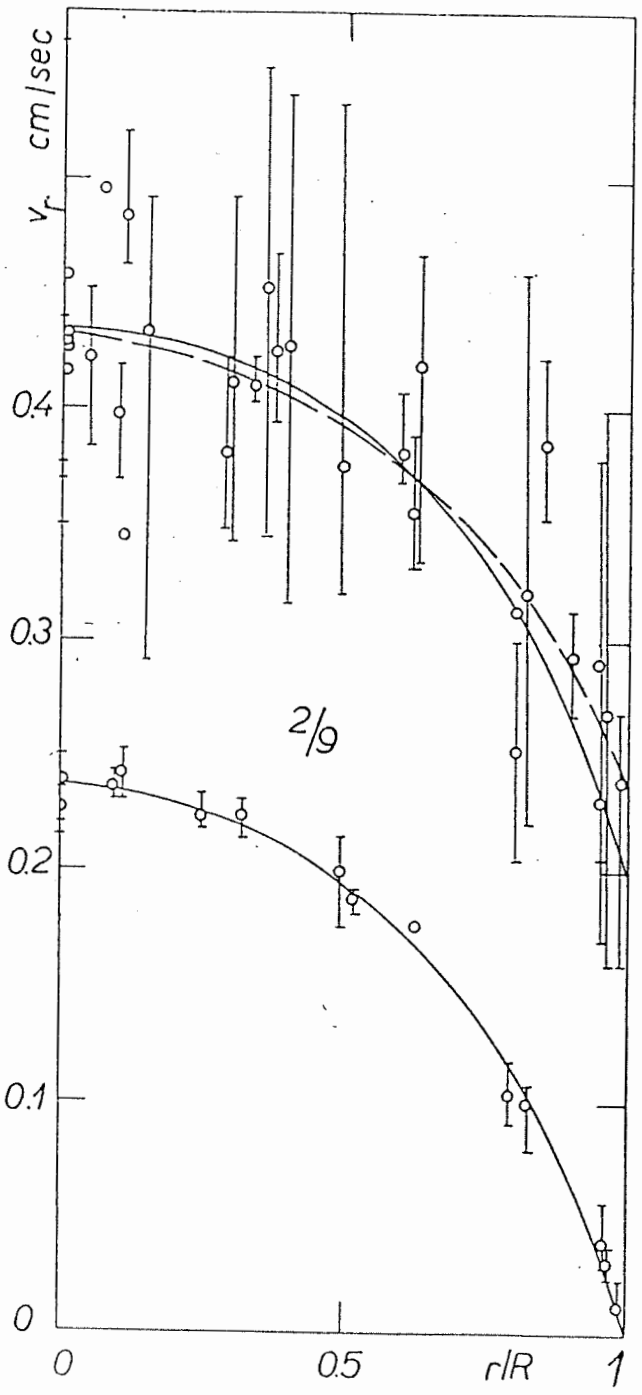

Figure 2.3. Velocity profile in spurting flow region with polybutadiene. Top curve: phase of flow corresponding to sudden velocity increase; bottom curve: phase of relatively constant rate of flow. (Bartos and Holomek, 1971).

technique. However, there are also opposite views (Den Otter, 1970, 1971) on these work, stating that the spurting flow is not related to slip at the wall for several types of polymer melts.

More recently, El Kissi and Piau (1990) visualized the flow inside the die by injecting a small quantity of silicon carbide particles (7 micron in diameter) as flow marker upstream of the capillary. They extruded high molecular silicon fluids (silicon gum) at room temperature, at pressure drop of 1.8 MPa. They observed the slip of the liquid at the wall. Figure 2.4 shows that the cluster of marker (in color of white) slips along the die wall with little deformation. Picture (f) was taken after picture (e).

2.2.3 Flow Birefringence

Birefringence is widely used to study polymer flow. This is an application of photo-elasticimetry in transparent flow medium. The interference patterns obtained from a transmitted polarized light wave across the polymer melt can be translated in terms of stresses. Birefringence can be used to study the flow both in the reservoir and inside the flow channel. This technique has been used by Philippoff and Gaskins (1958) as a rheological tool to measure the recoverable elastic strain of

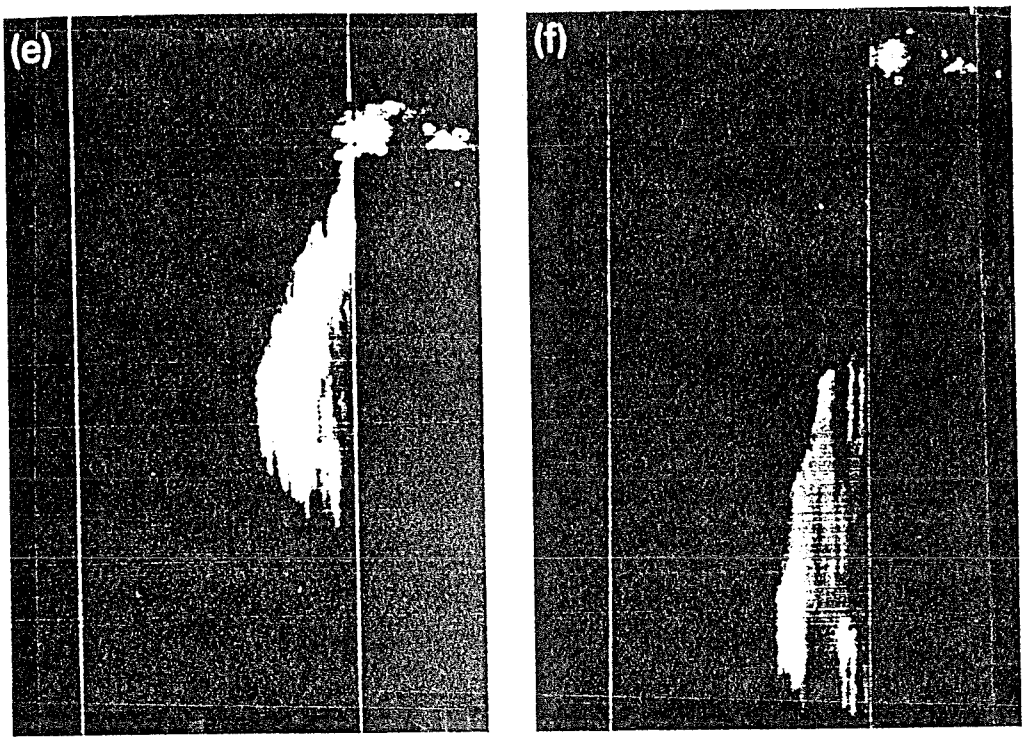

Figure 2.4. Flow visualization of silicon gum. The white clusters in both (e) and (f) are the flow marker. Picture (f) is taken a moment after (e) was taken. (El Kissi and Piau, 1990)

jellied gasoline and solutions of polyisobutylene in decalin. Schott and Kaghan (1959) appear to be the first to have used this technique to characterize flow instability of polymer melts through flat entry dies. They gave a qualitative description of the birefringence of branched polyethylene. They also reported heart-shaped bands of stress birefringence above the die entrance at low flow rates. At a critical flowrate the heart-shape bands evolved into pulsating distortions and occasional band of birefringence extended into the dark corners.

Tordella (1963) used flow birefringence to distinguish between branched and linear polyethylene types of flow behavior. For branched polyethylene he observed patterns similar to those reported by Schott and Kaghan (1959), but he reported a maximum of birefringence at the capillary inlet. At the critical flow rate, he observed fluctuations of this maximum. For linear polyethylene there was no maximum at the inlet and there were uniform birefringence bands along the length and parallel to the capillary walls at low flow rates. At a critical rate the birefringence bands broke up and a maximum appeared at the inlet. Tordella concluded that, for branched polyethylene, melt fracture is an inlet phenomenon; for linear polyethylene, melt fracture occurred in the die land. Vinogradov (1972) used birefringence to study polybutadiene melt flow. He related the pulsation interference pattern inside the die land to the stick and slip procedure. He observed alternating narrowing and broadening of interference pattern near the die wall, and he felt that the narrowing indicated high local shear stress which caused polymer melt change to high elastic state and consequently wall slip. More recently Beaufils et al. (1989) studied linear low density polyethylene, LLDPE, melt flow with sharkskin extrudate using birefringence technique. They observed the maximum values the of shear stress intensity were located at the die entrance and decreased along the die land. Moreover,

they found another increase just before die exit. They concluded there was a strong correlation between the development of the extrudate defect and the level of birefringence inside the die.

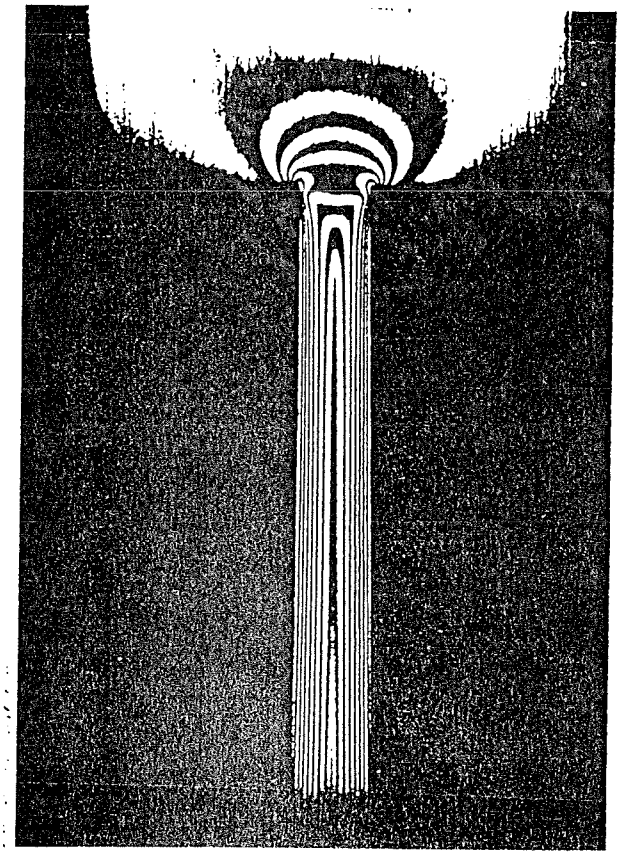

Figure 2.5. Birefringence patterns for the flow of LLDPE in a rectangular die. (Agassant et al. 1991)

Figure 2.5 represents birefringence patterns for the flow of LLDPE in a rectangular die. There is a high stress concentration at the sharp edge of the die entrance.

2.2.4 Summary

From many decades of studies, it is normally accepted that the flow patterns at the entry are divided into two categories of materials: branched polyethylene like and linear polyethylene like (Boudreaux and Cuculo, 1977-1978). The former features vortices at corner of the reservoir whereas the latter gives no or small vortices in the reservoir corner (Agassant et al., 1991). The birefringence observation confirms the concentration of stresses at the die entry is mainly responsible for the slip-stick phenomenon (Vinogradov, 1972). Beaufils et al. (1989) observed high concentration of shear stress near the exit of the die which is in line with the assumption that sharkskin is an exit phenomenon.

The most impressive observations inside the die land appear to be made by Bartos and Holomek (1971, using a cine camera) and El Kissi and Piau (1990, injecting a marked polymer at the upstream). Both of those two research teams proved the existence of slip at the die wall. However due to the technique limitations, Bartos and Holomek could not distinguish between real polymer-solid slip from the very high

shear rate near the die wall. The technique used by El Kissi and Piau gave a clearer view at the die wall during slip: no or not visible amount of polymer marked sticking on the die surface when slip happened. However there is still another possibility: the surface of the die wall had already been coated with the polymer melt before the marked polymer was injected into the flow (Figure 2.4). So, the marked polymer may slip at the surface of polymer instead of the die walls. On the other hand, in order to make the flow channel transparent to facilitate the visualization, nonmetallic materials (such as glass, quartz etc.) were used for the construction of dies (or windows) in those aforesaid observations. These nonmetallic surfaces may affect the flow pattern inside the die to some extent.

2.3 FLOW CURVES

2.3.1 Flow Curve and Bagley Correction

To understand the flow property of certain polymers, plots of pressure versus flow rate have been used for the flow through capillaries, slit and some other shape of flow channels. To obtain more quantitative information of the flow behavior, more specific relations were derived for the flow of Newtonian materials through a capillary. The apparent shear rate, $\dot{\gamma}_A$ and shear stress, σ_A, are respectively given by

$$\dot{\gamma}_A = \frac{4Q}{\pi R^3} \tag{2.1}$$

$$\sigma_A = \frac{PR}{2L} \tag{2.2}$$

where Q is the volumetric flow rate, R and L are the radius and length of the capillary, and P is the pressure drop across capillary length L. The plot of the apparent shear stress versus the apparent shear rate is called flow curve.

The ratio of shear stress to shear rate defines the viscosity of the fluid. For Newtonian fluids a plot of the viscosity versus the shear rate yields a straight line with zero slope. For polymer melts and solutions, the viscosity decreases with an increasing shear rate. The Rabinowitsch and Bagley corrections are usually used to obtain the true shear rate and the true shear stress. Bagley (1957) felt that there was an effective capillary length greater than the actual length due to the viscous resistance to flow caused by the velocity gradients in the converging stream entering the orifice of the capillary. The effective capillary length is defined as L + eR where e is a dimensionless number called the end correction. Placing this effective length in Equation 2.2 and rearranging it yields

$$P = \frac{2\sigma L}{R} + 2\sigma e \tag{2.3}$$

where σ is the true shear stress. Bagley (1957) found that the plots of P versus L/R at constant shear rate gave straight lines both above and below the critical shear rate at which extrudate distortion occurs. He also observed that for both branched and linear polyethylenes there was an inflection point at the critical shear rate. Den Otter (1970) and Utracki and Gendron (1984) and many others also made this observation. They found the plot of pressure loss versus shear stress for HDPE gave two sections divided by the critical shear stress. While for LDPE the plot was linear.

Philippoff and Gaskins (1958) suggested that the entrance effect was caused by both viscous and elastic effects, i.e.

$$e = n + \frac{S_R}{2} \qquad (2.4)$$

where e is Bagley correction (shown in Eq. 2.3), n is viscous correction and $S_R/2$ is the elastic correction, S_R is recoverable shear strain. Later Bagley (1961) showed how the elastic and viscous terms could be measured by assuming Hooke's law in shear:

$$\sigma = \mu S_R \qquad (2.5)$$

where μ is the shear modulus of elasticity. Using this relationship Bagley correction can be rewritten as

$$e=n+\frac{\sigma}{2\mu} \qquad (2.6)$$

The plot of e versus σ allows the viscous correction, the shear modulus of elasticity and the recoverable strain to be determined. Bagley observed that the onset of extrudate distortion occurred at a critical value of recoverable elastic shear strain.

2.3.2 Flow Curve Slope Change

Another important aspect in the flow curve analysis has been the relationship between the slope change of the flow curve and the extrudate roughness. Bagley (1957) made logarithmic plots of the shear rate versus the applied pressure for a branched polyethylene melt. At the critical shear rate (for the onset of extrudate distortion) a change in the slope was observed. The critical pressure at this change of slope varied with capillary length to radius ratio but the critical shear rate remained constant. He also found that the critical shear stress was about 0.1 MPa. Tordella (1956) also observed the slope changes for number of polymers but he didn't relate such change to the extrudate distortions. He believed that the change of slope was a valid rheological indicator. However, he didn't observe the similar changes in

slope for linear polyethylenes. Vinogradov and Manin (1965) reported that changes of slope in the flow curve marked the shear stress at which elastic turbulence started. Schott and Kaghan (1959) and Bartos (1964) made similar plots on branched polyethylenes, however, neither of them observed a change in slope at the critical shear rate.

More recently, Ramamurthy (1986) extruded both HDPE and LLDPE, and reported the changes in the flow curve slope. He proposed that the slope change indicated slip at the die wall, and the wall slip caused the sharkskin (surface roughness). Figure 2.6 shows the slope change from his experiments.

2.3.3 Discontinuity in Flow Curve

For linear polyethylene, discontinuities and hysteresis have also been an interesting subject discussed for several decades. Bagley (1958) first reported that when a linear polyethylene was extruded through a capillary at a constant pressure, there was a discontinuity in the plot of output versus applied pressure as shown in Figure 2.7. At a critical pressure the output becomes double valued and a hysteresis is described. As the pressure is increased, a point is reached at which the output jumps from a low to a high value. With further increases of pressure, the output continues to increase at the high value. As the pressure is decreased, the

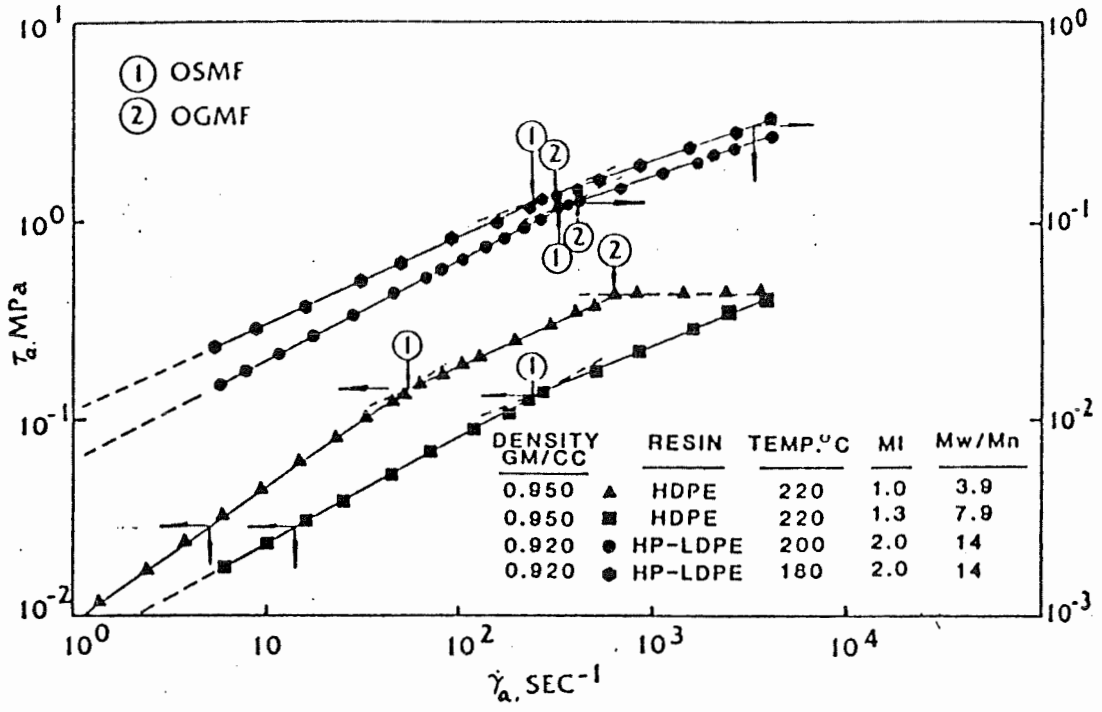

Figure 2.6. Slope change of HDPE and LLDPE flow curves. (Ramamurthy, 1986).

output decreases until a point is reached at which it jumps back to the lower value. The pressure at which this jump occurs is lower than the pressure at which the jump to the higher output occurs. With constant rate extrusion, Ballenger et al. (1971), Den Otter (1971) reported that there were oscillations of stresses. This phenomenon has also been reported by Utracki and Gendron (1984), Ramamurthy (1986), Kalika and Denn (1987), Lim and Schowalter (1989), Becker et

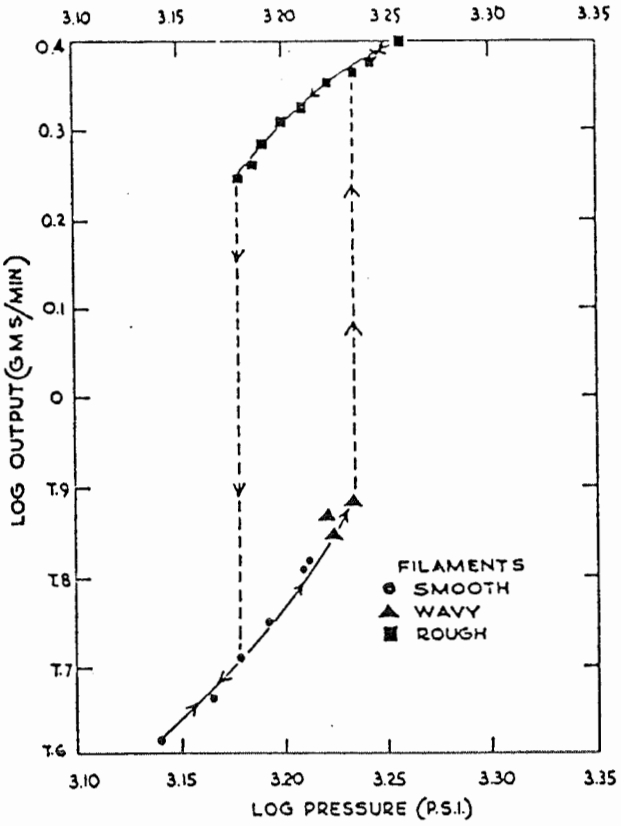

Figure 2.7. Flow of linear polyethylene through a flat entry capillary using capillary die, D=0.2445 mm, L/D=9. (Bagley et al., 1958).

al. (1991). Lim and Schowater used pressure transducer and hot film probe to monitor the die land pressure oscillations and corresponding wall slip.

There have been extensive studies on how various parameters affect the discontinuity phenomenon. Tordella (1963, 1969)

pointed out that the discontinuity itself was independent of capillary geometry. He also reported that it was independent of the capillary radius at fixed length to radius radio. On contrary, Bartos (1965) reported that larger diameters caused the discontinuity to occur at lower stresses. Tordella (1963), Bagley and Schreiber (1969), and Den Otter (1970, 1971) observed that the size of the jump of flowrate during discontinuity increased with capillary length. Tordella reported a well known figure based on HDPE extrusions (Figure 2.8). He observed a very small discontinuity when length to diameter value is equal to 1, but discontinuities increased remarkably at the higher L/D values. Sabia and Mullier (1962) reported that the extent of the hysteresis decreased with wider molecular weight distribution.

2.3.4 Summary

The flow curve has long been proved as an important information to analyze extrusion instabilities and related extrudate distortion. The Bagley correction is connected with flow pattern changes and the onset of extrudate distortion (Utracki and Gendron, 1984). Since the Bagley correction is the combination of both entry and exit pressure loss, Bagley corrections may be attributed to the both entrance part and exit part. To distinguish between two effects when extrudate distortion happens might be helpful to locate the source of

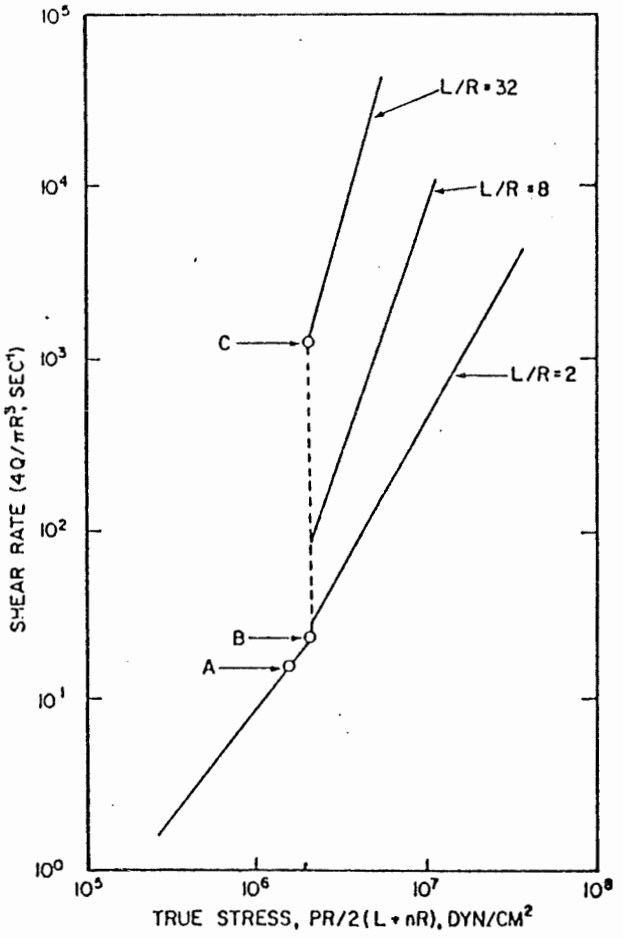

Figure 2.8. Schematic flow data representing increasing of flowrate jump at discontinuity as a function of L/R values based on HDPE extrusions (Tordella, 1963).

corresponding extrusion distortions. This is one of our objectives to conduct slit die experiments: we can determine the entrance and exit pressure loss separately.

Flow curve slope changes reflect the flow pattern changes,

possibly slip inside the die. However, this assumption needs more experimental evidence. El Kissi and Piau (1992) pointed out that the approach used by Kalika and Denn (1987) to calculate the slip velocity was incorrect because of slope change. El Kissi and Piau assumed the slope change was caused by shear-thinning effect. Under this assumption the calculated slip velocities were considerably smaller than the results obtained by Kalika and Denn.

Discontinuities in flow curve are the characteristics of linear polyethylenes, its severity (amount of pressure drop at constant flowrate extrusion or that of flow rate jump at constant pressure extrusion) depends on the nature of the polymers (molecular weight, molecular weight distribution, branching), and L/D value of the capillary channel. Discontinuities usually start with spurting flow featuring oscillations in pressure at constant flowrate extrusion and oscillations in flowrate at constant pressure. The frequencies of the oscillation depend on the dimensions of reservoir and flow channel. Smaller reservoir and length of the die increase the frequency. The oscillations correspond to the slip and stick procedure which is best explained by the state change theory proposed by Vinogradov (1972).

2.4 PARAMETERS AFFECTING EXTRUDATE DISTORTIONS

2.4.1 Extrusion Parameters

Extrusion parameters include temperature of melt and die, flow channel characteristics (length, radius, length to radius ratio, entry angle, material of the construction of the die), type of extrusion device (constant speed or constant pressure rheometers, and extruder). From the 1950's to nowadays, many researchers have studied the effect of temperature and flow channel geometry (Schott and Kaghan, 1959; Benbow and Lamb, 1963; Bartos, 1964; Den Otter et al., 1967; Ballenger et al., 1971; Vinogradov, 1972; Utracki and Gendron, 1984; Ramamurthy, 1986; Kalika and Denn, 1987; Cook et al., 1989; Beaufils et al., 1989, and Hatzikiriakos and Dealy, 1991). It may be summarized by the following:

1) Critical Shear Stress

The value of the critical stress for the onset of extrudate distortion is widely accepted to be within the range of 0.1 to 1 MPa. Experimentally, it has been shown that the critical stress increases slightly with temperature; the increase is so slight that many investigators (such as Ramamurthy, 1986) claimed that the critical shear stress is independent of temperature.

2) Parameters Affecting the Critical Shear Rate:

The critical shear rate for the onset of extrudate

distortion varies widely and no specific range has been given in the literature. It appears that the critical shear rate varies inversely with the viscosity (Howells and Benbow, 1962). Bagley (1961) and Schott (1964) also pointed out that the recoverable elastic shear strain, the shear modulus, and the normal force increase with temperature.

3) Geometry Effect

It is generally agreed that the critical stress and shear rate are independent of capillary geometry (Bagley 1957). For branched polyethylenes and most polymers, increasing the capillary length and decreasing the entry angle tends to diminish the severity of the distortion by increasing the critical shear stress or shear rate. However, there is an important exception for linear polyethylenes: increasing the capillary length increases the severity of the distortion (White, 1973). White felt that the disturbances which caused distortion were propagated rather than damped in the capillary. Although it is also generally agreed that the critical shear stress is independent of capillary diameter. Leonov (1984) modeled the stick-slip phenomenon by a simple linear model and he pointed out that there was a critical diameter of capillary only below that the stick-slip phenomenon would occur.

4) Die Materials

There is some evidence that the material of the die has an influence on the flow properties. Benbow and Lamb (1963) extruded branched polyethylene through dies of the same dimensions but made of brass, nylon/carbon black, copper nylon/fiber glass, nickel steel, mild steel, phosphor bronze, or silver steel. The critical shear stress for the onset of extrudate distortion decreases in descending order from 0.155 to 0.092 MPa for the die materials listed before. They also suggested that extrudate distortions could be diminished by choosing dies with cohesive energy density similar to that of the melt. Clegg (1957) performed experiments through glass dies with both polished and ground walls and saw no differences in the flow curves for polyethylene melts. He felt that this indicated no interaction between the melt and the die wall. Tordella (1963) extruded linear polyethylene through dies made of rough and polished stainless steel, glass, graphite, and polytetrafluoroethylene. He found that the critical stress at the onset of extrudate distortion remained the same. However, with the graphite die he did see bits of graphite on the emerging polymer stream. Metzger and Hamilton (1964) investigated linear polyethylene with dies of stainless steel, bronze, sintered bronze, and Teflon. They observed that the flow curves remained unchanged except with the Teflon die. Vinogradov et al. (1984) extruded

polybutadienes through steel, glass, and Teflon capillaries. They observed the flow curves of all the dies coincided at low shear rates. At a critical shear stress, Teflon dies caused a higher increasing rate of shear rate. They explained this phenomenon as the poor adhesion of polymer melt to the Teflon surface. They suggested that at the critical shear stress, there was stress concentration near the die exit, which caused local spurting there. Due to the good adhesion of polymer to the steel wall, spurting didn't extend to the upstream; while poor adhesion of polymer melt to the Teflon wall allowed spurting to be propagated to further upstream leading to wall slip. Therefore, for Teflon coated die, the stress values calculated was lower compared to those of other dies, showing as faster increase of shear rate in the flow curve. More recently, Ramamurthy (1986) studied the effect of die material on the extrusion of linear low density polyethylene: aluminum, copper, carbon steel, brass, bronze, and stainless steel dies were used. In addition to the suggestion given by Tordella (1963) and Metzger and Hamilton (1964) on the capillary extrusion, he found significant material effect on film extrusion: brass insert in film blown die eliminated the film roughness. Hatzikiriakos and Dealy (1991) studied high density polyethylene, HDPE by fluoroelastomer coated sliding die and found the coating caused wall slip to start at lower shear stress. They suggested there was slip between the

fluoroelastomer and polymer melt.

5) Device of Extrusion

The type of extrusion device may affect the occurrence of extrudate distortion. Den Otter et al. (1967), Tordella (1969), Ballenger et al. (1971), Den Otter (1971) found differences depending on whether the extrusion device is constant pressure type or constant rate type: there are pressure oscillations at spurting extrusion with constant rate type, whereas flowrate oscillations are observed with constant pressure type. However, there do not appear to be any differences in the flow patterns in the reservoir or in the extrudate distortions due to the type of rheometer. Recently, El Kissi and Piau (1990) compared pressure controlled and flowrate controlled extrusions through capillaries with silicone fluids, they reported similar flow curves.

Schott and Kaghan (1959) performed their experiments in a screw extruder and confirmed the results of earlier investigators who used gas driven rheometers. Ballenger et al. (1971) saw no differences in extrudate distortions in melts extruded by a screw extruder and an Instron rheometer (constant rate). In brief, in the literature, there does not appear to be any evidence that the type of apparatus affects extrudate distortion.

2.4.2 Material Parameters

1) Molecular Weight Effects

As early as in 1949, while studying the flow of polystyrene, Spencer and Dillon (1949) found an inverse relation between the weight-average molecular weight and the critical shear stress for the onset of extrudate distortion. The product of molecular weight and the critical stress was approximately constant. Bagley (1961) later reported that the product of the molecular weight and critical shear stress for linear polyethylene was constant and could be related to the recoverable elastic shear strain as:

$$\sigma_c M_W = (RT\rho) S_{RC} \qquad (2.7)$$

where σ_c is the critical shear stress for the critical elastic strain, S_{RC}, and M_W is the weight average molecular weight. R is the gas constant, T the absolute temperature, and ρ the polymer density. Benbow and Lamb (1963) also commented on the constancy of the product of molecular weight and critical shear stress for many polymers. Howells and Benbow (1962) believed that molecular weight and the degree of chain branching were the structural factors that influenced melt fracture. They felt that large molecular weight and low branching promoted melt fracture and led to low values of the critical shear stress. Since these structural factors have a similar influence on the melt viscosity, they also believed that polyethylenes with a similar melt index would have the

same critical stress. At constant melt index, the effects of molecular weight and chain branching cancel each other. Schreiber (1969) pointed out that if the weight average molecular weight was below 18,000, the flow discontinuity usually found for linear polyethylene should not be observable. He also reported that the blends of polyethylene made of components with widely different molecular weights are far more effective in reducing the viscosity discontinuity than blends with broader but more normally shaped distribution functions. Rudin (1970) felt that wider distributions should increase the occurrence of extrudate distortion since they promote melt elasticity. Den Otter (1970, 1971) reported that chain branching promoted the formation of the circulating secondary flow in the reservoir and decreased the angle of convergence of the funnel of fluid entering an orifice. Karbashewski et al. (1991) studied the effect of branching on the processability of linear low density polyethylenes. They concluded that, at constant molecular weight, the polymers with the higher proportions of linear polyethylene showed inferior processability in terms of onset of surface imperfections at lower extrusion rates.

2) Elasticity Effect

It is believed that the elastic properties of polymer fluids are responsible for the non-Newtonian behavior of these

fluids. It is also considered that elasticity is responsible for the flow instabilities that lead to extrudate distortions. Much efforts have been applied to separate the elastic and viscous effects in the extrusion process. Schreiber et al. (1965) have shown that a certain minimum molecular weight is necessary to produce sufficient molecular entanglement to promote melt elasticity. This is similar to the segmental entanglement theory of viscosity in which the critical molecular weight at which there are sufficient entanglements to affect the viscosity is defined by a change in slope on the logarithmic plot of viscosity versus molecular weight. They have determined that the critical molecular weight for the inception of elasticity is greater than twice that for the change in viscosity. Since the lower the molecular weight less elastic of the melt is, the low molecular weight increases the critical shear stress for the onset of extrudate distortion.

Vlachopoulos (1972) proposed that the product of recoverable shear strain and parameter of polymer molecular weights should be a constant, i.e.:

$$S_{RC}\left(\frac{M_z M_{z+1}}{M_w^2}\right)^{-1} = constant \qquad (2.8)$$

where S_{RC} is critical recoverable shear strain, M_w is weight average molecular weight, M_z and $M_{(z+1)}$ are the z and z+1 average molecular weights.

2.4.3 Summary

The anomalous extrusion phenomena such as sharkskin, spurting and gross fracture reflect the nature of the polymer molecular structure: combination of different length macromolecular chains; entanglement between those chains; portion of the branches etc. Therefore the characteristics of the polymer are bound to affect the extrudate quality. It is generally admitted that the higher the molecular weight the lower the critical shear stress (Spencer and Dillon, 1949, Schreiber, 1969). Vinogradov (1972) proposed a critical molecular weight, M_c corresponding to the change of the nature of the power dependence of the initial viscosity on the molecular weight. He pointed out that if $M/M_c > 10$, there must be a maximum value of loss modulus, G", at certain frequency which is corresponding to the onset at which the polymer changes to the elastic state. In extrusion, such a polymer will show flow instabilities and extrudate distortions. The molecular weight distribution is also an important factor and severity of the extrudate distortion is inversely related to the amount of low molecular, highly branched portion (Karbashewski et al., 1991).

The processing conditions are also the important factors. So far many factors (such as temperature and dimension of the die) have been studied by number of researchers. However, unlike the study of material effects, there are not widely accepted conclusions on the effects of different processing conditions (such as the dimension of the die).

Further, there is very little knowledge concerning the relationship between those factors and the coupling effects among them. In our work, we try to answer this question using a statistical approach.

2.5 MECHANISMS AND THEORIES

2.5.1 Different Views in the History

Many mechanisms and theories have been proposed through more than half a century of research work by many investigators. Table 2.1 lists the various authors and their explanations of the flow instability and extrudate distortion.

(1) As early as a half century ago, Nason (1945) proposed that extrudate distortion was a direct result of Reynolds turbulence in the melt flow. Turbulence occurs when a value of 1000 to 1500 for the Reynolds number is reached. Later Tordella (1957) pointed out that this relation predicts that

Table 2.1. Mechanisms of Instability and Extrudate Distortion.

Theory	Reference	Explanation
(1) High Reynolds turbulence	Nason (1945)	Distortion is the direct result of Reynolds turbulence in the melt flow.
(2) Difference of orientation between extrudate skin and core	Spencer and Dillon (1949)	Distortion is a die exit phenomenon.
(3) Melt fracture at die entry and in die land	Tordella (1956)	When the limit of elastic deformation is reached at high shear rates, melt fracture happens.
(4) Slip-stick on the die wall	Benbow et al. (1961)	The lack of adhesion between polymer melt and die wall causes surface distortion.
(5) Recoverable elastic strain	Bagley (1961) and Rudin (1970)	Extrudate distortion occurs at a critical values of the recoverable elastic shear strain.
(6) Deborah number	Metzner et al. (1966)	Large ratio of fluid relaxation time to the residence time results in flow instability.
(7) Melt state changing	Vinogradov (1972)	At critical shear stress, polymer melt changes its state from fluid to elastic which causes loss of adhesion of polymer at the die wall.
(8) Elastic friction at the wall	Uhland (1976)	At the die wall, the polymer follows the friction law, lower normal pressure facilitates slip and in turn extrudate distortion.
(9) Relaxation oscillation	Weill (1980)	The relaxation oscillatory flow causes both sharkskin and spurting, happening at entry for sharkskin; through whole the die for spurting.
(10) Wall slip	Ramamurthy (1986)	The wall slip indicated by slope changing of flow curve causes onset of sharkskin.
(11) Negative pressure at die exit	Tremblay (1989)	The negative pressure at edge of die exit leads to sharkskin.
(12) Slip acceleration at exit	Hatzikiriakos and Dealy (1992)	Polymer melt accelerates at the die exit because of low normal pressure.

the critical flowrate should vary directly with the radius and viscosity whereas experiments indicated that the critical flow rate varied with the third power of the radius and inversely with the viscosity. He concluded that Reynolds number is not a proper criterion for the flow instability. Further, many extrudate surface distortions have been observed at flowrates far below the critical (Beaufils et al., 1989) Reynolds number value suggested by Nason. There is a general agreement with Tordella's conclusion nowadays.

(2) Spencer and Dillon (1949) believed that extrudate distortion was due to differences in flow orientation between the extrudate skin and core. The fluid, as it passes through the die, is subjected to maximum orientation at the die wall. The orientation decreases progressively from the die wall to the center of the die so that an extrudate with a highly oriented skin covering a less oriented core. As the shear rate increases, the thickness of the skin also increases. Upon emergence from the die, the filament tends to recover from its oriented state, and since the skin is more oriented than the core, the filament buckles. Since relaxation occurs upon emergence from the die, Spencer and Dillon (1949) believed that buckling was a die exit phenomenon. Also, they found that the distortion occurred at a precise amount of shear orientation defined by the square of the ratio of the

extrudate diameter to the diameter of the die.

(3) In a series of publications, Tordella (1956, 1957, and 1958) suggested that the cause of extrudate distortions was irregularities in the flow of the polymer melt at the die entrance. As the shear rate is increased, the extent of elastic deformation is increased until at a critical shear rate the limit of elastic deformation is reached and the material fractures. The fracture is accompanied by an audible tearing noise and the emerging extrudate is distorted. According to Tordella, the extrudate distortion is due to the alternate flow from the converging flow region and the secondary circulating area above the die entrance as discussed in the section 2.2.1. Based on the birefringence observations, Tordella (1963) also concluded the discontinuity of linear polyethylene was caused by melt fracture. In contrary to the other polymer, he found the fracture happened in the die land rather than at the entrance.

(4) Benbow et al. (1961) introduced a slip-stick mechanism to explain flow instability and extrudate distortion. They believed that at and above a certain critical stress the polymer would experience intermittent slipping due to a lack of adhesion between the melt and the die wall. The slip relieves excessive deformation energy absorbed as a result of

flow through a die. This slip-stick process would result in an extrudate composed of alternative sections of melt with different deformation histories, an extrudate with irregular surface. In addition, slipping would seem to explain the discontinuity in the flow curve of linear polyethylene. Flow visualization experiments with silicone gums of various viscosities, polyethylene, polybutadiene, polyvinyl chloride, and polypropylene seemed to support this theory (Benbow et al. 1961, Benbow and P. Lamb, 1962, and Vinogradov, 1972). Later, many researchers (Maxwell and Galt, 1962, Lupton and Regester 1965, Blyler and Hart, 1970, Bartos and Holomek, 1971) have studied the slip mechanism and even obtained slip velocities at the wall. Blyler and Hart (1970) believed that slip occurred between layers of the polymer near the die wall rather than between the polymer-die interface. Ramamurthy (1986), Kalika and Denn (1987), and Hatzikiriakos and Dealy (1991), also calculated the slip velocities at the wall when extruding linear polyethylenes. The photograph made by El Kissi and Piau (1990) appears to be the most visible slip observation so far (Fig. 2.4). Therefore, the slip concept is becoming more and more acceptable among the researchers.

(5) Many investigators have considered the elastic nature of polymer melt to be responsible for the unstable flow which leads to extrudate distortion. Bagley (1960) introduced the

term "elastic turbulence" in reference to a formulation involving elastic compliance given by Tordella (1958).

$$N_J = QJ\eta / R^3 \qquad (2.9)$$

This formulation is analogous to kinetic or Reynolds turbulence. Q is the volumetric throughput of a fluid with viscosity η through a die of radius R. J is the elastic compliance of the fluid. Rudin (1970) also related extrudate distortion to the elastic nature of the melt. He felt that any processing variations which would decrease the elasticity of the polymer would diminish the severity of the extrudate distortion. These variations include increased die length, increased temperature, and the incorporation of polymeric additives to the polymer melt. Also anything that would influence the breakdown and recovery of the molecular entanglement structure would influence melt elasticity. Based on this theory, it is expected to find a critical elastic strain related to unset of extrudate distortion. Bagley (1961) showed how the critical elastic strain could be determined by plotting the end correction against the true shear stress assuming Hooke's law in shear. He was able to relate this to the occurrence of melt fracture as discussed earlier (Eq. 2.5).

(6) First introduced by Reiner (1964) and developed by

Metzner et al. (1966), the Deborah number, $N_{Deb}=\theta/t$ was defined to describe the influence on the flow field of unsteady elastic responses. θ is the characteristic relaxation time of the fluid and t is the time scale of the process; i.e. the residence time of the fluid in the changing velocity field. The Deborah number is the ratio of time scales involving the fluid properties and the residence time of the fluid in a deformation process. Large residence time and small Deborah number imply fluid-like behavior while small residence time and large Deborah number imply solid-like behavior. The resulting instability of the flow field caused by solid-like behavior leads to extrudate distortion.

(7) Vinogradov and Insarova (1972) proposed the theory of state change of polymer melt during extrusion. He pointed out that a polymer passed from the fluid to the high elastic state with an increase in the shear rate and the polymer would cease to behave as a fluid under shear. This is accompanied by various forms of flow perturbation at the die exit, entrance and inside the die. He also suggested that the perturbations at the die entrance and exit are due to stress concentrations in these zones; while the transition of a polymer to the high elastic state near the walls inside die caused slip-stick process or continuous slippage along the die wall. The kind of slip (whether slip-stick or continuous slip) depends on the

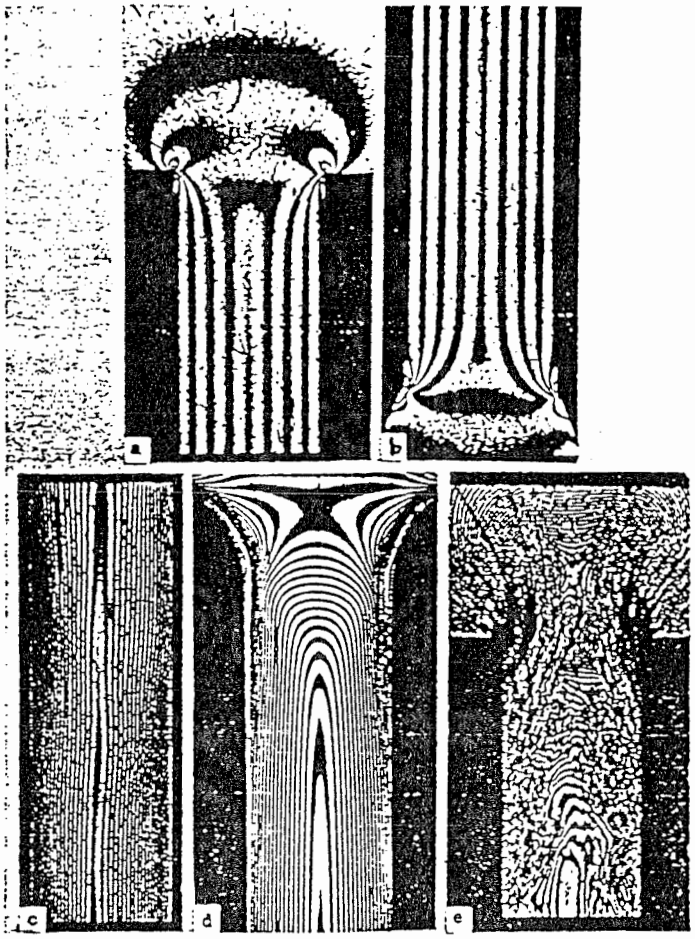

Figure 2.9. Birefringence observation of polybutadiene flow (room temperature) made by Vinogradov and Insarova (1972) in explaining the state changing theory.

velocity of the polymer. At further higher flowrates, melt fracture occurs. He used birefringence technique to observe this state change. The typical patterns are shown in Figure 2.9. The polymer was polybutadiene and extrusion was conducted through a transparent die at room temperature. Part (a) shows

the die entry at shear stress of 0.063 MPa; part b is the die exit at same shear stress; part c shows middle part of the die at shear stress of 0.316 MPa; part d depicts the smooth die entry at shear stress of 0.398 MPa; and part e shows die entry at shear stress of 0.562 MPa. Parts a and e show concentrations of stresses at the die entry; similarly, part b shows the stress concentration at the die exit. In part c, there is alternating narrowing and broadening of the interference bands along the die wall. Vinogradov and Insorava explained the narrow zones corresponded to an increase in stresses up to the critical value and the transition of the polymer to the high elastic state. This caused a reduction of the adhesion of the polymer to the wall and also resulted in

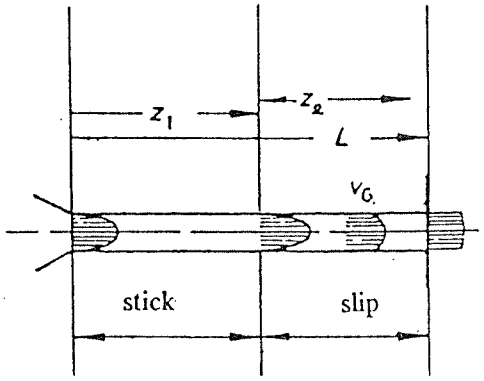

Figure 2.10. Elastic friction model (Uhland, 1976). Z_1 is stick zone, the Z_2 is slip zone.

slippage. Such slippage allowed relaxation of polymer, and in turn caused transition of polymer to the fluid state and sticking to the die wall again. Vinogradov (1981) also related this critical stress to the maximum value of the loss modulus, G" in sinusoidal dynamic measurements. He pointed out that the maximum in the loss modulus curve corresponded to the transition of polymer from the fluid to the high-elastic state, and this value is independent of molecular weight and temperature. When he plotted the modulus/frequency (G''/ω) and shear stress/shear rate($\sigma/\dot{\gamma}$) together, the critical shear stress and maximum loss modulus coincided. This state change theory gives better understanding of spurting phenomenon and lay the foundation for a further analysis based on the elastic friction theory.

(8) In 1976, Uhland (1976) proposed a model based on the Coulumb Friction Law for solids stating that the friction between two surfaces is proportional to the normal pressure. In pressure flow, the pressure decreases linearly along the flow direction. Therefore, according to Uhland's assumption the friction between the polymer and the die wall becomes weaker and weaker in the flow direction. Therefore, at some point in the die land, the polymer begins to slip at the wall. As shown in Figure 2.10, the model predicts that there are two flow regions in the die: a first region, Z_1 in the upstream

part of the die, where the fluid sticks to the wall; and a second region, Z_2 in the downstream part of the die, where the fluid slips at the wall. For shear stresses above a critical value, an instability region is found at the exit of the die. In this region, a sudden decrease of the shear stress can occur. He suggested that this mechanism seemed to explain the discontinuity in the flow curve of linear polyethylenes. Hatzikiriakos and Dealy (1992) also suggested that the slip happened at certain position of the die land.

Based on the state change theory (proposed by Vinogradov, 1972), Leonov (1984) proposed a simple linear model to describe the pressure oscillations and surface roughness. He assumed that the polymer melt behaves as an elastomer at high shear rate. At certain flowrate, the polymer begins to slide at the solid wall causing an increae of flow rate and a decrease of shear stress. He proposed the following function:

$$\sigma_w=\sigma_0(1-v/v_\infty) \tag{2.10}$$

where σ_w is shear stress at the wall σ_0 is the critical shear stress at which slip starts, V is velocity of polymer at the die surface, V_∞ is a constant depending on the properties of polymer and die wall material. Under the assumption that the polymer behaves as elastomer and slides along a rigid surface

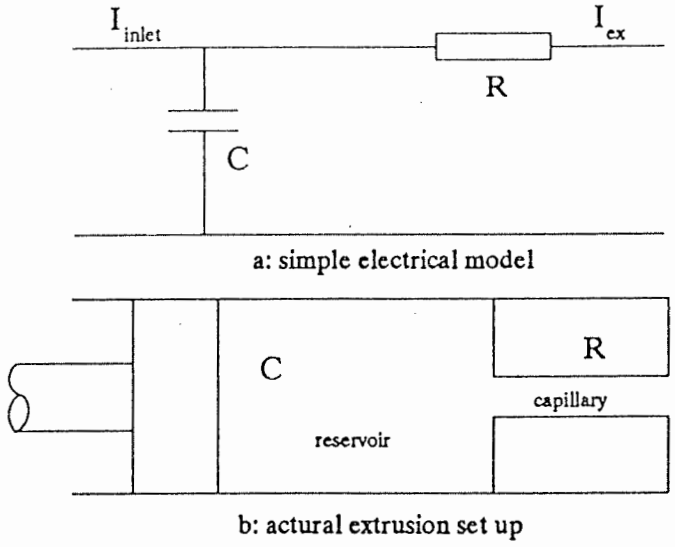

Figure 2.11. The simple electrical model proposed by Weill (1980) to describe capillary flow with upstream reservoir. He simulated the reservoir by a capacitor and the capillary by a resistor.

by means of migration of polymeric bonds (some segments or macromolecules), $V_\omega=\lambda_0/\theta$ (Moore, 1972), where λ_0 is the mean distance between the adhesive (polymer-to-die wall) bonds without slip, and θ is the average life time of these bonds.

(9) Weill (1980) proposed a relaxation oscillation theory to explain spurting and sharkskin phenomena of linear polyethylenes. He felt that both these extrudate distortions are caused by relaxation oscillation. The only difference is that: for spurting, the oscillation happens through the whole

die whereas for sharkskin, the oscillation only happens at the die entry. The oscillations are caused by two transitory flows: compression and decompression assuming the polymer is compressible. The polymer is first compressed in the reservoir. During this compression flow, the pressure head measured at the die reservoir increases. At certain critical pressure, the depression flow begins. This time, pressure decreases and flowrate increases. Weill (1980) simulated this oscillation procedure by a simple electrical circuit, an oscillator (Figure 2.11). He related the capacitor in the oscillator to the reservoir above the capillary; and the resistor to the capillary. The frequency of such oscillation depends on the dimension of reservoir and capillary as well as the plunger (pushing the polymer out of capillary) speed. He concluded that if the whole die was considered as the resistive part of the oscillator, one could obtain a good description of the pressure and flow rate oscillations. The pertinent parameters R and C could specify the period. This is accompanied with spurting flow. On the other hand, if only the die entry region is considered as the resistive part, the die itself acts as a damping element and melt flow at the exit gives rise to the sharkskin phenomenon. This time there is no measurable flow rate oscillation although there are high frequency pressure oscillations in the reservoir. He pointed out that the oscillation periods for spurting and sharkskin

are 2 and 0.02 seconds respectively. The amplitudes of pressure oscillations for these two phenomena are 10 and 0.1 MPa respectively. Experimentally, he obtained a linear dependence of the oscillating period on the reservoir size. Although his theory is working relatively well for linear polyethylene, it could not explain the fact that there is no oscillation flow for branched polyethylene which has similar compressibilities as linear polyethylene. Moreover, his suggestion that the high frequency pressure oscillations are associated with sharkskin does agree with experimental results. Beker et al. (1991) used a frequency analysis technique to study sharkskin. They didn't observe any characteristic oscillation frequency and the pressure fluctuations have very low intensity. According to our slit die extrusion, when sharkskin happens the pressure fluctuations in the reservoir are similar to that are when extrudate is smooth: sharkskin related pressure oscillations do not exit or are not observable. His suggestion of sharkskin originating at the entry is a unique point of view over this very controversy issue. Other and more accepted explanations include exit effect (Vinogradov 1984, Tremblay, 1989) and slip inside die (Ramamurthy, 1986).

(10) Although the wall slip mechanism has been suggested several decades ago, Ramamurthy (1986) studied in more details

of the relation between wall slip and flow curve as well as extrudate distortion (shark skin and gross fracture) for polyethylenes. He concluded that the sharkskin phenomenon was due to the failure of polymer adhesion at the die wall. He stated that the slip started at the beginning of the flow curve slope change as shown in Figure 2.6. He plotted the apparent shear rate, $\dot{\gamma}_a$ versus reciprocal of radius (Mooney's method) to obtain the slip velocities (Figure 2.12) at the die wall and he reported that the slip started at an apparent shear stress of 0.1 MPa. Kalika and Denn (1987) obtained similar slip velocities with similar LLDPEs (Figure 2.13) using dies with different L/D values. Their work has given rise to a new wave of research interest on relationship between slip velocity and extrudate distortion since the late 80's. Further, Ramamurthy (1986) found a strong effect of die construction material on the blown film surface roughness: using alpha brasses he found no melt fracture following certain ''induction time''. However, such strong effect has not been found with capillary die extrusion. On the other hand, Ramamurthy (1986) found the adding of fluoroelastomer to the linear low density polyethylene improved the extrudate quality very much. He felt the reason was the good adhesive ability of fluoroelastomer which preventing the slip at the die wall. However his conclusion has not been widely accepted. There are many controversial arguments on the role of

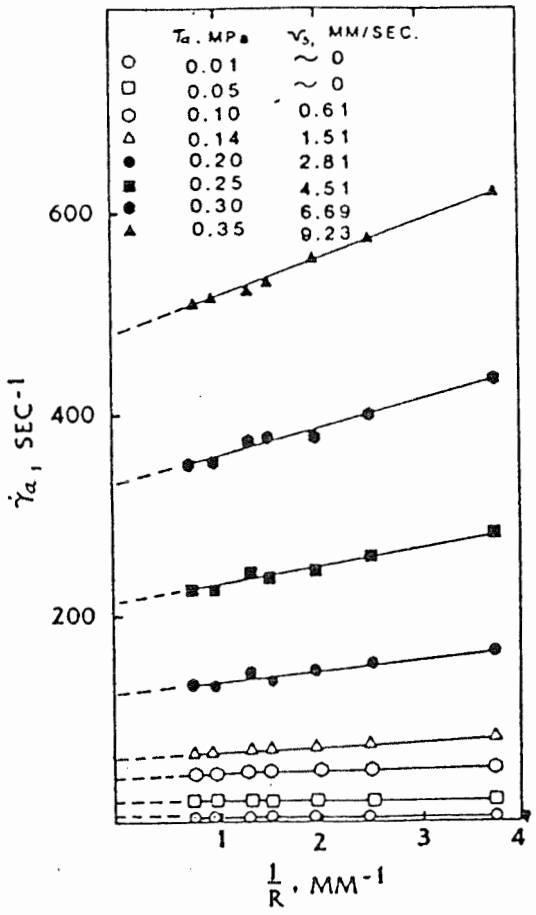

Figure 2.12. Wall slip measurements for 1 MI LLDPE at 220 °C (Ramamurthy, 1986).

fluoroelastomer. Some people (Hatzikiriakos and Dealy, 1991) believe there is slip between the elastomer and the polymer melt. In opposition to Ramamurthy's calculation, Piau et al. (1990) pointed out that the slip velocity calculated was greatly affected by neglecting the pressure loss stating that the real slip velocity was one order less than the results reported by Ramamurthy (1986). Therefore the actual relation

between the wall slip and extrudate distortion still remains an interesting question for further studies.

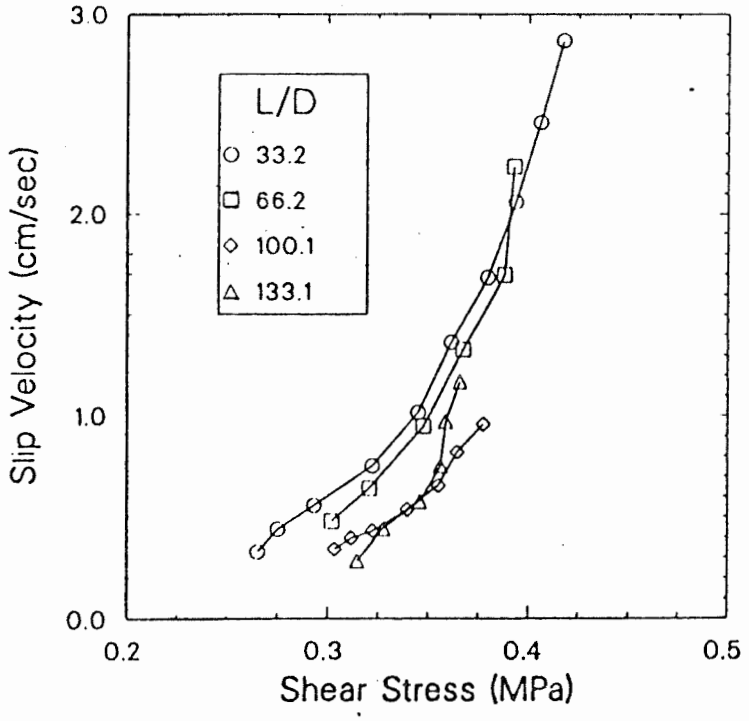

Figure 2.13. Slip velocity as a function of wall shear stress for 1 MI LLDPE (Kalika and Denn, 1987).

(11) More recently, Tremblay (1991) related sharkskin phenomenon to the negative pressure near the exit edge of the die. Using a finite element program, he obtained negative pressures existing at the die exit, as shown in Figure 2.14. Part (a) is the picture of extrudate at exit with magnification=1; part (b) with magnification = 200 near the maximum negative pressure point. The figure shows the maximum negative pressure point is located at about one micron out of

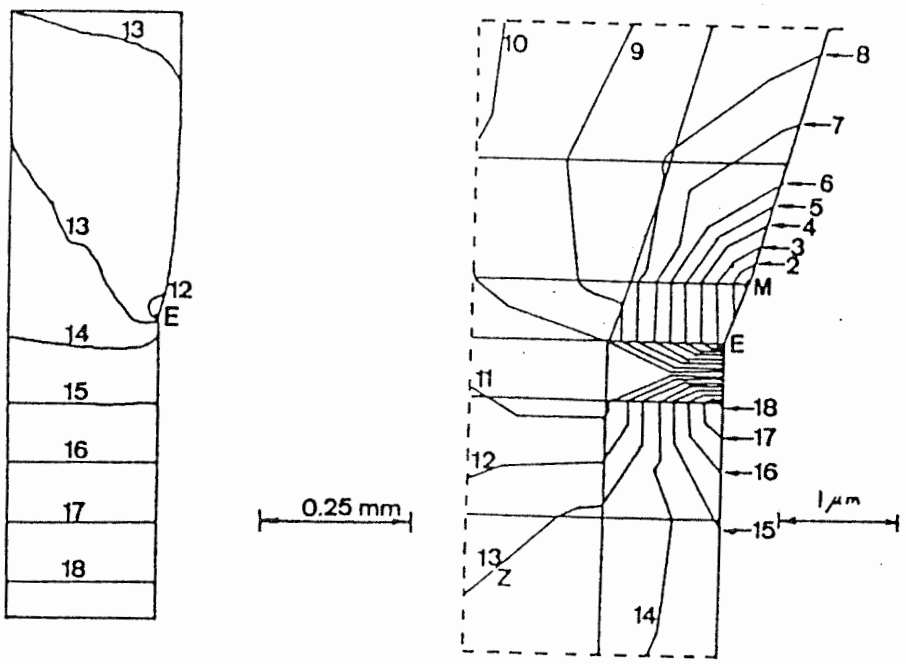

Isobars represent pressures: (1): - 3.12 MPa, (2): -2.86 MPa, (3): -2.6 MPa, (4): -2.34 MPa, (5): -2.08 MPa, (6): -1.82 MPa, (7): -1.56 MPa, (8): -1.3 MPa, (9): -1.04 MPa, (10): -0.78 MPa, (11): -0.52 MPa, (12): -0.26 MPa, (13): 0 MPa, (14): 0.26 MPa, (15): 0.52 MPa, (16): 0.78 MPa, (17): 1.04 MPa, (18): 1.3 MPa.

Figure 2.14. Pressure profile at the exit of die calculated by finite element method (Tremblay, 1991). (a) magnification=1, (b) magnification=200, M=maximum negative pressure, Z=zero pressure.

the die edge (indicated by ''M''). According to Tremblay, such negative pressure creates cavities in the polymer melt very close to the die lip. The growth and coalescence of these voids would then lead to sharkskin at the die exit. A sequence of photographs taken by Tremblay from a video film of linear polydimethylsiloxane melt extrusion at the exit of an orifice die has shown that the fracture of the polymer occurs at the die exit and not further down the extrudate.

Tremblay's suggestion gives a further explanation to the assumption that sharkskin phenomenon caused by exit effect. Combining his suggestion and ''exit stress concentration'' proposed by Vinogradov (1972), the sharkskin phenomenon could be caused by both stress concentration just before the exit and high value of negative pressure just out of the exit. If negative pressure plays an important role in causing sharkskin, the strength of adhesion of polymer to the solid die surface and the cohesion of the bulk of the polymer should be important. This may explain the strong die material effect observed by Ramamurthy (1986) when he just changed the exit part of the die in blown film procedure.

(12) Hatzikiriakos and Dealy have made systematical studies on wall slip phenomenon. They found that the wall slip not only depends on the shear stress but also on the pressure.

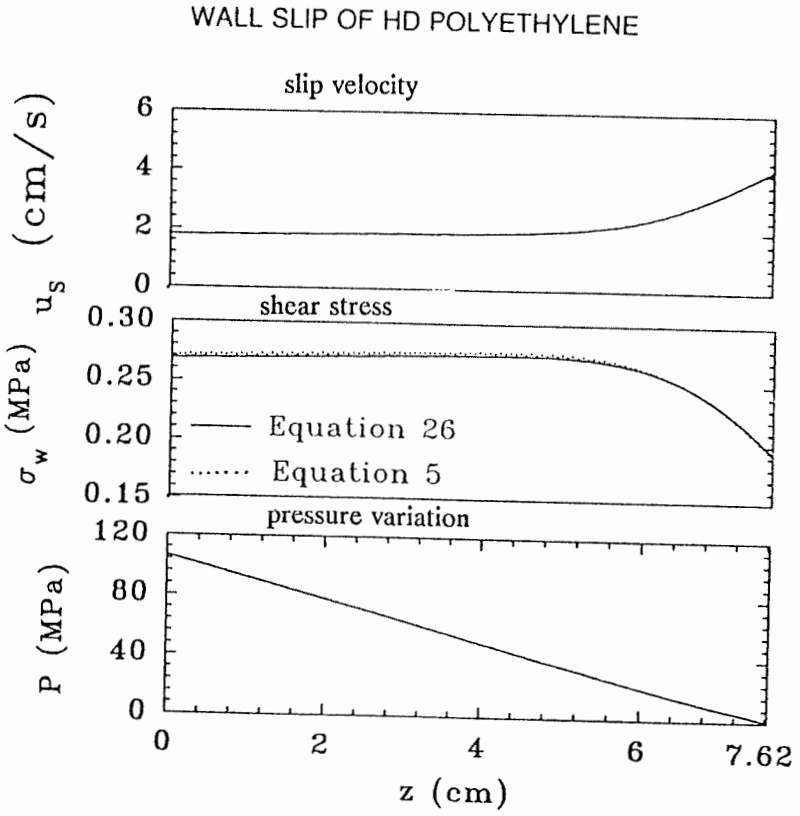

Figure 2.15. Prediction of slip velocity acceleration near the die exit (Hatzikiriakos and Dealy, 1992). Three curves (from the top to the bottom) represent slip velocity, shear stress, and normal pressure.

Since the pressure varies in the flow direction, the wall slip velocity will also depend on the position in the die. They proposed a model to predict how wall slip varies along the die. Figure 2.15 shows the predictions of the slip velocity, shear stress, and pressure variations along capillary dies of three diameters. The figure shows acceleration of slip velocity near the exit of the die. Hatziriakos and Dealy pointed out that the combination of this acceleration and high concentration of shear stress at the entrance caused extrudate

roughness. Their theory brought a new concept of how slip affects extrudate appearance.

2.5.2 Summary

Although there have been so many proposed mechanisms, the most acceptable causes of extrudate distortions now are (Utracki and Gendron, 1984) the followings.

(a) **"Entrance Effect":** the critical deformation that polymer melt experienced at the die entry causes extrudate distortion (Tordella, 1956, 1958);

(b) **"Exit Effect":** unstable polymer flow near the die exit causes the surface roughness (Vinogradov, 1972, Tremblay, 1991, Hatzikiriakos and Dealy, 1992);

(c) **"Slip Effect":** the polymer slippage at the die wall is responsible for the extrudate distortion (Benbow et al., 1961, Ramamurthy, 1986).

Regarding the relation of those mechanisms to the extrudate distortion, it is generally agreed that the surface roughness, usually called as sharkskin is caused by exit effect (Vinogradov et al., 1984, Becker et al. 1991, Tremblay, 1991); whereas spurting and gross fracture are caused by entry deformation and die slip (Vinogradov, 1972, Kalika and Denn, 1987, El Kissi and Piau, 1990).

CHAPTER 3

EXPERIMENTAL

3.1 EXPERIMENTAL METHODS

The extrudate roughness was studied through three sets of experiments.

(I) **Capillary die experiments based on ''screening design''**

Capillary die experiments were carried out according to a statistical approach, ''screening design''. This method allowed us to evaluate many parameters affecting extrudate roughness but to avoid too many extrusion runs. It was designed to understand what parameters are the most important ones to extrudate roughness. The details are presented in Chapter 4.

(II) **Two-hole die experiments**

A two channel capillary die (two-hole die) was used to observe wall slip and its related extrudate roughness. Two channels have same L/D values but different diameters. Different flow behaviors have been observed for two channels subjected to the same pressure head. Two-hole die experiments are to be presented in Chapter 5.

Table 3.1. The properties and molecular weights of polymers used.

No.		polymers (producers)	Density (g/ml)	Melt index (dg/min.)	Mn (g/mole)	Mw (g/mole)	Mz (g/mole)	Mw/Mn
1	HDPE	HDPE 4352N (Dow Canada)	0.95	4.0	17,300	83,300	252,400	4.82
2	HDPE	HDPE 12065 (Dow Canada)	0.96	0.9	20,800	118,800	2,415,000	5.71
3	HDPE	HDPE 16A (Du Pont Canada)	0.95	0.25	17,900	140,500	1,393,000	7.85
4	HDPE	HDPE 62020 (Dow Canada)	0.95	0.3	18,800	161,500	1,235,000	8.59
5	LLDPE	LLDPE 2517 (Dow Canada)	0.92	25.0	21,700	70,900	150,000	3.27
6	LLDPE	LLDPE 2535 (Dow Canada)	0.92	6.0	20,800	88,800	243,000	4.27
7	LLDPE	LLDPE 12J1 (Du Pont Canada)	0.92	1.0	17,000	99,300	327,000	5.84
8	LLDPE	LLDPE 2045 (Dow Canada)	0.92	1.0	16,700	108,400	484,000	6.49
9	LLDPE	LLDPE 13J4 (Du Pont Canada)	0.92	1.0	23,800	128,000	546,400	5.39

(III) Slit die experiments

A slit die was also used to observe instant die wall slip along the die land. The instant pressure variations were monitored by three pressure transducers along the die land. Slit die experiment will be discussed in Chapter 6.

3.2 POLYMERS

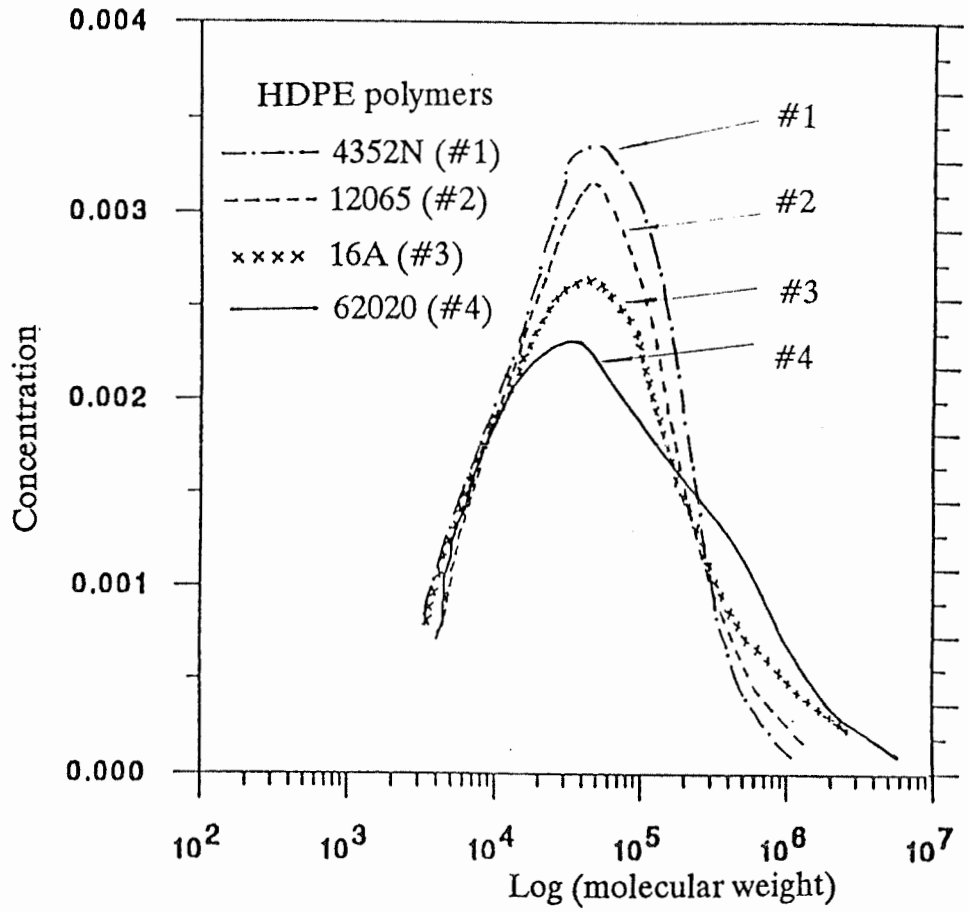

Figure 3.1. Molecular weight distributions of HDPEs, measured by GPC, using viscosity detector.

Four HDPE and five LLDPE polymers were used. They were commercial products from Dow Canada and Du Pont Canada. These polymers according to the suppliers, contain no additives other than antioxidants. The properties and various molecular weights of these polymers are listed in Table 3.1. Molecular weights (except LLDPE 13J4) were measured by Professor Rudin

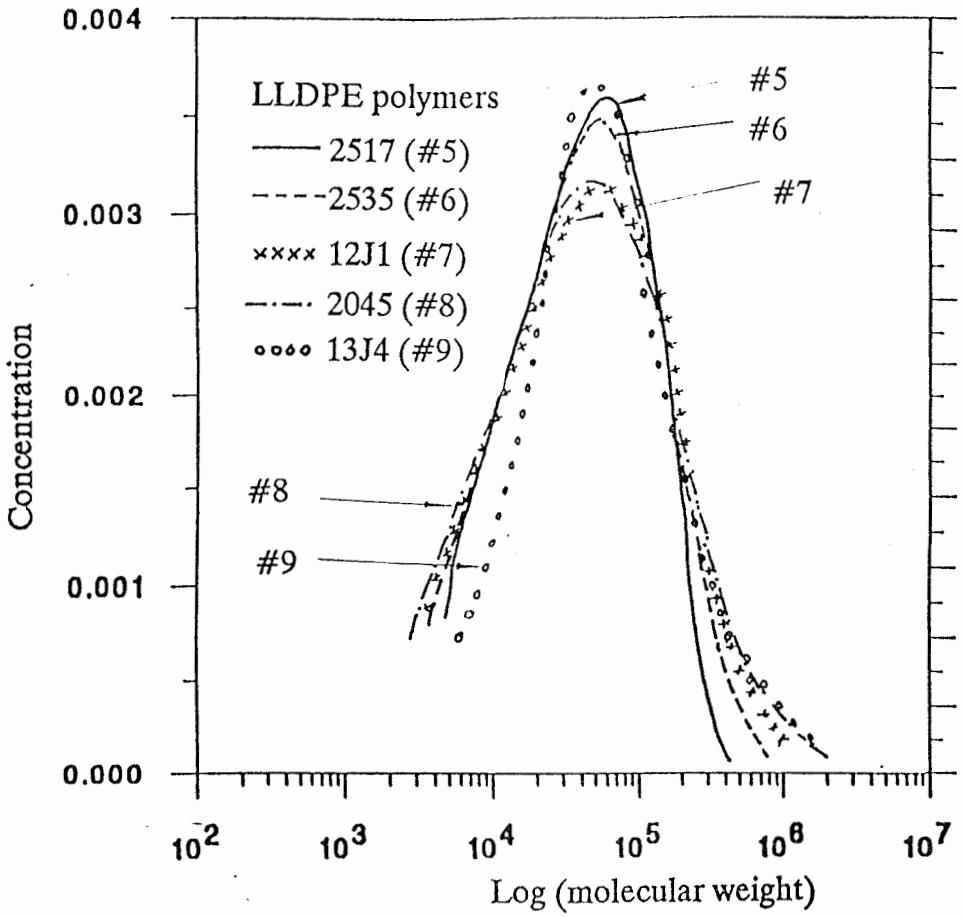

Figure 3.2. Molecular weight distributions of LLDPEs, measured by GPC, using viscosity detector.

of University of Waterloo, through GPC (Gel Permeation Chromatography) using viscosity detector. Molecular weights of LLDPE 13J4 was measured by R. E. Murray of Du Pont Research Center in Kingston, Canada. Since the production of LLDPE 13J4 has been stopped, no sample was available for molecular weight measurements at the University of Waterloo. Molecular weight distributions of various HDPE and LLDPE polymers from GPC are shown in Figure 3.1 and 3.2 respectively. These polymers were selected to have various molecular weights. In Table 3.1, they are listed in ascending order of weight averaged molecular weight, Mw, for both HDPE and LLDPE polymers. It should be pointed out that these polymers are not only different in various molecular weights but also in molecular weight distribution. We found it virtually impossible to find commercial polymers with the same molecular weight distribution and different molecular weights. However, as shown in Table 3.1, molecular weight distributions (denoted by Mw/Mn) increase with weight averaged molecular weights.

Four HDPE polymers show similar Mn values but different Mw and Mz values. Figure 3.1 shows that four curves almost coincide at the low molecular weight side (<10,000 g/mole), but separate towards higher molecular weight region. Increasing contents of high molecular weight molecules (>100,000 g/mole) from #1 to #4 polymers seems to cause the

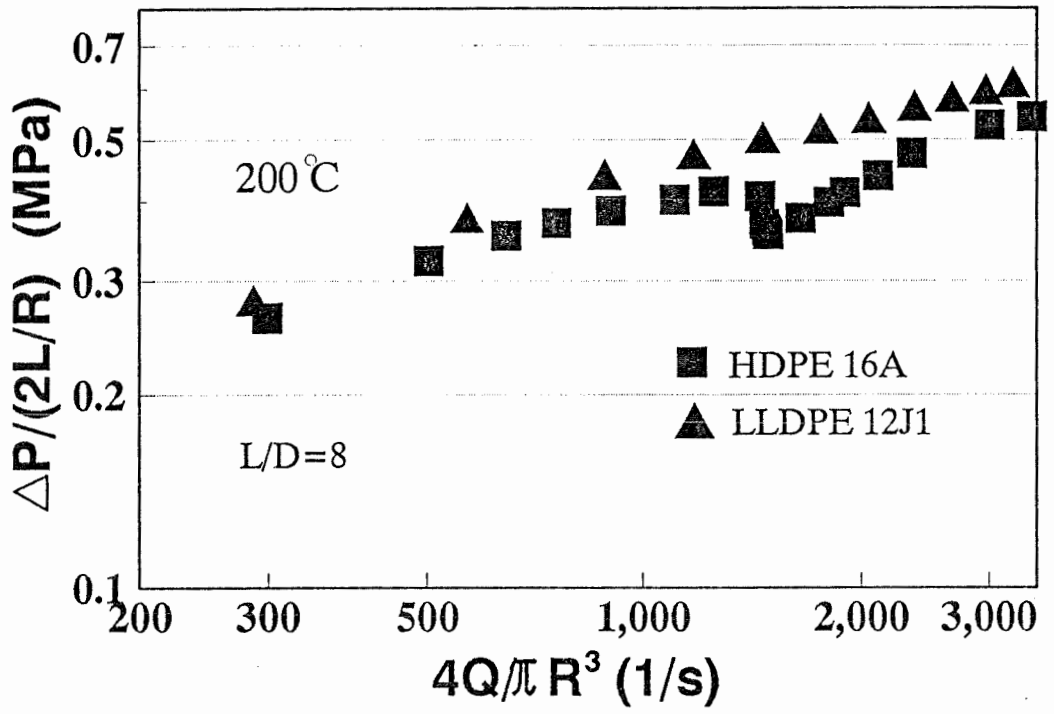

Figure 3.3. Flow curves of HDPE 16A and LLDPE 12J1 at 200 °C using an extruder.

wider and wider molecular weight distributions in the same order. For LLDPE polymers, Mw and Mz values show constant increase from #5 to #9 polymers, while Mn values don't show the similar trend (Table 3.1). That implies increasing contents of the high molecular weight molecules from #5 to #9 polymers. Similarly, Figure 3.2 shows such trend by longer and longer "tails" towards the higher molecular weight region.

The high molecular weight molecules in both HDPE and LLDPE polymers could influence the extrudate roughness. This will be elaborated in Chapter 4 using a statistical method.

These polymers are of different rheological properties. As the examples, the flow curves for HDPE 16A and LLDPE 12J1 are presented in Figure 3.3. Those are obtained through the extrusions from a capillary die (diameter=1.59 mm and L/D=8) at 200 °C. The extrusions were conducted using an extruder (to be presented later). The figure shows different rheological behaviors between the two polymers. HDPE shows obvious discontinuity while LLDPE doesn't. We will find different patterns of extrudate distortions between the HDPEs and the LLDPEs through the discussions in the following chapters.

The Bagley corrections of HDPE 16A and LLDPE 12J1 are shown in Figure 3.4. The corrected values are pressured as "e" in

$$\sigma = \frac{P_{res}}{4\left(\frac{L}{D} + e\right)} \quad \textbf{(3.1)}$$

Where σ is shear stress at wall, P_{res} is the reservoir pressure, and L/D is the length/diameter ratio of the die. The data are shown in three temperatures. Three dies with various L/D values (4, 10 and 24) were used. For LLDPE 12J1, the e

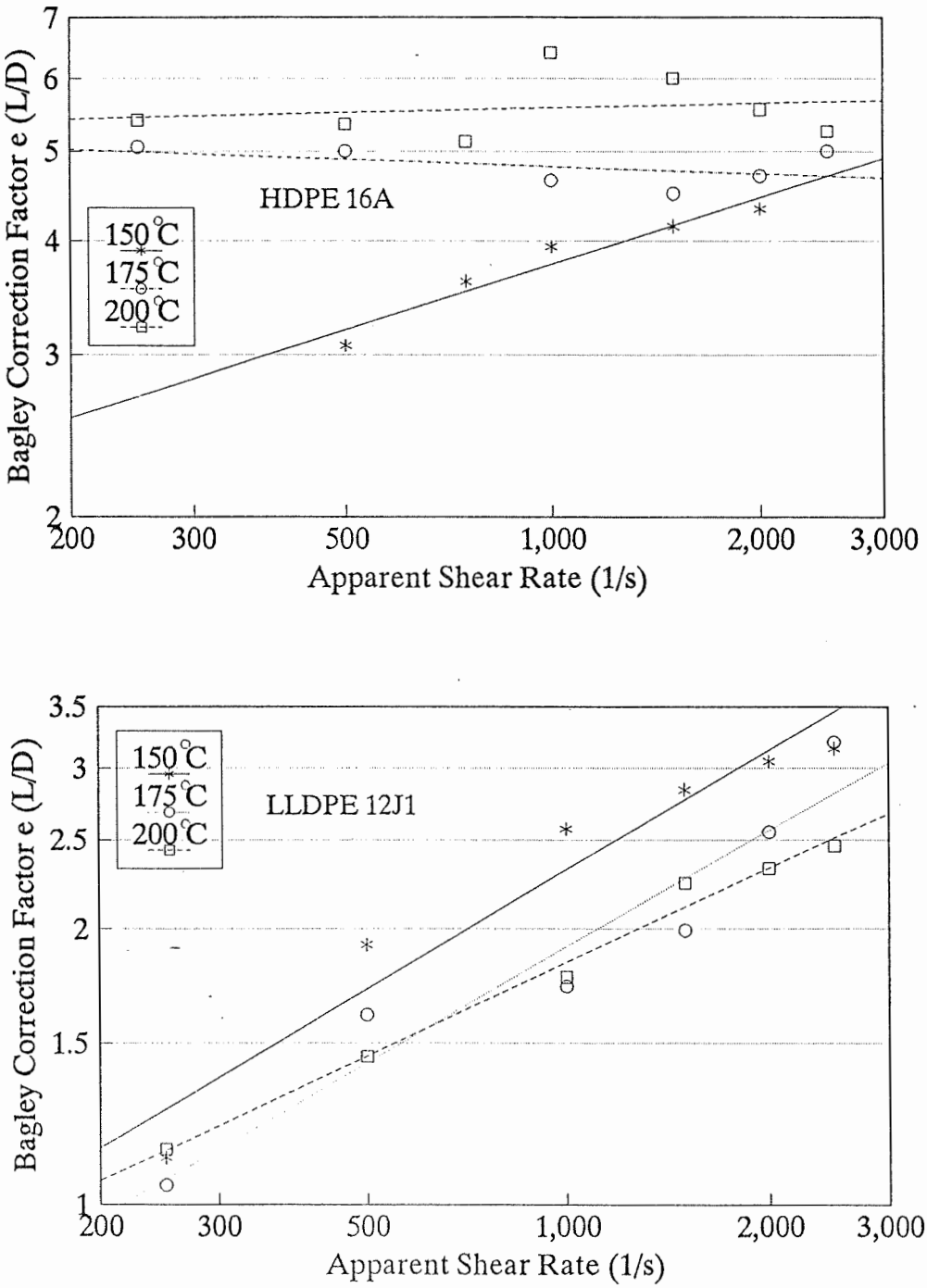

Figure 3.4. Bagley corrections for HDPE 16A and LLDPE 12J1.

value increases with apparent shear rate gradually; while for HDPE 16A, the e value increases monotonously with apparent shear rate at 160 °C but not at 175 and 200 °C.

It was hard to obtain straight line when plotting the pressure values against L/D values within instable region. Consider the discontinuity of flow curve in Figure 3.3 for HDPE 16A, the poor linearity might be caused by slip-velocity differences among the dies under the same shear stress. Therefore, using a series of capillary dies, it is hard to obtain accurate Bagley corrections in the instable flow region, especially for the polymers like HDPE 16A. The entrance and exit effects for pressure will be better examined by slit die which will be presented in Chapter 6.

3.3 EXTRUDER

All the extrusions were conducted through a single screw extruder (manufactured by ''Killion Extruder Inc.'', U.S.A.). The diameter of the extruder barrel was 45 mm; and length to diameter (L/D) ratio of the barrel was 24.

A computer aided PID (Proportional Integral Derivative) control system was used to set temperatures along the extruder barrel, the adapter and the die. The temperatures can be

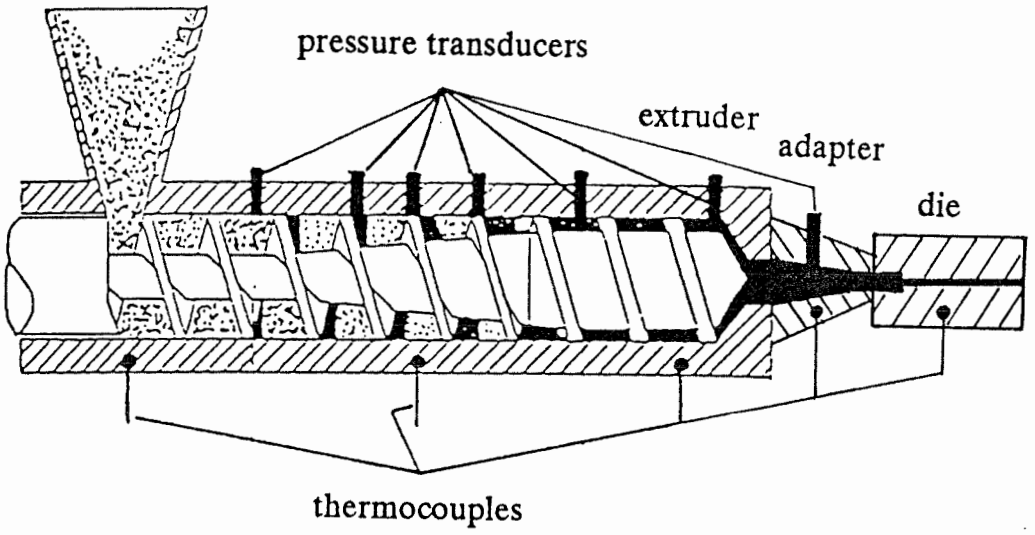

Figure 3.5. The arrangements of thermocouples and pressure transducers along extrusion line.

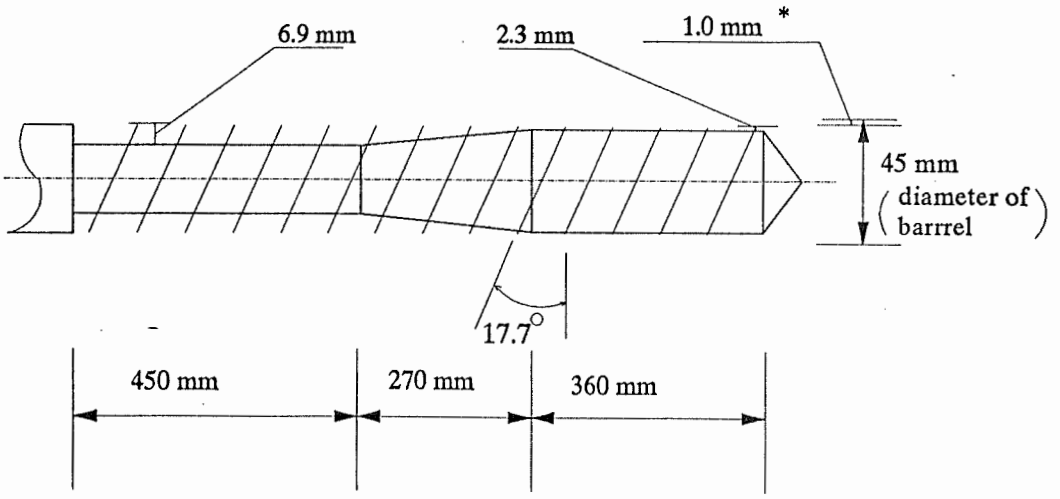

*: gap between the barrel and tip of the flight

Figure 3.6. Sketch of the extruder screw.

maintained at the given values within ±1 °C. Five pressure transducers were installed along the extruder barrel; and one in the reservoir (prior to the entrance of die). The temperature and pressure variations can be recorded and saved by a personal computer. The arrangements of thermocouples and

Table 3.2. The characteristics of various dies.

	material	entrance angle	L/D value	diameter (mm)
#1	steel	180 degree	8	1.59
#2	steel	180 degree	8	0.79
#3	steel	180 degree	24	1.59
#4	steel	180 degree	24	0.79
#5	steel	60 degree	8	1.59
#6	steel	60 degree	8	0.79
#7	steel	60 degree	24	1.59
#8	steel	60 degree	24	0.79
#9	brass	180 degree	8	1.59
#10	brass	180 degree	8	0.79
#11	brass	180 degree	24	1.59
#12	brass	180 degree	24	0.79
#13	brass	60 degree	8	1.59
#14	brass	60 degree	8	0.79
#15	brass	60 degree	24	1.59
#16	brass	60 degree	24	0.79

pressure transducers are shown in Figure 3.5. It should be pointed out that, when the slit die was used (the details of it will be discussed later), three more pressure transducers were installed along the die land, which is not shown in Figure 3.5.

The screw of the extruder features three zones, typical

type for extrusion of crystalline polymers such as polyethylene. The details of the screw are given in Figure 3.6.

3.4 EXTRUSION DIES AND ADAPTERS

Sixteen different single channel capillary dies were used; and their characteristics are listed in Table 3.2. These dies feature various material, diameter, entrance shape, and L/D values. They were used in screening design experiments.

A special two-hole die was also used besides normal single channel capillary dies. It comprises two channels with different diameters but same L/D value. The details are shown in Figure 3.7. As shown in the figure, the two channels were subjected to the same pressure head. The die could be heated by electrical heating bands and the temperature of the die was controlled. The temperatures at the exits of two channels was checked by a thermocouple probe (manufactured by Omega Engineering Inc.). The temperature differences between the two were found to be less than 2.5 °C. Two hole die was designed to observe wall slip and related extrudate roughness by comparing two flow streams from two channels.

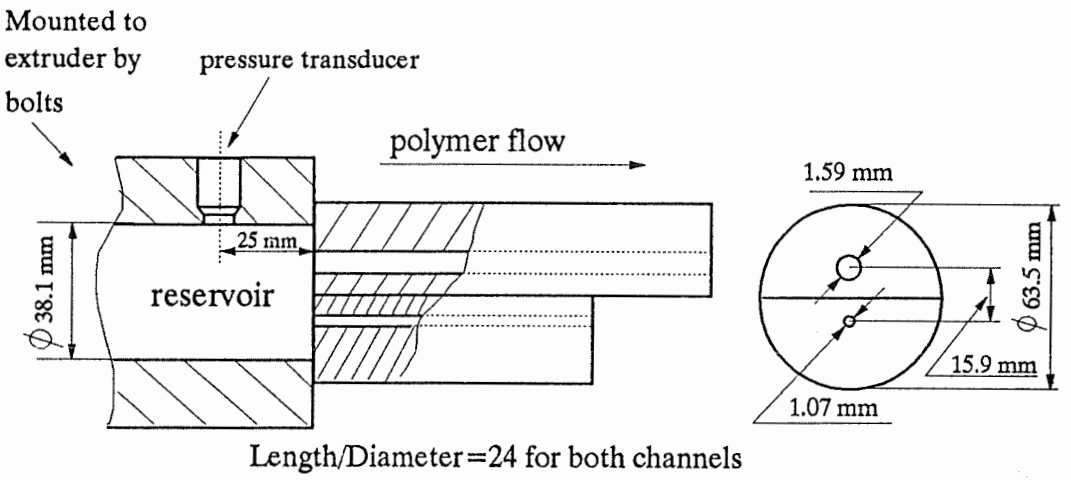

Figure 3.7. Sketch of two-hole die.

A slit die was used to study wall slip inside the die land. The dimensions of the die and arrangement of the pressure transducers are shown in Figure 3.8. The die was made of stainless steel. The surface roughness of the die was less than 0.86 micron. Three pressure transducers were flush mounted at the die surface along the slit die, and another one was installed in the reservoir. The pressure transducers were connected to a data acquisition system which was able to collect pressure measurements from each transducer at a rate of 1000 per second.

Two different adapters (flat and tapered) were used

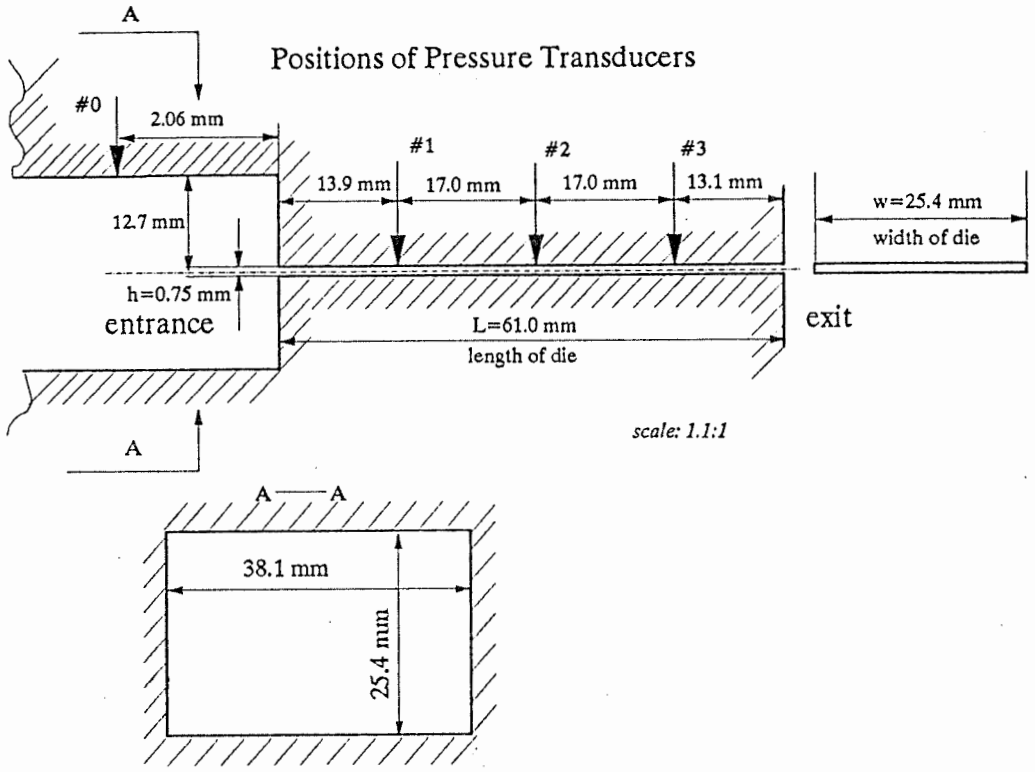

Figure 3.8. Structure of slit die.

(Figure 3.9) for capillary dies listed in Table 3.2. The tapered adapter was designed to diminish the stagnant zone. Both adapters were used for "two level design" in screening design experiments (Chapter 3) when only the flat entrance dies were used. Only flat adapter was used for "three level design" in screening design (Chapter 3).

The pressure transducers used are the PT series products from Dynisco. The response time of the transducer reported at

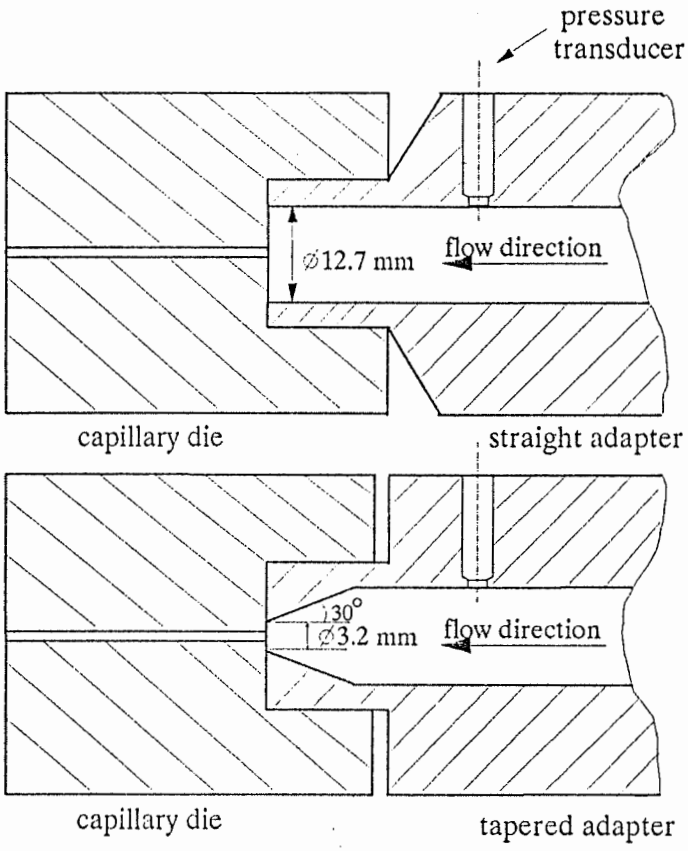

Figure 3.9. Flat and tapered adapters.

0.013 second (information from Dynisco). In our laboratory test, the transducer has detected pressure variations (during extrusion) in 0.05 second. Each pressure transducer was calibrated by a pressure meter over the pressure range of 0 to 8000 psi (about 55 MPa). The calibrations of four pressure transducers are reported in Figure 3.10. The correlation coefficient of each linear regression was higher than 0.999.

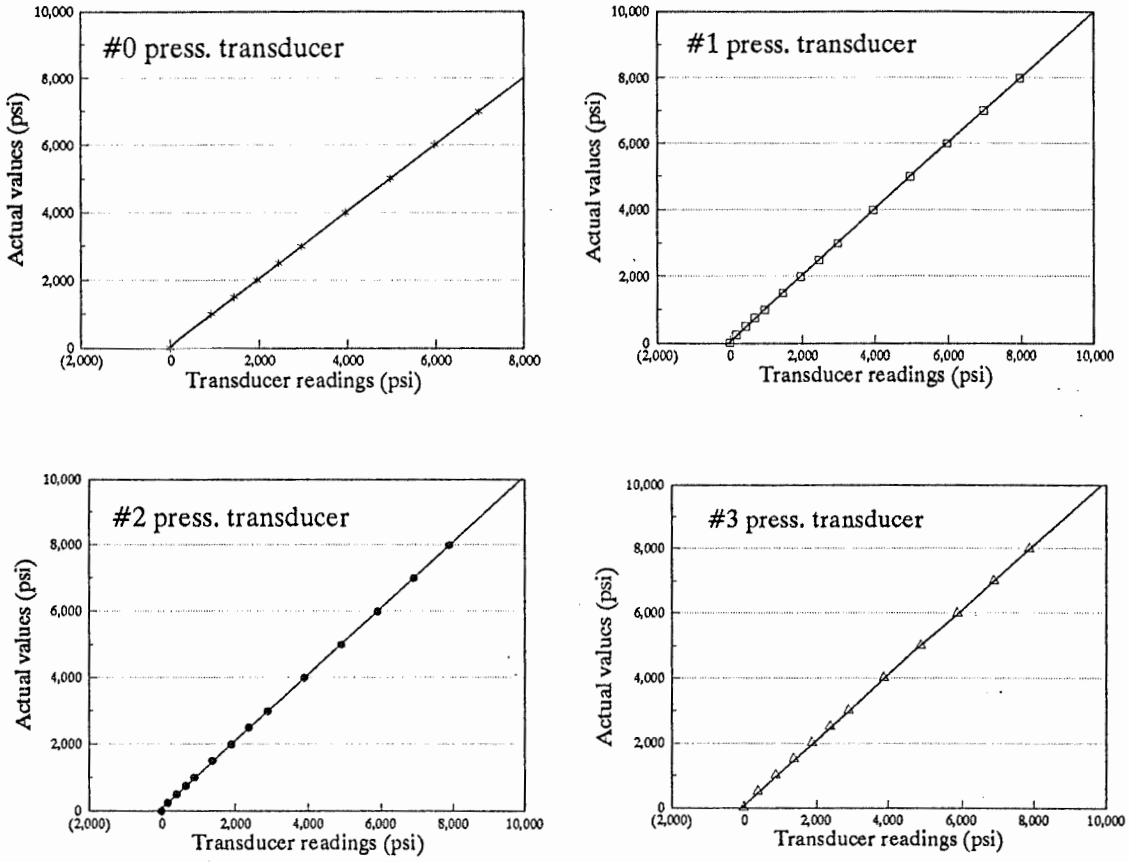

Figure 3.10. Calibrations of pressure transducers. The numbers correspond to the positions shown in Figure 3.8.

CHAPTER 4

SCREENING DESIGN STUDIES

4.1 INTRODUCTION

There are mainly three types of factors affecting extrudate roughness: 1) polymer properties, 2) processing conditions and 3) die geometries. The number of these factors may exceed 10, 20 even more. Because of so many factors involved, the study of such multi-factor system needs a lot of experimental work. For instance, if one wants to study 10 parameters, the fully crossed experiments would require **1024** extrusion runs with all parameters varing between 2 levels. These experiments are obviously lengthy and costly to conduct. It is now possible using an analysis called screening design to study many parameters with a limited number of extrusions and be able to separate main effects from two-factor interaction effects.

Such screening design is based on what is known as the Plackett-Burman design, Hadamard matrix or fractional factorial design (Wheeler, 1989). This design makes it possible to distinguish rapidly between active and inert parameters. It also provides information regarding specific two-parameter interactions, if any. The main advantages of these designs are: i) for a given number of parameters, the

number of runs needed is minimum; ii) this number is a function of the design resolution that one wants to obtain; iii) each main effect is estimated independently of all other main effects with the same precision; iv) the main effects can be estimated and isolated from the two-parameter interactions by combining a set of runs (basic runs) and a set of complementary runs (reflected runs). Screening designs are therefore the perfect tool now to quantify the effects of many parameters on a response variable.

In this work, a 32 run design was used: 16 extrusions of basic runs and 16 extrusions of reflected runs. It is necessary to give a few definitions to facilitate further discussion.

(1) **Screening Design:** a special arrangement of 32 extrusions capable to evaluate main effects and group of two interaction effects. The 32 extrusions comprise 16 of basic runs and 16 of reflected runs.

(2) **Basic Runs:** one half of a **Screening Design** composed of 16 extrusions, the conditions (processing, geometry, polymer type) of each extrusion are arranged based on screening design method.

(3) **Reflected Runs:** another half of a **Screening Design** with the other group of 16 extrusions to obtain the true main effects by combining the results with those of the **Basic Runs**.

(4) **Main Effects:** The pure effect of an individual parameter causing an increase or decrease of the response variable (the variable here is the extrudate roughness) when the parameter is varied from low level to the high level (such as shear stress changed from 0.2 MPa to 0.3 MPa).

(5) **Two Parameter Interaction Effects:** The extra effect in addition to the algebraic sum of main effects. For example, for a simple two parameter (X and y) system, the over all effect could be written as: over all effect (extrudate roughness) = main effect of X + main effect of Y + two parameter interaction effects of X and Y. If there is no interaction effects, the third term is zero. However, usually it is not.

4.2 PROCEDURE OF SCREENING DESIGN STUDIES

The whole procedure of the screening design comprises three steps: 1) extrusion of the polymer through various capillary dies to obtain extrudate with various appearances (smooth or rough); 2) evaluation of extrudate roughness; 3) analyze roughness data to evaluate the effect of the various parameters.

4.2.1 Evaluation of Extrudate Roughness

To facilitate the statistical analysis, the appearance

(smooth or rough) of the extrudates must be translated into numerical values. Surface defects can be characterized by a dimensionless volume-averaged roughness. However, as the roughness was determined using a video camera with an image analyzer of limited capacity, we chose the following definition for a dimensionless roughness, F_R:

$$F_R = \frac{\int_0^L |(R_{upper} - R_a)|\, dl + \int_0^L |(R_{lower} - R_a)|\, dl}{2\, R_a\, L} \qquad (4.1)$$

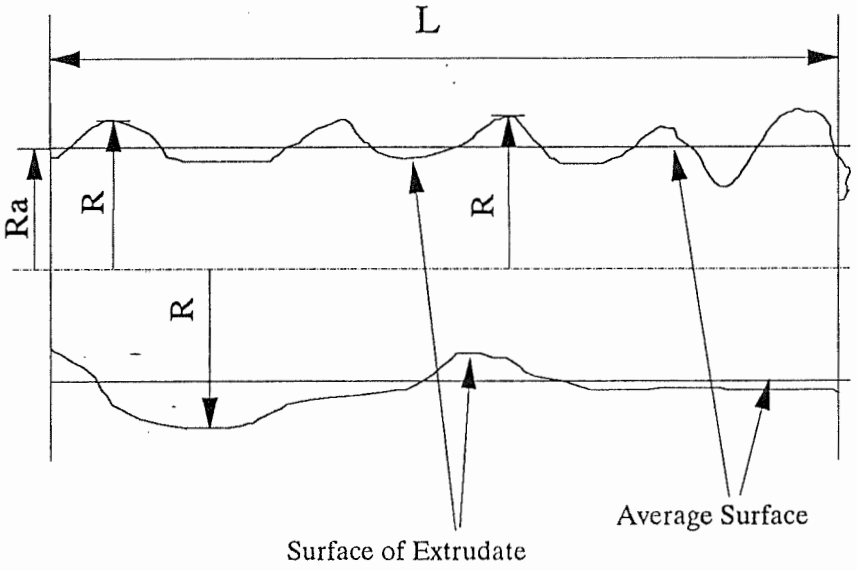

Figure 4.1. Sketch of rough extrudate.

As illustrated by Figure 4.1 for an arbitrary deformed extrudate, F_R is obtained by integrating over both the upper and lower contour lengths of an extrudate image. R_{upper} and R_{lower} are the free surface radii of the upper and lower parts of the picture. R_a is the average radius. F_R is hence the ratio of the total rough area over the total projected area of the extrudate. This is obviously an approximation for the surface roughness of cylindrical extrudates, but it is valid on a relative basis.

The device to measure roughness consists of a camera, a PC computer, and a special video monitor. First, an extrudate sample is photographed by the camera and a magnified image is displayed on the video monitor. The extrudate is enlarged up to 50 times and then the enlarged image is analyzed using a software provided by Coreco Inc. For the sake of convenience, areas were calculated in pixel. Since the parameter F_R is dimensionless, the unit used in the calculation does not affect the value of F_R. The resolution of the monitor is 0.01 mm per pixel. In other words, the unit for area calculation is 0.0001 mm^2. To determine the precision of this measurement technique, we measured the same object five times and found the average deviation of 0.039%.

Figure 4.2 shows photographs of three typical extrudates

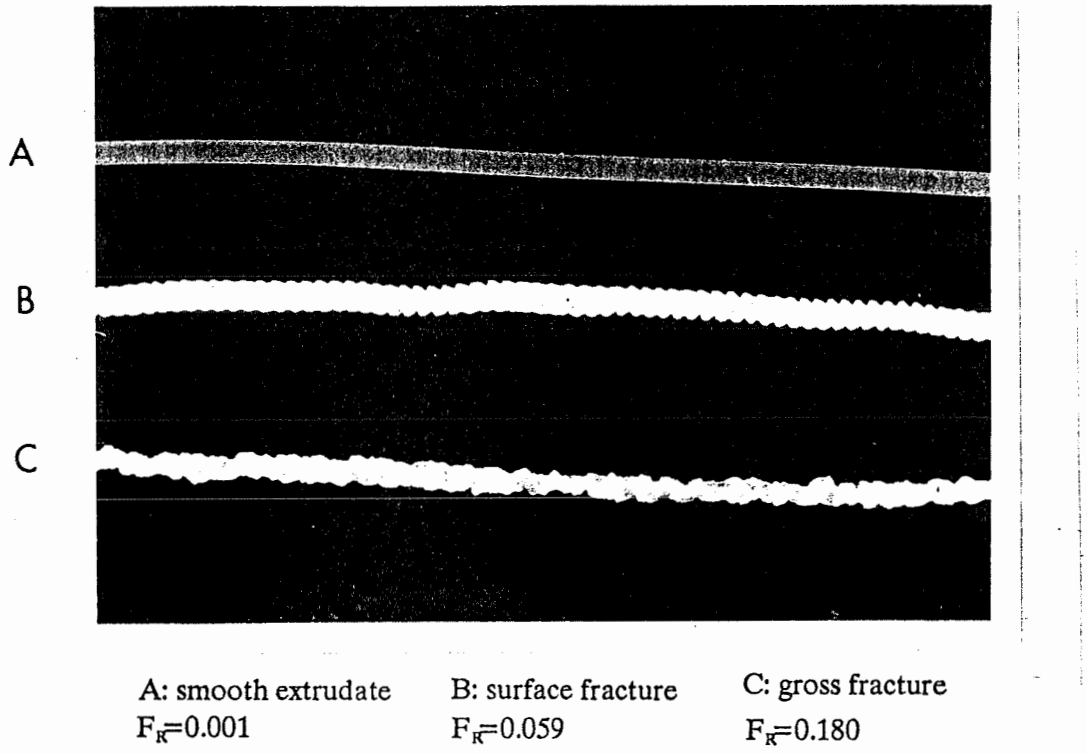

Figure 4.2. Typical extrudate appearances and roughness in terms of F_R. ''A'' is a smooth extrudate; ''B'' is a surface fracture extrudate; ''C'' is a gross fracture extrudate.

and their F_R values. A is a smooth extrudate with F_R equal to 0.001, barely measurable; B is the photograph of an extrudate with a surface fracture(sharkskin) with a value of F_R equal to 0.059; in the case of a gross fracture shown in C, the value of F_R becomes quite large (here 0.18). In this work, surface fracture and gross fracture will not be treated separately. However, for many measurements, the F_R value was found to be greater than 0.01 but less than 0.1 corresponding to surface fracture, while a few values of the F_R greater than 0.1 were

obtained corresponding to gross fracture.

4.2.2 Statistical Analyses

The F_R values obtained were analyzed using a statistical software called SAS. The software has been run through MUSIC operating system on the mainframe of Ecole Polytechnique.

4.3 TWO LEVEL SCREENING DESIGN

4.3.1 Descriptions

Table 4.1. Parameters for Two Level Screening Design.

Label	Parameters	Level -	Level +
A	Type of polymer	LLDPE 13J4	HDPE 16A
B	Additive	No	Added
C	Recycling	0	2
D	Type of adapter	Tapered	Straight
E	Material of die	Steel	Brass
G	Diameter of die	1.59 mm	0.79 mm
H	L/D value of die	8	24
K	Melt temperature	170°C	210°C
M	Die temperature	160°C	220°C
N	App. shear stress	0.2 MPa	0.3 MPa

The influence of 10 parameters on extrudate surface was studied using cylindrical dies. A low and a high value (level "-" and level "+") were assigned to each parameter (Table 4.1). The parameter values for each run were determined by using the screening design. The letters refer to the parameters throughout this Two Level Design, except *F*, *I*, *J*, *L*, and *O* which were used for interactions between parameters. The list of parameters covers most of the parameters believed to affect surface roughness of polymer extrudates. A linear low-density polyethylene (LLDPE 13J4, Du Pont Canada) and a high-density polyethylene (HDPE 16A, Du Pont Canada) were chosen respectively as the low and high level for the parameter describing the type of polymer. Specifications of these two polymers are given in Table 3.1. The additive was a fluoroelastomer, Viton (FREEFLOW 12 of Du Pont), a product used as a polyolefin processing aid. The Viton was pre-blended to the polyethylene granules at a ratio of 1:100 using a counter-rotating twin screw extruder. Recycling at level "+" refers to resin which has been processed through the extruder twice. We used two entrance adapters as illustrated in Figure 3.9. One gives a flat (180°) entrance and the other a 60° tapered entrance to eliminate corner vortices. Two die materials were used: stainless steel and brass. Brass was reported to be a good material for film blowing dies

(Ramamurthy, 1986). Eight cylindrical dies of diameter equal to 1.59 mm (1/16") and 0.79 mm (1/32") with L/D values of 8 (low) and 24 (high) were used (#1, #2, #3, #4, #9, #10, #11, and #12 dies in Table 3.2). The smaller diameter die is taken as the "+" level. We also considered the effects of die temperature and melt temperature. The melt temperature was either 170°C or 210°C, while the die temperature (controller set point) was set at 160°C or 220°C. Finally, the apparent shear stress was taken as 0.2 or 0.3 MPa, which is within the normally accepted critical shear stress range of 0.1 MPa to 1 MPa. This value was obtained by controlling the RPM of extruder which determines the pressure at the die entrance reservoir. With measured pressure values, we can calculate the apparent shear stress by

$$\sigma_w = \frac{P_{res}}{4L/D} \quad \textbf{(4.2)}$$

where σ_w is the apparent shear stress at the die wall, P_{res} is the pressure measured in the entrance reservoir, L and D are respectively the die length and diameter. To distinguish between interaction effects and effects of individual parameters, we conducted two groups of experiments: the basic runs and the complementary or reflected runs. In our study, each group consisted of 16 extrusions. Tables 4.2 and 4.3 give the experiment arrangements for each group. A "+" sign means

Table 4.2. The Arrangement of Basic Runs for Two Level Design.

	A	B	C	D	E	G	H	K	M	N
1	-	-	-	-	-	-	-	-	-	-
2	-	-	-	-	-	-	+	+	+	+
3	-	-	-	+	+	+	+	+	-	-
4	-	-	-	+	+	+	-	-	+	+
5	-	+	+	+	+	-	-	+	+	-
6	-	+	+	+	+	-	-	-	-	+
7	-	+	+	-	-	+	+	-	+	-
8	-	+	+	-	-	+	-	+	-	+
9	+	+	-	-	+	-	-	-	+	+
10	+	+	-	-	+	-	+	+	-	-
11	+	+	-	+	-	+	+	+	+	+
12	+	+	-	+	-	+	-	-	-	-
13	+	-	+	+	-	-	-	+	-	+
14	+	-	+	+	-	-	+	-	+	-
15	+	-	+	-	+	+	+	-	-	+
16	+	-	+	-	+	+	-	+	+	-

that the particular parameter is set at the high level as indicated in Table 4.1; a "-" sign stands for the low level. For each extrusion, the 10 parameters were set at the levels indicated in the two tables. The levels of some parameters were changed from one experiment to another. As Table 4.2 shows, parameter *A* was the least frequently changed and parameter *N* the most frequently changed. The reflected runs followed the same design as the basic runs, but all the levels were inverted. For example, the first extrusion in the basic runs required all the parameters to be at low level, and those of the first reflected runs were all at high level. Two-

Table 4.3. Arrangement of Reflected Runs for Two Level Design.

	A	B	C	D	E	G	H	K	M	N
1	+	+	+	+	+	+	+	+	+	+
2	+	+	+	+	+	+	-	-	-	-
3	+	+	+	-	-	-	-	-	+	+
4	+	+	+	-	-	-	+	+	-	-
5	+	-	-	-	-	+	+	-	-	+
6	+	-	-	-	-	+	+	+	+	-
7	+	-	-	+	+	-	-	+	-	+
8	+	-	-	+	+	-	+	-	+	-
9	-	-	+	+	-	+	+	+	-	-
10	-	-	+	+	-	+	-	-	+	+
11	-	-	+	-	+	-	-	-	-	-
12	-	-	+	-	+	-	+	+	+	+
13	-	+	-	-	+	+	+	-	+	-
14	-	+	-	-	+	+	-	+	-	+
15	-	+	-	+	-	-	-	+	+	-
16	-	+	-	+	-	-	+	-	-	+

parameter effects could thus be isolated by combining the results of the basic and reflected runs.

It should be mentioned that the main effects (those of individual parameters) and the interaction effects cannot be determined independently using the results of only the basic or reflected runs. Table 4.4 shows the confounding patterns (Wheeler, 1989) for both the basic and reflected runs. The letters at the top of the table correspond to the parameters listed in Table 4.1; in addition, the letters not in Table 4.1 (*F*, *I*, *J*, *L*, and *O*) represent interaction effects. The two-

Table 4.4. Confounding Patterns of Basic and Reflected Runs for Two Level Design.

Labels in Design	A	B	C	D	E	F	G	H	I	J	K	L	M	N	O
Basic Runs															
Two-factor Interactions	· BC	· AC	· AB	· AE	· AD	· AG	· BE	· CK	· AH	· AK	· CH	· AM	· CN	· CM	· AN
	· DE	· EG	· DG	· CG	· BG	· BD	· CD	· EM	· BK	· BH	· EN	· BN	· EH	· EK	· BM
			· HK		· HM	· CE			· DM	· DN		· DH			· DK
			· MN		· KN	· HN			· GN	· GM		· GK			· CH
						· KM									
Reflected Runs															
Two-factor Interactions	BC	AC	AB	AE	AD	AG	BE	CK	AH	AK	CH	AM	CN	CM	AN
	DE	EG	DG	CG	BG	BD	CD	EM	BK	BH	EN	BN	EH	EK	BM
			HK		HM	CE			DM	DN		DH			DK
			MN		KN	HN			GN	GM		GK			CH
						KM									

letter groups of the basic and reflected runs sections are the two-parameter interaction effects that are confounded with the corresponding main effects (indicated by the letters at the top) of the same column. Take parameter *A* as an example: in the basic runs, its effect is confounded with the negative effects of interactions *BC* and *DE*. In the reflected runs, however, it is confounded with the positive effects of interactions *BC* and *DE*. Since *BC* and *DE* make exactly opposite contributions to the basic and reflected runs, the pure main effect of *A* is easily obtained by adding the effects from the basic and reflected runs together, i.e.

$$A = \frac{[A+(-BC-DE)] + [A+(BC+DE)]}{2} \quad (4.3)$$

The *BC* and *DE* interactions can also be obtained using

$$BC + DE = \frac{-[A+(-BC-DE)] + [A+(BC+DE)]}{2} \quad (4.4)$$

This is how confounding effects are screened out.

In order to test the reproducibility of the extrudate roughness, we selected six different extrusion conditions for repeated experiments. These were runs number 1, 5, 7, 8, 14 and 16 in the reflected run arrangement (as indicated in Table 4.3). To ensure true repetitions, each extrusion experiment was conducted at least four hours after the previous one. The results of these repeated experiments are shown in Figure 4.3, in terms of roughness factor F_R. Except for run #16, the deviations between the F_R (response) values for the three repeated experiments are small, demonstrating that roughness can be reliably reproduced under specified conditions.

4.3.2 Results and Discussions

All the F_R values measured for the total of 32 extrusion runs are listed in Table 4.5. They were statistically analyzed to determine the effects of each individual parameter and of interactions; the results are shown in Table 4.6. Four rows of

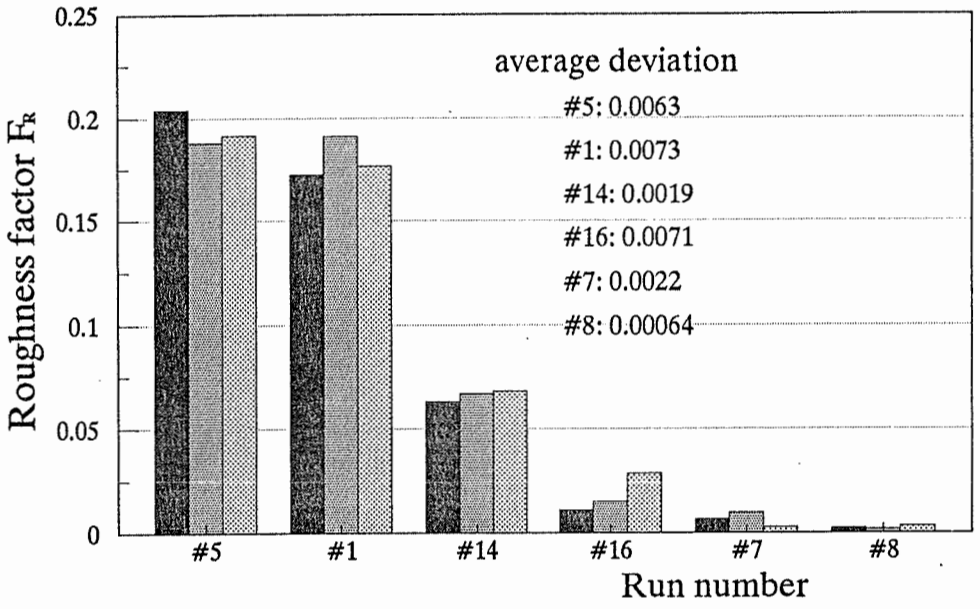

Figure 4.3. Repeatability of extrudate roughness. The average deviation from the mean value from three repeated tests is shown for six different runs.

data represent the effects calculated from the basic runs, reflected runs, main effects (using Equation 4.3) and interactions (using Equation 4.4).

With the screening design it is possible to distinguish between individual effect of each parameter by examining how the F_R value is affected when parameters are shifted from the low(-) to the high(+) level. Figure 4.4 depicts the effect of each of the 10 parameters on F_R. These values were obtained by combining the statistical results of the basic and reflected runs reported in Table 4.6. In decreasing order of importance of the parameters are: apparent shear stress, die diameter,

Table 4.5. Measurement and Predictions of Extrudate Roughness from Two Level Design. The "prediected" values were obtained by Equ. 4.6.

	Basic Runs (F_R)		Reflected Runs (F_R)	
	Measured	Predicted	Measured	Predicted
1	0.0012	0.0049	0.1901	0.1867
2	0.0050	0.0082	0.0016	0.0024
3	0.0014	0.0049	0.0022	0.0042
4	0.0009	0.0191	0.0007	0.0028
5	0.0098	0.0049	0.1871	0.1867
6	0.0117	0.0082	0.0008	0.0024
7	0.0075	0.0049	0.0056	0.0042
8	0.1990	0.0191	0.0023	0.0028
9	0.0079	0.0042	0.0009	0.0049
10	0.0072	0.0028	0.0013	0.0191
11	0.1838	0.1867	0.0008	0.0049
12	0.0067	0.0024	0.0009	0.0082
13	0.0013	0.0042	0.0105	0.0049
14	0.0008	0.0028	0.0542	0.0191
15	0.1861	0.1867	0.0080	0.0049
16	0.0012	0.0024	0.0153	0.0082

die L/D, polymer type, the use of Viton, recycling, die temperature, type of entrance adapter, die material, and melt temperature. The last six parameters show very small (not significant) contributions to the roughness factor.

As expected the apparent shear stress at the die wall is the most significant parameter with a contribution to the F_R value of 0.05. This confirms most observations reported in the literature, i.e. that above a critical shear stress, severity of roughness increases with shear stress.

Table 4.6. Analyzed Effects of Different Parameters in Terms of F_R.

Labels in Design	A	B	C	D	E	F	G	H	I	J	K	L	M	N	O
	F_R x 100														
Basic Runs	4.21	0.71	0.31	-0.24	-0.01	-4.48	4.54	4.44	-4.60	0.28	0.09	-0.03	-0.23	4.75	-4.32
Reflected Runs	3.73	1.04	-1.07	-0.40	0.62	4.09	5.13	4.17	5.08	-0.40	0.50	0.64	-0.63	5.39	4.10
Combinations	3.97	0.88	-0.38	-0.32	0.31		4.84	4.30			0.29	0.30	-0.43	5.07	
Interaction Effect	-0.24	0.17	-0.69	-0.08	0.32	4.29	0.30	-0.14	4.84	-0.34	0.21	0.34	-0.20	0.32	4.21

The second most significant parameter is the die diameter with a contribution to roughness similar to shear stress. Hence, using a smaller diameter results in more severe roughness. This is predicted by the analysis of Leonov (1986) who proposed a critical diameter above which the slip-stick phenomenon will not occur. In other words, under certain conditions, a smaller die is likely to cause stick and slip and consequently cyclic melt fracture and rough extrudate. Large effects of the cylindrical diameter or gap dimension for other flow geometries on the viscosity - shear rate curves are usually interpreted in terms of slip at the die wall. For example, Mourniac (1991) has shown that slippage for highly loaded rubber melts increases with decreasing gap or capillary

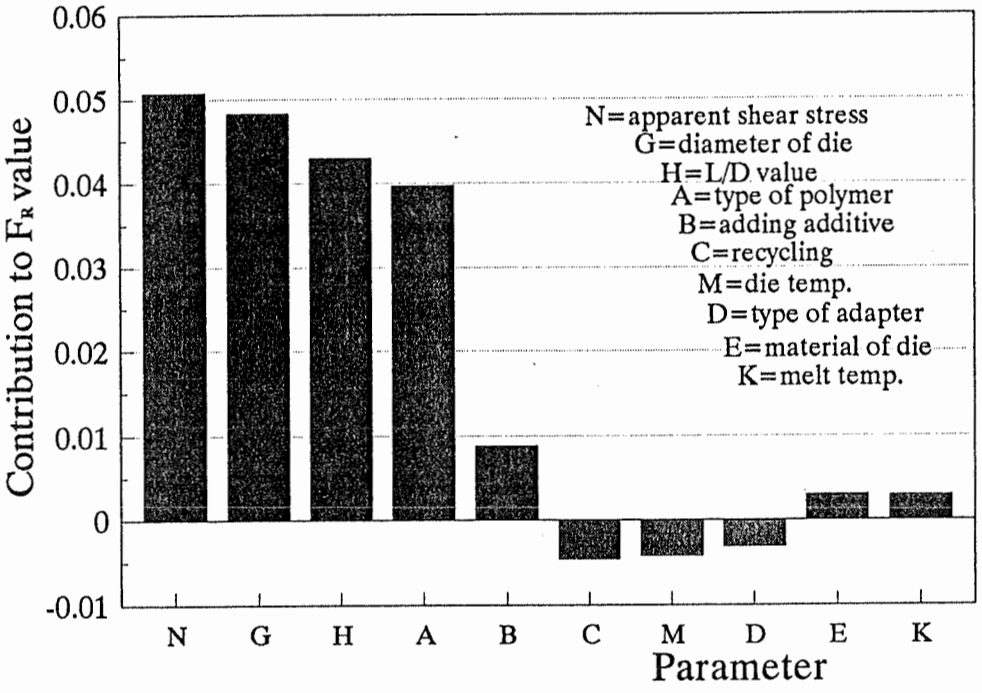

Figure 4.4. Main effects of ten parameters from Two Level Design.

diameter. However, as far as we are aware, there has been no report in the literature of die diameter effects on surface defects. Besides the arguments given by the two previous authors, generally, the dimensions of die has little effect on critical shear stress (Boudreaux and Cuculo, 1978).

Next in importance is the effect of the die L/D. The use of a larger L/D value (24 compared to 8) results in a roughness increase (F_R value) of 0.042. This large effect is puzzling as one would normally expect the contrary. Entrance and exit (extrudate swell) effects decrease with increasing

L/D. If roughness results from unstable flow at the die entrance, a longer die will allow the polymer melt to relax and produce a smoother extrudate than a shorter die. Boudreaux and Cuculo (1978) have cited many authors who reported larger flow curve discontinuities when using larger L/D values (Bagley et al.,1958, and Tordella, 1963). Some authors refer to this as die land fracture, but the physical reason for the larger discontinuities at larger L/D remains unclear.

One plausible explanation comes from the work of Cogswell (1993) who suggested that stress induced polymer crystallization on the die wall at the entrance causes a flow restriction which vanishes at high enough pressure. Since polymer melt of longer die subjects to higher pressure, such crystallinity effect might explain the differences between the polymer flows in longer and shorter dies.

In order to rule out viscous dissipation effects, motion and energy equations were solved for the steady fully developed flow of power-law fluids assuming isothermal wall boundary conditions. For the longer die at a shear rate of 750 s^{-1} the temperature increase near the capillary wall and close to the exit, in the case of HDPE is less than 3 °C. This is not large enough to account for the more severe extrudate distortion for longer die. It should be pointed out that

normally polymer flow in the die is not isothermal, but between isothermal and adiabatic. Therefore, the actual temperature increase could be higher. However, the higher melt temperature in longer die should not lead to more serious extrudate distortion but to the contrary. Pressure effects on the melt viscosity are also believed to be negligible for the conditions in which we operated. According to Hatzikiriakos and Dealy (1992), the viscosity increase of HDPE due to an operating pressure of 10 MPa would be of only 2%.

In addition, since we used **apparent** shear stress in this Two Level Design, the actual shear stress is larger in the large L/D die than that in the small L/D die because of entrance pressure loss. This entrance effect will be further discussed in Three Level Design.

The fourth most significant parameter is the polymer type: the HDPE produced greater roughness than the LLDPE. As many researchers (Vinogradov, 1972, Petrie and Denn, 1976, and Ramamurthy, 1986) reported, linear polymers show instability with shear stress somewhere above 0.1 MPa. The exact value varies with the type of polymer. Further, the HDPE produces discontinuities in the flow (shear stress - shear rate) curve (Bagley et al. 1958) and the flow becomes unstable at high shear stresses. When extruding the HDPE, we observed the

typical discontinuities in the flow curve, but not when extruding the LLDPE. Also, with the HDPE a sudden change in the extrudate appearance with increasing flow rate was observed, whereas the changes in the LLDPE extrudate were rather gradual. As described in Table 3.1, the two polymers have different molecular weights, MW, and molecular weight distributions, MWD, both of which affect their flow behavior. Further, even at same MW and MWD, according to the studies of Karbashewski et al. (1991), higher linear portion leads to extrudate imperfections at the same extrusion rates. Linear portion in HDPE is higher than that in LLDPE. Therefore HDPE is likely to produce extrudate roughness at lower shear stress than LLDPE does. Such consideration agrees with our results.

We expected much stronger effects on extrudate roughness by adding 1% of Viton to the polymers. The addition of Viton contributes only 0.008 to the F_R value, but it increases the extrudate roughness. Although the Viton was pre-blended to polyethylene using a counter-rotating twin screw extruder, the mixing and/or the experimental time may have not been sufficient to allow enough Viton to reach the die wall surface where it could be active.

The remaining five parameters are shown in Figure 4.4 to have very little effects on extrudate roughness. The

properties of these polyethylenes are not significantly affected by recycling. The use of a taper entrance adapter does not contribute much to roughness reduction. Changing the die material (brass vs. stainless steel), its temperature, and the melt temperature are shown to have insignificant effects on roughness. These observations are restricted to the two particular polyethylenes. More polymers will be investigated later in this Chapter with Three Level Design.

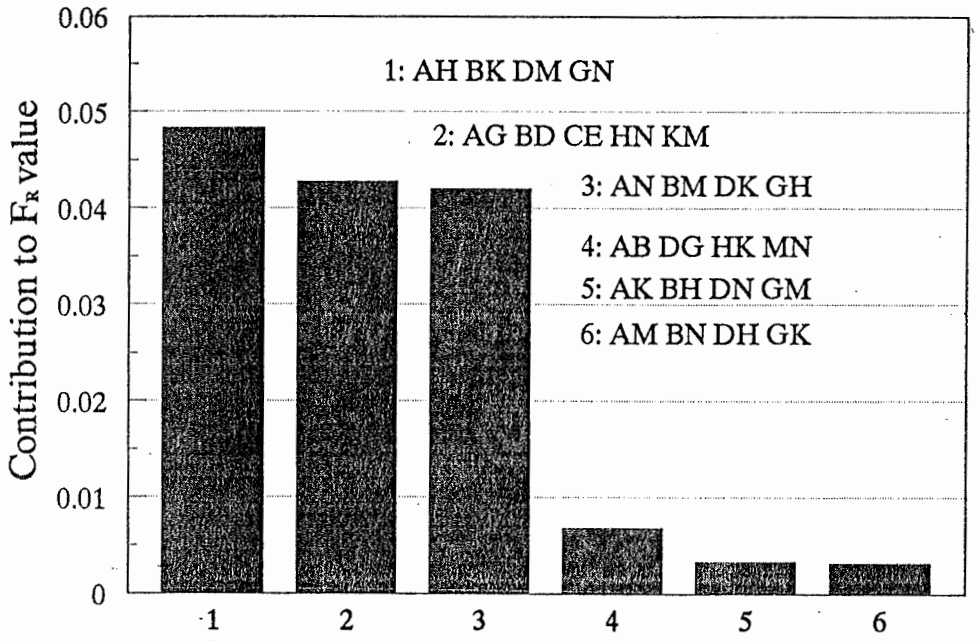

Figure 4.5. Effects from groups of two-parameter interactions on extrudate roughness. The two-letter pairs stand for the interactions between two parameters. Each bar represents a group of 4 or 5 two-parameter interactions (indicated after ``1'',``2''...``6'').

This experimental design enabled us not only to screen the main effects of the various individual parameters, but to determine also interaction effects. Our results show that the interactions are very strong, comparable to those of main effects. The interaction effects are reported in Figure 4.5. The bars in the figure represent groups of interactions, labelled 1 to 6. The two-letter groups listed stand for the interactions between pairs of parameters listed in Table 4.1. It can be seen that groups 1, 2 and 3 have considerable effects on extrudate roughness. These three groups involve the interactions between apparent shear stress (*N*), diameter of the die (*G*), L/D values of die (*H*), and type of polymers (*A*), the four most active parameters. The contribution of group 1 is made up of the interactions *AH BK DM* and *GN*. Since the individual effects of *B*, *K*, *D* and *M* were shown to be small, interactions *AH* and *GN* are the most significant factors in this group. In other words, the effect of group 1 is virtually those of *AH* (type of polymer - die L/D) and *GN* (die diameter - apparent shear stress). By the same analysis, group 2 reflects those of *AG* (type of polymer - die diameter), *HN* (L/D - apparent shear stress), while group 3 reflects the interactions of *AN* (type of polymer - apparent shear stress) and *GH* (die diameter - L/D). As discussed above, the interaction with the L/D parameter may be physically explained

by the effect of pressure. For similar shear stress, the polymer melt subjects higher pressure in the higher L/D die. Since the pressure affects the crystallinity procedure (Cogswel, 1993) and extrudate appareances, when using high L/D die at high pressure, one could expect more severe effect on crystallinity.

In groups 4, 5 and 6, the interaction effects are small. The four active parameters interact with inert parameters. In other words, when the two active parameters are set to higher levels, the effects will be as strong as those of the two individual parameters with no extra interaction effects.

Eliminating the inert parameters which have no or a low contribution to roughness, the statistical results presented in Table 4.5 can be expressed as:

$$F_R = 0.02915 + 0.02539N + 0.02414G + 0.02152H + 0.01985A + 0.0242GN + 0.0214AG + 0.0210GH \quad (4.6)$$

where the first term on the right-hand side of the equation is the average value for the roughness factor and the other numerical values are the half contributions of the active parameters and of their interactions. This model can be used with caution to predict the roughness of extrudate under given conditions. It is restricted to the two particular polyethylenes used. The predictions for the 32 extrusion runs

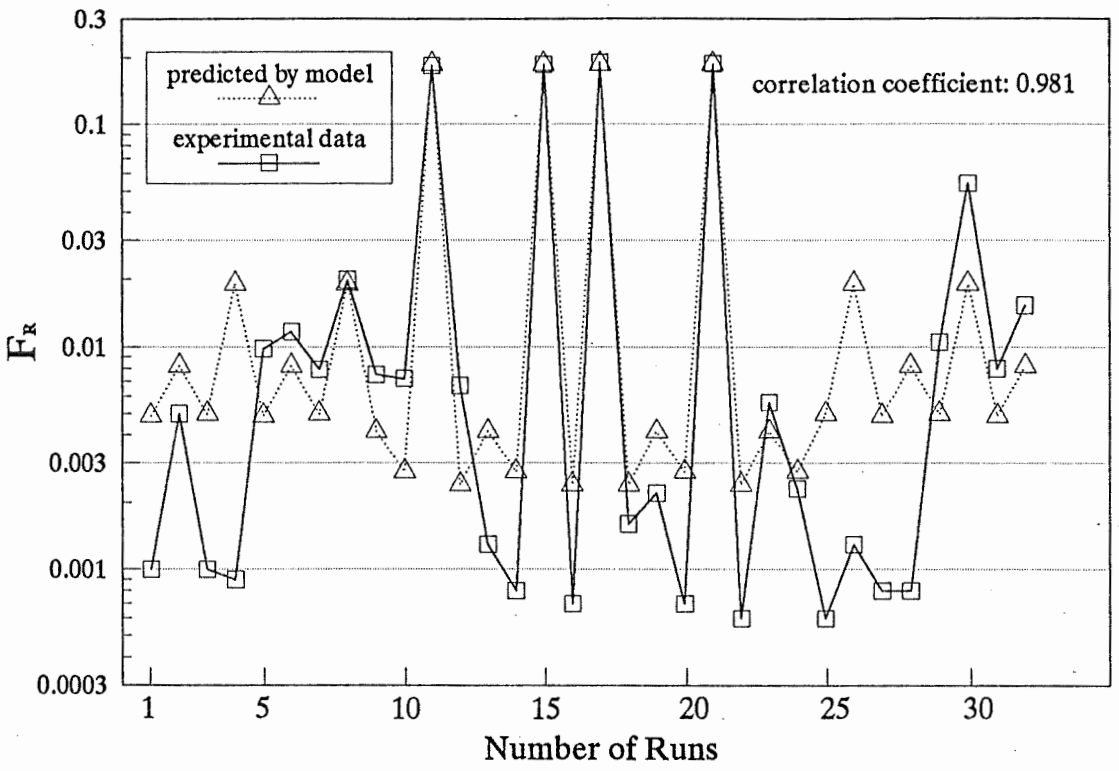

Figure 4.6. Comparison between the statistical model predictions and the data. All F_R values from 32 runs are depicted in the figure.

are compared to the experimental F_R values in Table 4.5 and in Figure 4.6. The model predicts the higher values very well. For the lower values, the predictions are not very good. This is due in parts to the difficulty of obtaining accurate measurements for low values of F_R. The correlation coefficient is 0.98.

4.4 THREE LEVEL SCREENING DESIGN

4.4.1 Descriptions

In this Three Level Design, two new parameters (molecular weight and entrance angle) and six other parameters used in Two Level Design (material of die, diameter of die, L/D value of die, melt temperature, die temperature and apparent shear stress) were analyzed.

Although the previous Two Level Design provided some interesting evaluations over 10 parameters, there is another important parameter, **molecular structure** of polymers which has not been involved. Due to complexity of such a structure, it is not proper to identify any polyethylene by a single parameter. Usually such diversity between various polyethylenes can be characterized by four parameters: 1) molecular weight, 2) molecular weight distribution, 3) long chain branching, and 4) short chain branching (Karbashewski et al. 1991). As we mentioned in Chapter 3, it was not possible to find commercial polymers with identical molecular weights but different molecular weight distributions, nor with identical molecular weight distributions but different molecular weights. Therefore, we only used molecular weight, Mw (weight average molecular weight) as property parameter.

In order to identify the sensitivity of Mw, three levels were used, level 1, 2 and 3. Therefore, it is called "Three Level Design" in following discussion. However, Mw is the only

parameter varied between three levels, while the others still vary between 2 levels. The details of experimental arrangement will be discussed later.

Besides the molecular weight effect, effect of die entrance angle was also included. The importance of entrance angle has been discussed by a number of authors (such as Schreiber et al. 1960, Han, 1973). The previous Two Level Design indicated the type of adapter didn't affect the extrudate roughness very much. Since the diameters (either 0.79 or 1.59 mm) of the flat-entry dies are always smaller than that (3.18 mm) at the exit of the tapered adapter, the tapered adapter diminished the size of stagnant zone and vortex, but it didn't eliminate sharp edge at the entrance. There are following reasons for not using adapter shape as a parameter again: 1) such effect is not important proved in Two Level Design, 2) the dies with tapered entrance can't fit onto tapered adapter (i.e. parameters type of adapter and entrance angle of the die could not be involved in one screening design). If the dies with tapered entrance were to be used with the tapered adapter, one would find the diameter of the die entry would be larger than that of the adapter exit. It will cause two consecutive converging flows, and that should definitely be avoided.

''Recycling'' and ''Additives'' effects are also omitted this time. Recycling showed almost no effect on extrudate roughness according to Two Level Design. The blending of extrusion additive, Viton, was not gratified in terms of dispersion. Therefore we did not study the effect of Viton in Three Level Design.

The roughness evaluation was the same as that used in two level design. The roughness factor F_R was also used.

Table 4.7. Parameters of Three Level Design for HDPE.

Label	Parameters	Level 1	Level 2	Level 3
A	Mw *	83300 (g/mole) (Dow 4352N)	118800 (g/mole) (Dow 12065)	161500 (g/mole) (Dow 62020)
D	Entrance angle	60 deg.	180 deg.	
E	Die material	steel	brass	
F	Die diameter	1.59 mm	0.69 mm	
G	Die L/D value	8	24	
H	Melt temperature	210 deg. C	170 deg. C	
I	Die temperature	220 deg. C	160 deg. C	
J	App. shear stress Corr. shear stress	0.2 (MPa)	0.35 (MPa)	

*: weight average molecular weight

Table 4.8. Parameters of Three Level Design for LLDPE.

Label	Parameters	Level 1	Level 2	Level 3
A	Mw *	70900 (g/mole) (Dowlex 2517)	88800 (g/mole) (Dowlex 2535)	108400 (g/mole) (Dowlex 2045)
D	Entrance angle	60 deg.	180 deg.	
E	Die material	steel	brass	
F	Die diameter	1.59 mm	0.69 mm	
G	Die L/D value	8	24	
H	Melt temperature	210 deg. C	170 deg. C	
I	Die temperature	220 deg. C	160 deg. C	
J	App. shear stress Corr. shear stress	0.25 (MPa)	0.45 (MPa)	

*: weight average molecular weight

The Three Level Design was applied to both HDPE and LLDPE polymers. The details of the assignments for each parameter for HDPE extrusion are shown in Table 4.7. The labels in the tables representing certain parameters will be used through the discussions of the Three Level Design.

The first parameter in Table 4.7 is weight average molecular weight, Mw. Three HDPE polymers, Dow 4535N, Dow 12065 and Dow 62065 were assigned to level 1, 2, and 3 in

order of increasing Mw. The Molecular properties are shown in Table 3.1.

The second parameter is the entrance angle. Level 1 was set at 60°, while level 2 at 180°. The next three parameters are the die material, die diameter and die L/D value. The values of level 1 of these three parameters are the same as those of level (-) in Two Level Design. The values of level 2 of these three are the same as those of level (+) in the Two Level Design. There were 16 dies (shown in Table 3.2) used in this design to meet the dimensional and material diversity of the dies.

The next two parameters, melt and die temperatures were set to the same values but in reverse order to that in Two Level Design, since lower temperature is believed to produce higher extrudate roughness (Beaufils et at, 1991).

The last parameter is the shear stress. The required values were obtained by controlling the RPM of the extruder (refer to discussion of the apparent shear stress in Two Level Design). Since the HDPE polymers used here are less sensitive to apparent shear stress than the HDPE resin in Two Level Design, 0.35 MPa is assigned to level 2, and 0.2 MPa to level 1. The variation of that parameter in Two Level Design was

between 0.2 and 0.3 MPa. This time both **apparent shear stress** and a **corrected shear stress** were used to define this parameter. We feel that the apparent shear stress (Equation 4.2) is not the true shear stress in the capillary. If there is substantial pressure loss at the entrance (which is usually the case at high shear stress), the apparent shear stress calculated by Equation 4.2 will be higher than actual shear stress inside die. Under the same apparent shear stress, the die with a larger L/D will be subjected to higher shear stress than the smaller L/D die. In order to clarify entrance effects, a **corrected shear stress** was also used for Three Level Design,

$$\sigma_{corr} = \frac{P_{res}}{4\,(L/D+e)} \quad \textbf{(4.5)}$$

Where e is the entrance correction factor, (Bagley correction factor). According to our experience, one cannot obtain precise but only relative values of e, when flow instability (especially wall slip) happens. Therefore, instead of measuring Bagley corrections for each polymer, two assumed e values (one for low and one for high shear stress) obtained from measuring HDPE 16A were used for the three HDPE polymers (similar assumptions were made for LLDPE polymers as discussed later). Therefore we call such shear stress ''corrected shear stress'' instead of true shear stress. Here, corrected shear stress is still set at 0.25 MPa and 0.35 MPa for level 1 and

level 2. Correcting factor, e for 0.2 MPa is 4.5 and for 0.35 MPa is 5.3.

A similar arrangement was used for the LLDPE polymers as shown in Table 4.8. Compared to the arrangement for the HDPE, only the first and eighth parameters were changed. Dowlex 2517, Dowlex 2535, and Dowlex 2045 are assigned to level "1", level "2", and level "3" with increasing of Mw for first parameter; 0.25 MPa and 0.45 MPa are assigned to level "1" and "2" to the eighth parameter. The reason of increasing shear stress values is that these LLDPE polymers start to show extrudate roughness at higher apparent shear stress than the HDPE polymers do. Two e values for three LLDPE polymers (obtained from measuring LLDPE 12J1) were used to calculate corrected shear stress: 1.3 for shear stress of 0.25 MPa and 2.4 for shear stress of 0.45 MPa.

Accordingly, there will be two almost identical Three Level Designs for each type of polymer, one with the apparent shear stress and the other with the corrected shear stress. We will call them Three Level Design with apparent shear stress and Three Level Design with corrected shear stress. Applying these two to both HDPE and LLDPE polymers, there will be four Three Level Designs in total.

As mentioned in discussions of Two Level Design, the pure main effects only can be evaluated by combining the results of basic and reflected runs. The same principle applies to Three Level Design here. Therefore, both basic and reflected runs were conducted.

The details of basic run arrangement (for both HDPE and LLDPE polymers) are shown in Table 4.9. The first column corresponds to the run number. The letters at the top represent parameters (explained in Table 4.7 and 4.8). The numbers in each row represent the level at which the particular parameter should be set. The reflected run arrangement is described in Table 4.10.

Recall the discussion over Table 4.4 for the Two Level Design, the main effects are confounded with groups of two-parameter interactions. The similar confounding pattern for Three Level Design is shown in Table 4.11.

The first row is the labels used in the calculation. The meanings of letters A, D, E, F, G, H, I, and J are given in Tables 4.7 and 4.8 for HDPE and LLDPE respectively. The second row lists the main effects that can be analyzed, for the corresponding parameters in the first row. Note, in the Three Level Design, the parameter A (molecular weight effect) varies

Table 4.9. The arrangement of Basic Runs for Three Level Design.

	A	D	E	F	G	H	I	J
1	1	1	1	1	1	1	1	1
2	1	1	1	1	1	2	2	2
3	1	2	2	2	2	2	2	2
4	1	2	2	2	2	1	1	1
5	2	2	2	1	1	1	1	2
6	2	2	2	1	1	2	2	1
7	2	1	1	2	2	2	2	1
8	2	1	1	2	2	1	1	2
9	3	1	2	2	1	1	2	2
10	3	1	2	2	1	2	1	1
11	3	2	1	1	2	2	1	1
12	3	2	1	1	2	1	2	2
13	2	2	1	2	1	1	2	1
14	2	2	1	2	1	2	1	2
15	2	1	2	1	2	2	1	2
16	2	1	2	1	2	1	2	1

between 3 levels, two main effects, effect A′ and effect A′′ (in second row) can be evaluated instead of one. Therefore the numbers of main effects can be analyzed are more than the number of parameters. Whereas in the Two Level Design, only one main effect can be analyzed for each parameter. Therefore the number of main effects is equal to that of parameters. As shown in Table 4.4, there is no second title row.

Effect A′ is called linear effect as illustrated by Figure 4.7, a. If roughness when parameter A at level 1 is F_1, at level 2 is F_2 and at level 3 is F_3. Then effect A′ is

Table 4.10. The arrangement of Reflected Runs for Three Level Design.

	A	D	E	F	G	H	I	J
1	2	2	2	2	2	2	2	2
2	2	2	2	2	2	1	1	1
3	2	1	1	1	1	1	1	1
4	2	1	1	1	1	2	2	2
5	3	1	1	2	2	2	2	1
6	3	1	1	2	2	1	1	2
7	3	2	2	1	1	1	1	2
8	3	2	2	1	1	2	2	1
9	2	2	1	1	2	2	1	1
10	2	2	1	1	2	1	2	2
11	2	1	2	2	1	1	2	2
12	2	1	2	2	1	2	1	1
13	1	1	2	1	2	2	1	2
14	1	1	2	1	2	1	2	1
15	1	2	1	2	1	1	2	1
16	1	2	1	2	1	2	1	2

$(F_3+F_2)/2-(F_1+F_2)/2$. If this value is positive, the extrudate roughness increases with increasing molecular weight, Mw. Effect A" is $F_2-(F_1+F_3)/2$, shown in Figure 4.7, b. The small absolute value of effect A" indicates that the extrudate roughness increases linearly with Mw. If A" is positive, the increase of Mw from level 1 to level 2 is more pronounced than that from level 2 to level 3; if A" is negative, the increase of extrudate roughness from level 2 to level 3 is more significant than that from level 1 to level 2.

The rest of second row (Table 4.11) comprises the other

Table 4.11. Confounding Patterns of Basic and Reflected Runs for Three Level Design.

Labels in Design	A		D	E	F	G	H	I	J	K	L	M	N	O
Main Effect	A'	A"	D	E	F	G	H	I	J					

Basic Runs

Two-factor Interactions	- DE	- DG	- A'E	- A'D	- A'G	- A'F	- A'I	- A'H	- A"I	- A'J	- DH	- DI	- DJ	- EJ
	- FG	- EF	- A"G	- A"F	- A"E	- A"D		- A"J		- A"H	- EI	- EH	- FH	- FI
	- HI	- IJ									- FJ	- GJ	- GI	- GH

Reflected Runs

Two-factor Interactions	DE	DG	A'E	A'D	A'G	A'F	A'I	A'H	A"I	A'J	DH	DI	DJ	EJ
	FG	EF	A"G	A"F	A"E	A"D		A"J		A"H	EI	EH	FH	FI
	HI	IJ									FJ	GJ	GI	GH

parameters represented by letters D, E, F, G, H, I, and J (defined in Table 4.7 and 4.8).

Note letters K, L, M, N, and O represent no main effect but only the interaction effects. For example, interaction effect of A"I can be obtained by subtracting the effect of the reflected run from that of the basic run of J (see discussion of Equation 4.4).

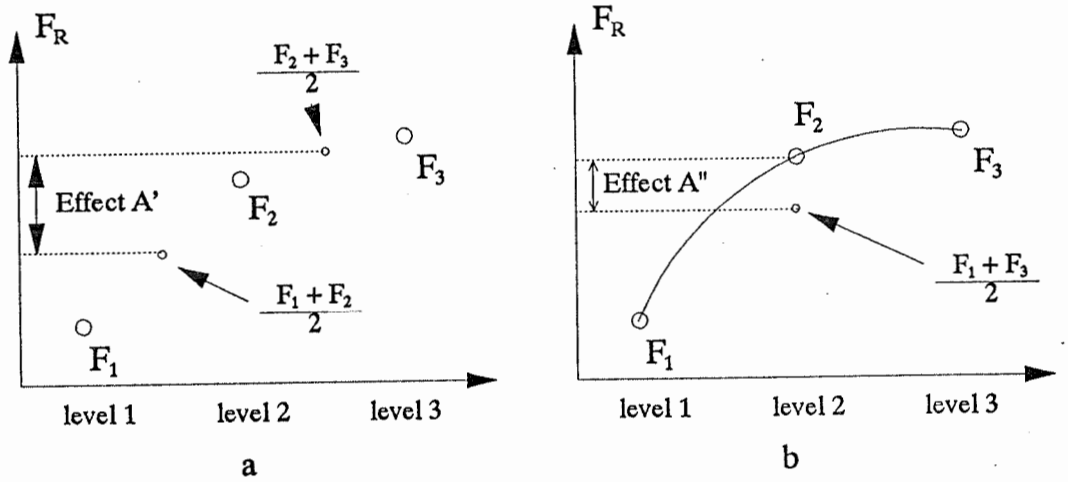

Figure 4.7. Diagrams of two main effects. a: linear effect (A') and b: quadratic effect (A").

In order to verify the reproducibility of such extrudate roughness, several repeated runs were made. For the HDPE polymers, experiments #11 , #12 of basic runs, and #7, #8 of reflected runs were repeated twice. Figure 4.8 shows these repeated values. In each cluster of the bars, the left one is the first repeated value; the middle one is second repeated value; and the right one, the initial value.

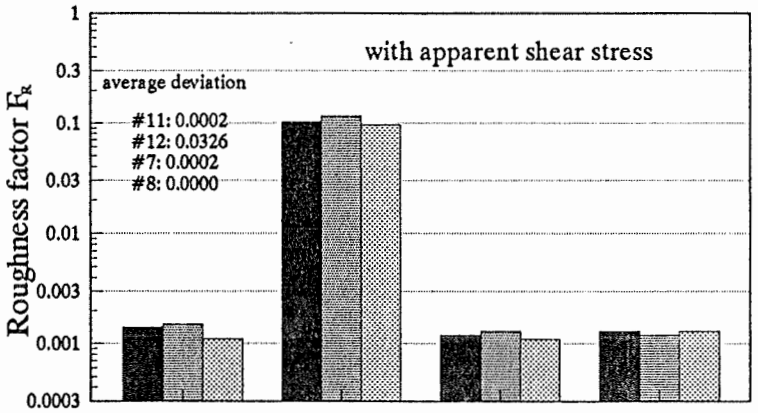

#11 of basic run	#12 of basic run	#7 of reflected run	#8 of reflected run
0.0014	0.1022	0.0012	0.0013
0.0015	0.1151	0.0013	0.0012
0.0011	0.0954	0.0011	0.0013

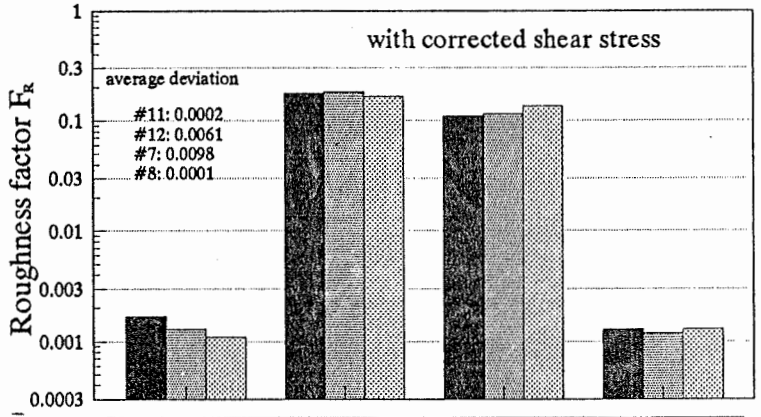

#11 of basic run	#12 of basic run	#7 of reflected run	#8 of reflected run
0.0017	0.1780	0.1113	0.0013
0.0013	0.1818	0.1157	0.0012
0.0011	0.1661	0.1356	0.0013

Figure 4.8. Repeatability of extrudate roughness for HDPE. The average deviation from the mean values of three repeated tests is shown for four different runs.

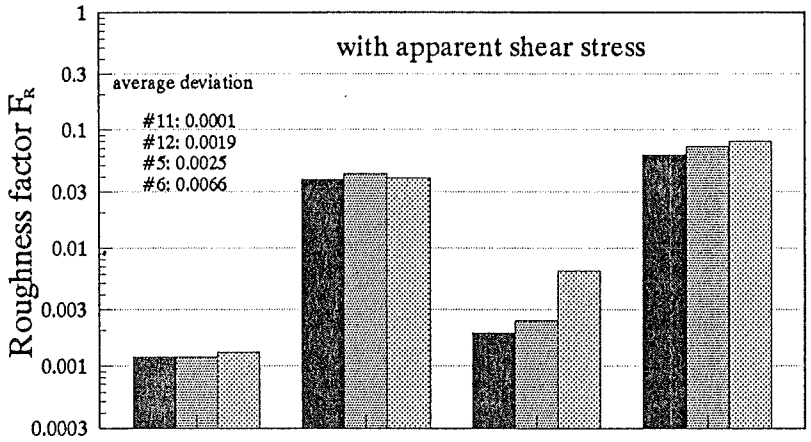

#11 of basic run	#12 of basic run	#5 of reflected run	#6 of reflected run
0.0012	0.0380	0.0019	0.0613
0.0012	0.0428	0.0024	0.0726
0.0013	0.0388	0.0064	0.0798

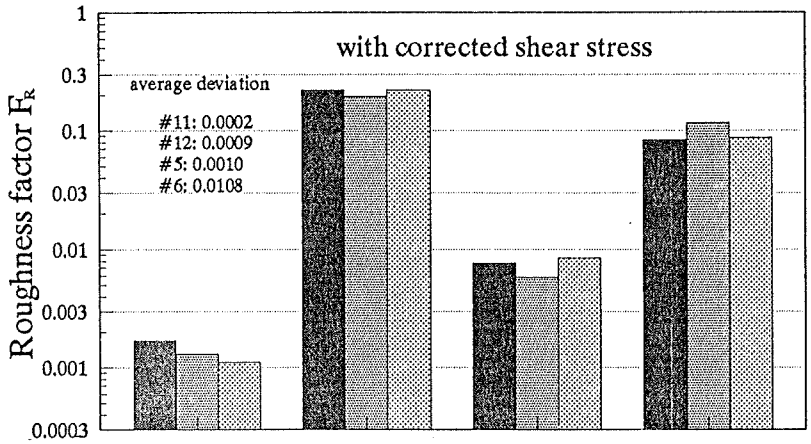

#11 of basic run	#12 of basic run	#5 of reflected run	#6 of reflected run
0.0017	0.2218	0.0077	0.0834
0.0013	0.1948	0.0058	0.1157
0.0011	0.2213	0.0085	0.0866

Figure 4.9. Repeatability of extrudate roughness for LLDPE. The average deviation from the mean values of three repeated tests is shown for four different runs.

Table 4.12. Measured F_R values for HDPE polymers.

	With Apparent Shear Stress (F_R)		With Corrected Shear Stress (F_R)	
	Basic Run	Reflected Run	Basic Run	Reflected Run
1	0.0012	0.0185	0.0122	0.1687
2	0.0234	0.0026	0.0422	0.0016
3	0.0163	0.0010	0.0056	0.0011
4	0.0026	0.0092	0.0025	0.0118
5	0.0010	0.0027	0.0245	0.0023
6	0.0070	0.0248	0.0013	0.0501
7	0.0028	0.0018	0.0098	0.1208
8	0.0019	0.0013	0.0029	0.0013
9	0.0152	0.0012	0.0322	0.0011
10	0.0036	0.0012	0.0018	0.0105
11	0.0013	0.0021	0.0014	0.0141
12	0.1042	0.0030	0.1753	0.0016
13	0.0022	0.0169	0.0027	0.0190
14	0.0016	0.0143	0.1726	0.0152
15	0.0303	0.0022	0.0208	0.0246
16	0.0093	0.0229	0.0097	0.0456

For LLDPE polymers, #11, #12 of basic runs and #5 and #6 of reflected runs were repeated twice. The results are reported in Figure 4.9 in the same pattern as that of Figure 4.8.

Each of the repeated extrusion experiment was conducted at least four hours after the previous one after extruder had been shut off. Figures 4.8 and 4.9 show good repeatability in terms of F_R values. This demonstrates reliability of those extrudate roughness data in such conditions.

4.4.2 Results and Discussions

All the F_R values for HDPE and LLDPE are listed in Tables

Table 4.13. Measured F_R values for LLDPE polymers.

	With Apparent Shear Stress (F_R)		With Corrected Shear Stress (F_R)	
	Basic Run	Reflected Run	Basic Run	Reflected Run
1	0.0014	0.0105	0.0013	0.2152
2	0.0011	0.0026	0.0011	0.0027
3	0.0024	0.0012	0.0765	0.0010
4	0.0024	0.0114	0.0027	0.0136
5	0.0094	0.0036	0.0017	0.0073
6	0.0105	0.0712	0.0104	0.0866
7	0.0021	0.0011	0.0046	0.0546
8	0.0219	0.0051	0.0129	0.0022
9	0.0198	0.0015	0.2137	0.0022
10	0.0023	0.0012	0.0018	0.0558
11	0.0012	0.0282	0.0014	0.0315
12	0.0398	0.0022	0.2213	0.0024
13	0.0113	0.0015	0.0120	0.0012
14	0.0036	0.0016	0.0040	0.0012
15	0.0086	0.0025	0.1099	0.0023
16	0.0100	0.0018	0.0030	0.1022

4.12 and 4.13. They were statistically analyzed according to the screening design. The analyzed results for HDPE and LLDPE polymers are shown in Tables 4.14 and 4.15. The first row lists analyzed results from the basic runs. The second gives the results from the reflected runs. The third row contains main effects obtained by

(results of basic runs + results of reflected runs)/2

(see Equation 4.3 for an example). The forth row represents the two-parameter interaction or a group of two-parameter interactions.

The main effect reflects how much changing a given

Table 4.14. The analyzed results in terms of F_R values for HDPE.

Labels in Design	A		D	E	F	G	H	I	J	K	L	M	N	O
Main Effect	A'	A"	D	E	F	G	H	I	J					
	with apparent shear stress (F_R x 100)													
Basic Runs	1.39	-1.40	0.61	-0.67	-1.64	1.42	-0.64	1.71	2.05	-1.32	1.45	-1.37	-0.70	1.04
Reflected Runs	-0.02	-0.60	-0.28	-0.06	0.40	0.48	0.32	-0.28	0.86	0.30	0.58	0.15	0.06	-0.41
Main Effect	0.69	-1.00	0.16	-0.36	-0.62	0.95	-0.16	0.71	1.46					
Interaction Effect	-0.71	0.40	-0.44	0.30	1.02	-0.47	0.48	-1.00	-0.59	0.81	-0.43	0.76	0.38	-0.73
	with corrected shear stress (F_R x 100)													
Basic Runs	3.94	-0.36	3.18	-4.01	-0.72	-0.77	-0.08	0.50	5.43	-4.20	0.52	0.90	-3.82	3.74
Reflected Runs	2.83	-0.86	3.24	2.44	1.60	0.60	0.17	0.10	4.90	3.73	1.31	0.81	3.03	2.68
Main Effect	3.38	-0.61	3.21	-0.78	0.44	-0.09	0.04	0.30	5.17					
Interaction Effect	-0.56	-0.25	0.03	3.22	1.16	0.68	0.12	-0.20	-0.27	3.96	0.40	-0.05	3.42	-0.53

parameter from level "1" to level "2" (except parameter A) affects the extrudate roughness. In the case of parameter A, the effects A' and A" impart the linear and quadratic effects of the molecular weight described in Figure 4.7.

Table 4.15. The analyzed results in terms of F_R values for LLDPE.

Labels in Design	A		D	E	F	G	H	I	J	K	L	M	N	O
Main Effect	A'	A"	D	E	F	G	H	I	J					
	with apparent shear stress (F_R x 100)													
Basic Runs	0.57	0.09	0.17	-0.21	-0.20	0.36	-1.05	0.58	0.82	-0.36	0.08	-0.61	0.07	0.44
Reflected Runs	0.83	-0.37	-1.18	-0.52	1.23	0.50	-0.90	-0.24	1.33	0.71	1.19	0.55	-1.26	-0.59
Main Effect	0.70	-0.14	-0.51	-0.37	0.51	0.43	-0.98	0.17	1.08					
Interaction Effect	0.13	-0.23	-0.68	-0.15	0.71	0.07	0.01	-0.41	0.26	0.53	0.56	0.58	-0.67	-0.52
	with corrected shear stress (F_R x 100)													
Basic Runs	5.70	-4.52	-0.23	2.01	-0.27	2.33	-3.24	5.09	7.55	-5.72	0.40	-2.67	0.62	-2.05
Reflected Runs	2.31	0.84	3.66	0.50	3.98	2.03	1.38	0.95	6.74	2.18	3.78	1.89	3.71	0.61
Main Effect	4.00	-1.84	1.71	1.26	1.85	2.18	-0.93	3.02	7.15					
Interaction Effect	-1.70	2.68	1.94	-0.76	2.13	-0.15	2.31	-2.07	-0.40	3.95	1.69	2.28	1.55	1.33

The main effects of HDPE polymer shown in Table 4.14 are plotted in Figure 4.10, where the upper part is the results with the apparent shear stress, and the bottom part, the results with the corrected shear stress.

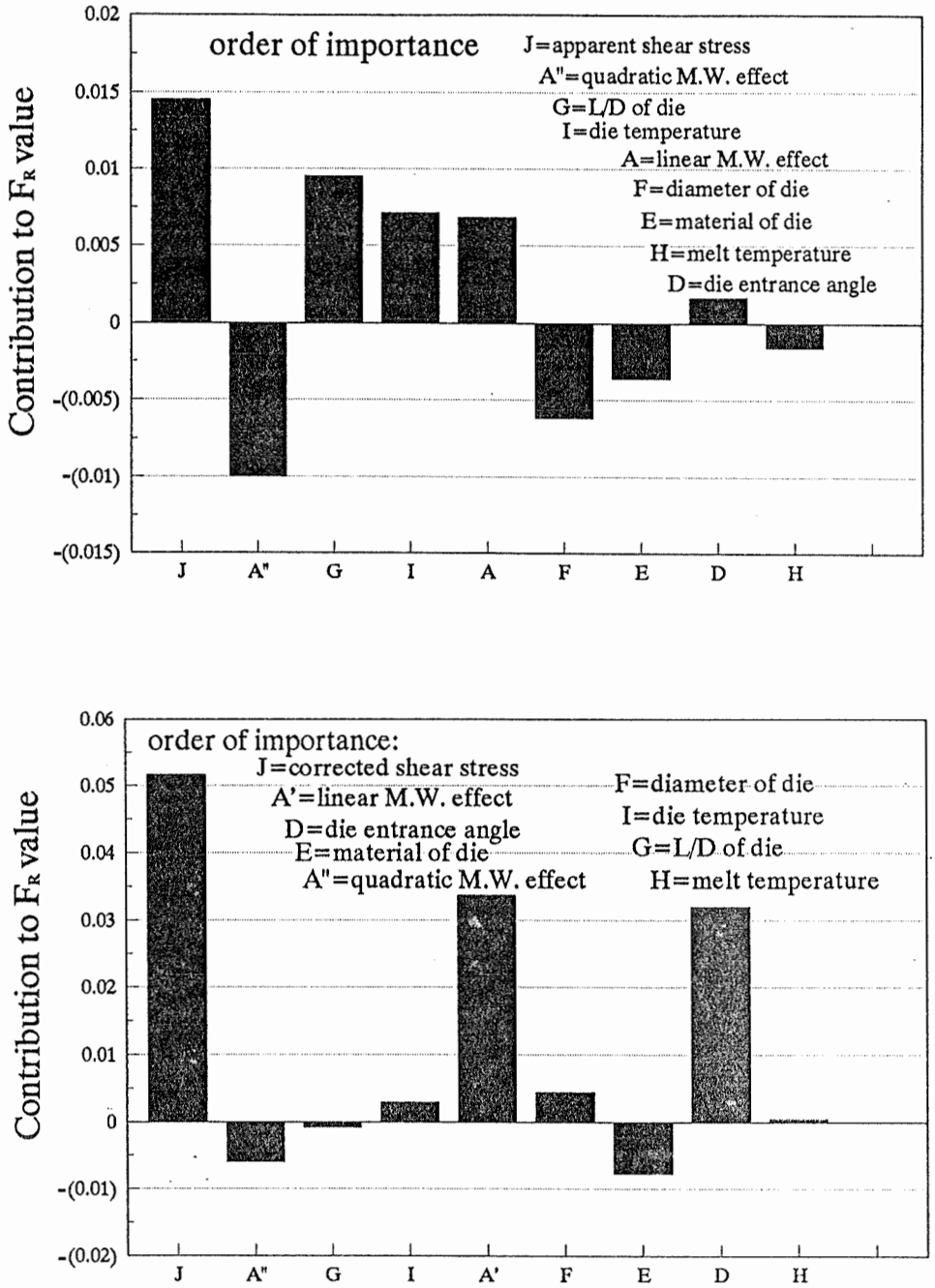

Figure 4.10. Main effects of 8 parameters on F_R values of HDPE polymers. The results for design with apparent shear stress at the top; with corrected shear stress at the bottom.

The results with apparent shear stress (shown as the upper part of the Figure) resemble those of the Two Level Design to some extent. Recall the results of the Two Level Design: the four active parameters were **the apparent shear stress, the L/D values of die, the diameter of the die and the type of polymer.** Three of these four reappear here. The apparent shear stress comes again as the most important one, the quadratic effect of molecular weight (such effect can be related to the Type of Polymer which appeared in the Two Level Design, they all reflect the polymer effect) comes second, and the L/D value is rated as the third important parameter. Although the polymers used are different in Two and Three Level Designs, such similar results are obtained. It appears that this screening design method is fairly reliable. Since the major contributions in the Two Level Design come from HDPE 16A (it produced all the high-level extrudate roughness), the results there mainly reflect the properties of HDPE. Resemblance of these two results demonstrates the similar effect given by different HDPE polymers to extrudate roughness. The diameter effect didn't show as an important parameter here.

The effects of shear stress and polymer properties are the dominating parameters. Of all the results from three analyses (Two Level Design, Three Level Designs with the

apparent shear stress and the corrected shear stress), these two parameters always come as the important ones.

Strong effect of the type of polymer from the Two Level Design and the effect of molecular weight, Mw reflects the importance of polymer properties. HDPE 16A in the Two Level Design has a higher Mw than LLDPE 13J4 and HDPE 16A was shown to cause more extrudate roughness. This is in line with the results of the Three Level Design: higher Mw leads to more severe roughness. The differences between the HDPE and LLDPE will be further discussed later with the Three Level Design of LLDPE polymers. It should be noted that the relative importance of the quadratic effect A" in upper part of Figure 4.10 is stronger than the linear effect A', while the order is reversed in the bottom part of the Figure. Recall the discussion over the meaning of A' and A"; a strong negative effect of A" indicates that an increase of Mw from level "2" to level "3" causes much more increase on F_R than the increase from level "1" to level "2" does. That implies that in average, the F_R value at level "2" is similar or even smaller than that at level "1", while the F_R value at level "3" is quite high compared to that at level "2". This nonlinear phenomenon is consistent with the molecular distribution of these three polymers as explained before (shown in Figure 3.1).

According to Ajji et al. (1992) the larger the molecular weight, the worse the extrudate appearance would be. Table 3.1 shows weight average molecular weight Mw increases from level 1 to level 3. The molecular differences are better illustrated in Figure 3.1. There are more larger molecules in HDPE 62020 than in HDPE 12065. Whereas the differences are less between HDPE 12065 and HDPE 4352N. Therefore, HDPE 62020 is likely to cause larger F_R values. On the other hand, practically, we found that HDPE 12065 had a second smooth zone observed in separate extrusion. This happened in the apparent shear stress range of 0.3 MPa to 0.35 MPa. In this shear stress range, the extrudate roughness was less severe than that below 0.3 MPa. This can cause unusual low F_R for the level "2" of Mw. However, in a higher shear stress range, above the second smooth zone, strong negative effect should diminish. The bottom part of Figure 4.10 does show an increase of the effect A' and a decrease of that of A". This time the actual shear stress is higher due to use of the corrected shear stress since pressure loss was taken into account. The shear stress of level 2 has exceeded the second smooth zone. Therefore, the effect is more linear like indicated by strong effect of A'.

The L/D effect, ''G'', is not an important parameter according to results shown in the bottom part of in Figure 4.10. Using the apparent shear stress, the L/D effect is quite

strong (shown in upper part of the figure). The reason is that the strong L/D effect obtained with the apparent shear stress was quite possibly caused by unequal real shear stress inside die.

The shear stress ''J'', the weight average molecular weight, ''A'' and die entrance angle ''D'' are the three active parameters according to the results with the corrected shear stress. The other parameters are quite inert.

The strong entrance angle effect, ''D'', suggests that the upstream converging flow is quite important. The 180° angle entry causes higher degree of elastic deformation of the polymer melt than the 60° entry does. It is important to stress through this study that such effect is more important than most parameters, such as temperature, at least for HDPE polymers studied. Tordella (1956) proposed that the elastic deformation at die entry caused extrudate roughness. According to the birefringence observation by Vinogradov (1972), the higher concentration of stresses was found for a 180° die entry than for a tapered die entry. He suggested that such a high stress level could make the polymer behave more like an elastomer and trigger wall slip. Therefore, the entrance flow and related wall slip are the possible mechanisms for HDPE extrudate roughness.

Similar studies have been conducted for three LLDPE polymers. The results are shown in Figure 4.11, where the upper part presents the results with the apparent shear stress and the lower part is those with the corrected shear stress. Since the results from the apparent shear stress may be marred by entrance pressure loss, we will consider the results based on both the corrected shear stress and apparent shear stress.

The pattern of effects on F_R shown by the upper part of Figure 4.11 is not similar to that of the two level design, although in both cases the apparent shear stress was used. This suggests that the results of the Two Level Design reflect mainly the behaviour of HDPE 16A. A screening design study (details are not shown here) of only LLDPE 13J4 (used for Two Level Design) gave a pattern of importance unlike that of Two Level Design but like that of upper part of Figure 4.11. Therefore, it suggests that the mechanism of extrudate roughness of LLDPE is different from that of HDPE. There is no obvious active and inert group of parameters.

The shear stress effect ''J'' is once again the most important parameter of all. This confirms the strong effect obtained through the previous analyses. This effect is strong

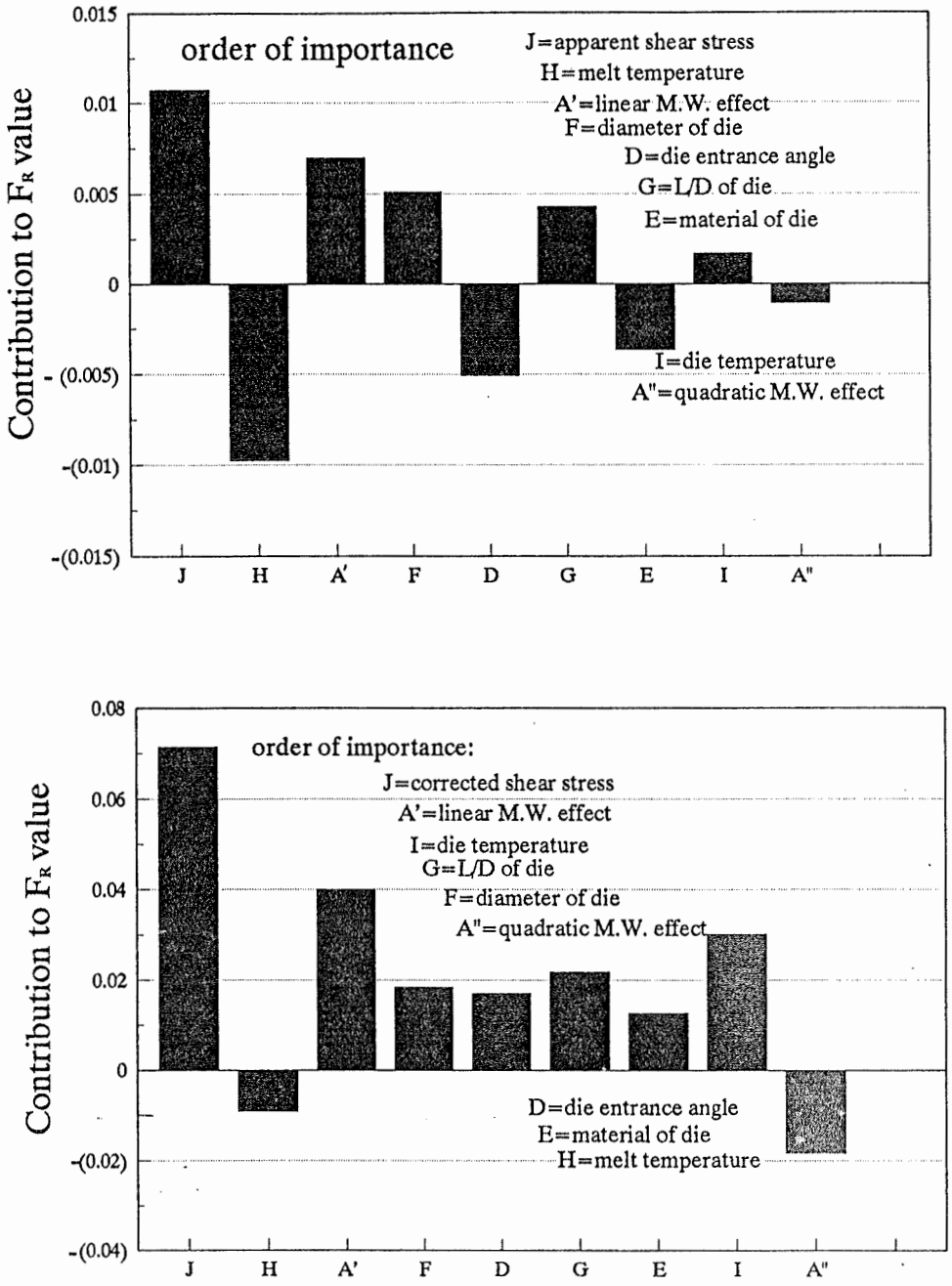

Figure 4.11. Main effect of LLDPE polymers from Three Level Design. Top: result with apparent shear stress; Bottom: result with corrected shear stress.

for both HDPE and LLDPE polymers.

The molecular weight, Mw, stands as the second important parameter of all when considering the results using corrected shear stress. Here, the effect is linear which is in line with the gradual increase of large molecule content in the three LLDPE polymers shown in Figure 3.2. Such gradual increase causes gradual increase of extrudate roughness from level 1 to level 3. On the other hand, Ajji et al, (1992) pointed out the effect of minimum molecules was strong on extrudate roughness: smaller of this minimum value, more severe the extrudate roughness. Small molecules tend to migrate to the melt/solid interface and act like bonding layer. Smaller are the minimum molecules, the weaker is the bonding, and more chance of extrudate roughness. Figure 3.2 shows that minimum molecules are smaller and smaller from level 1 to level 3 polymers. In that sense, level 3 polymer is more likely to cause extrudate roughness.

Temperature seems to be a sensitive parameter here, more notable than it is for HDPE polymers. The negative effect of melt temperature shown in upper part of Figure 4.11 is surprising, since normally the reversed results are expected. The negative value implies that F_R increases with increasing melt temperature. It is not an error in the experiments,

because such negative effects appears four times (Figure 4.4, upper part of Figure 4.10 and Figure 4.11). The only non negative effect is also very small (bottom part of Fig 4.10). Compared to the result with corrected shear stress, such negative effects remain the same value (-0.01) but its relative importance drops to the least important one. It should be noted that the average F_R value in the apparent shear stress is 0.0092. While with the corrected shear stress, F_R is 0.03194. The contribution of temperature (-0.01) are constant for both cases. Therefore, in the former case, the average F_R value is low, the temperature effect can be considered important. While in the latter case, the average value is high, the temperature effect appears to be not important. That might be explained as that the temperature is important to surface roughness, such as shark skin, (with low F_R values); while not so to gross fracture (with high F_R values).

It is unclear what causes the negative-going tendency of such effect. Beaufils et al (1991) observed that the LLDPE extrudate roughness was more severe at 145°C than at 205°C, but differences diminished for experiment carried at higher and higher shear stresses. The maximum shear stress they reported was 0.27 MPa. At further higher shear stresses, the difference might be even smaller, but it is not certain whether there

will be a reversed temperature effect.

On the other hand, the die temperature effect ''I'' is found as the third important parameter, a moderate active one, according to the results based on the corrected shear stress. That reflects roughness of LLDPE is related to the viscosity and adhesion of polymer melt near the die wall. On contrary, die temperature effect is rather negligible for HDPE. Such difference indicates different mechanisms of extrudate roughness for LLDPE and HDPE. According to our observations, LLDPE shows gradual development of roughness: from surface roughness to gross fracture (no sudden increase of slip); while HDPE shows rather abrupt start of roughness: from smooth to gross fracture or spurting (this phenomenon will be further discussed in two-hole die experiments of next chapter). Surface roughness is an exit phenomenon, and increases as the residual elastic energy of the extrudate surface increases. If the die temperature decreases, viscosity of the polymer contacting that die wall increases, which causes higher shear stress, and higher elastic energy in the outside layer of polymer stream. When polymer emerges from the die, more severe surface roughness can be expected. Since LLDPE shows more pronounced surface roughness, it is more sensitive to the die temperature. For HDPE, the spurting and gross fracture are caused by vigorous wall slip through the die. The die

temperature will be less effective on such slip. Therefore, HDPE roughness is less sensitive to the die temperature.

Die geometry, L/D, ''G'', diameter, ''F'', and entrance angle ''D'' of die show less important effects. The L/D effects don't change very much when using the apparent shear stress and corrected shear stress. It is because, the entrance pressure loss is smaller here than that for HDPE, and the distortions are more of the surface type due to exit flow.

Based on the Three Level Design, the two parameter interaction effects can also be evaluated. Due to present resolution of experiments we cannot obtain every single interaction effects. The components of each interaction group are listed in Table 4.11. These groups consist of one up to three two-parameter interactions.

The effects of these interaction groups are reported in Tables 4.12 and 4.13 for HDPE and LLDPE polymers respectively. It is found that the interactions are quite comparable to the main effects in terms of contributions to the F_R values.

Figure 4.12 shows some major interaction effects from the Three Level Design with the corrected shear stress for the HDPE polymers. The format of the figure is the same as that of

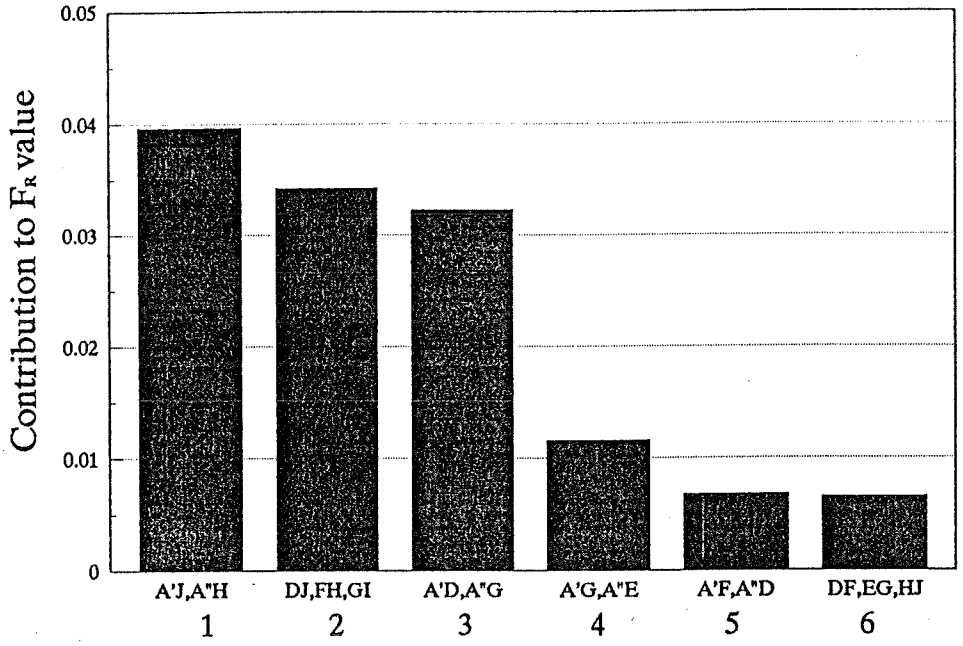

Figure 4.12. Effects of group of interactions for HDPE polymers from Three Level Design with corrected shear stress.

Figure 4.5. The figure shows notable contributions to the F_R values. Consider group 1 which contains interactions between A'J and A''H, as an example, the contribution reaches 0.04. Compared to main effects of J (0.05) and A'(0.035) (shown in the bottom of Figure 4.10), the interaction effect is of the same order. Moreover, since H is not an active parameter, the interaction A"H should not be strong either. Therefore the effect of group 1 is mainly the interaction of A'J. On the other hand, the interactions between two inert parameters or

one active and one inert parameter are not very strong.

Figure 4.13 shows the interactions for LLDPE polymers from the Three Level Design with the corrected shear stress. Looking at group 1 again, we find the same level of contribution to the F_R value from this group. If the interaction between A"H is small due to low activity of H, the total contribution is mainly from A'J. By coincidence, this effect is the same (0.04) as that shown in Figure 4.12 for HDPE polymers. Note group 3 has only one interaction A'I, with a contribution of about 0.023. Since parameter "I" (die temperature) is not as active as parameter "J" (corrected shear stress), interaction A'I should be smaller than A'J. This confirms the major contribution of group 1 is from A'J. It also gives an important reference value of individual interaction when we analyze the interaction in groups (where the individual interaction is not available).

In short, the two-parameter interaction effects are strong and the contribution to F_R is at the same level as the main effect provided the two main effects are strong.

4.5 SUMMARY OF SCREENING DESIGN STUDIES

Shear stress is the most important factor affecting the

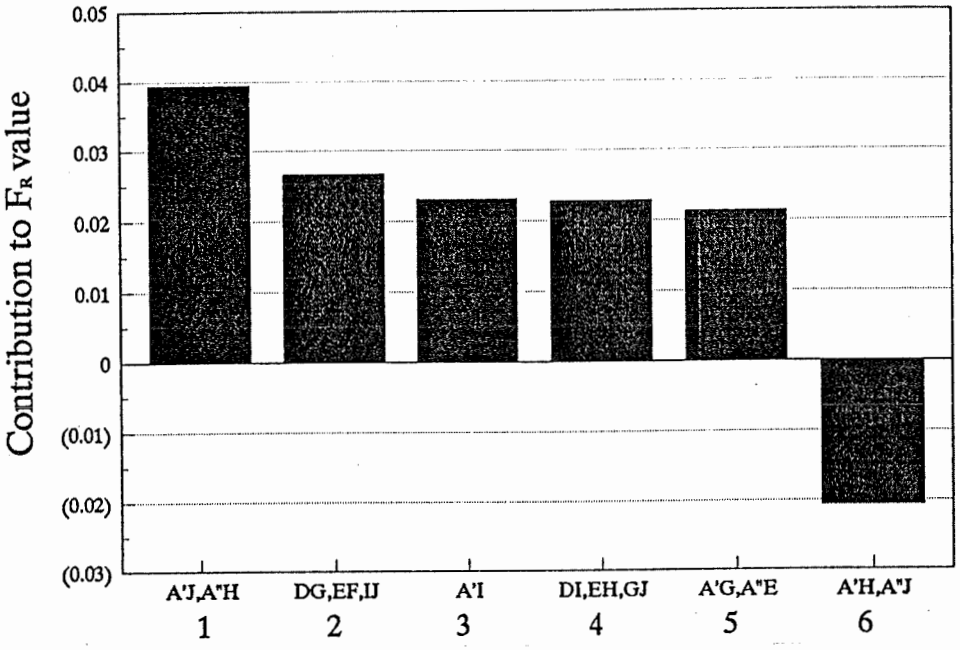

Figure 4.13. Effects of group of interactions for LLDPE polymers from the Three Level Design with the corrected shear stress.

extrudate roughness, as clearly shown by the results discussed here, whether using the apparent or the corrected shear stress. This corroborates the work done by many investigators stating that there is a critical shear stress at which extrudate roughness occurs (refer to Chapter 2). However, for the first time the relative importance of the shear stress compared to other parameters is clearly shown.

Molecular weight is the second important parameter of all

according to our results. Higher molecular weight leads to higher F_R values.

The importance of other parameters cannot be concluded generally. For HDPE polymers, shear stress, molecular weight and entrance angle are the active parameters while the others are inert. For LLDPE polymers, there are no distinct active and inert groups of parameters, although shear stress and molecular weight are still the first two most important parameters.

Two-parameter interactions from two active parameters have the same effect as the main effect. The interaction between one active and one inert parameters is less strong as well as those between two inert parameters.

The Screening design provides another approach to verify the mechanism of extrusion roughness. If some assumption is true, the related parameter will show higher degree of importance in the analyzed results. Further, if only a few parameters are important, that may suggest a simple mechanism. On the other hand, if the importance of various parameters is not clear-cut divided, the extrusion may be affected by many parameters. Therefore, HDPE and LLDPE polymers appear to have different mechanisms behind the extrudate roughness.

The strong entrance angle effect for HDPE supports the assumption that high stress level at the entrance result into large amount of stored elastic energy, which will be released as extrudate roughness. This might be a major cause of extrudate roughness for HDPE. Extrudate roughness of LLDPEs was found to be affected by various parameters not only a few. The final appearance of the extrudate reflects the combining effects of many parameters. We may call the mechanism for HDPE a ''simple type'', while that for LLDPE a ''combined type''.

CHAPTER 5

TWO-HOLE DIE EXTRUSION

5.1 INTRODUCTION

For a polymer flow inside a capillary die without slip shear stress at the wall is:

$$\tau_w = \frac{\Delta P R}{2L} \tag{5.1}$$

where R and L are the radius and length of the capillary. ΔP is the pressure drop along the capillary. For Newtonian fluid, the shear rate at the die wall is:

$$\dot{\gamma}_N = \frac{\Delta P R}{2\mu L} \tag{5.2}$$

where μ is the viscosity. If the polymer melt is assumed as a power law fluid, the shear rate at the wall can be written as

$$\dot{\gamma}_p = \left(\frac{\Delta P R}{2mL}\right)^{1/n} \tag{5.3}$$

where m is the consistency index and n is the shear thinning index for the power law model.

According to the Equation 5.1, at given temperature,

different capillary dies with the same L/D ratio should have the same shear stress at die wall as long as the pressure drop through the die is identical. If we consider a polymer as a power law fluid, it should exhibit the same shear rate (Equation 5.3). As a result, if two channels with the same L/D are subjected to the same pressure head, the shear stress and the shear rate in the two channels should be equal (assuming that the entrance pressure drops are the same for the dies with identical L/D). The apparent shear rate can be calculated from the extrusion flow rate:

$$\dot{\gamma}_A = \frac{4Q}{\pi R^3} \tag{5.4}$$

where Q is volume flowrate. Normally, Rabinowitch analysis should be used to obtain the corrected wall shear rate:

$$\dot{\gamma}_c = \left(\frac{3n+1}{4n}\right)\frac{4Q}{\pi R^3} \tag{5.5}$$

As shown in Figure 3.7, the two-hole die consists of two channels with identical L/D = 24. According to Equation 5.1 the shear stresses at die wall are equal for both channels.

If there is no slip, since L/D values of the two channels are equal, the apparent shear rate should be equal in both channels (Equation 5.3). Equation 5.5 gives the shear rate

form which can be calculated through the flowrate.

If there is a sudden slip, flowrates will jump to higher values. Usually, to detect such a slip, a series of dies with the same L/D value but different diameters are needed. The apparent shear rates at a given shear stress are plotted against the reciprocal of the diameter. Then the slip velocity can be calculated from the slope of the curve (Mooney's plot). Figure 2.12 gives an example reported by Ramamurthy (1986). This is the most widely used approach to evaluate slip velocity so far. However, it depends critically upon the entrance correction. Usually it is not easy to find precise end corrections for all the dies near the instable region. Further, if the slip velocity in the large diameter die is higher than that in the small die, the slip will be negative based on this method which is not correct. Hence, for some slip situation, this method would not apply. The two-hole die enable us to observe slip through a direct comparison between the apparent shear rates from two channels especially when slip occurs in one channel. There are three possibilities:

1) If no slip happens, the shear rates are equal in both channel;

2) If slip happens in both channels, one can observe jumps of apparent shear rates in both channels. The apparent shear rate from the small channel will be higher than that

from large channel according to Mooney's Equation.

3) If slip happens in just one channel, that channel gives a jump of the apparent shear rate, while the other channel exhibits unchanged or even lower flowrate. Such obvious differences in the apparent shear rate under the same pressure head will clearly indicate slip.

The two-hole die was mounted on the same single screw extruder used for screening design studies described in Chapter 3. All the extrusions were conducted at 200 °C. The measured pressure in the reservoir was used to calculate the apparent shear stress for both channels by Equation 5.1.

The flowrate was measured by cutting and weighing the emerging extrudates from the two channels (assumed density 0.8 g/mL was used to convert mass flowrate into volumetric flowrate). The apparent shear rates were obtained using the measured flowrates by Equation 5.4.

In this work, two HDPE and one LLDPE polymers were used: HDPE 16A from Du Pont, HDPE 12065 from Dow, and LLDPE 12J1 from Du Pont. Their properties are listed in Table 3.1

5.2 RESULTS AND DISCUSSIONS

5.2.1 Discontinuity of Flow Curves

Various discontinuities can be observed on the flow curve of HDPEs and LLDPEs. Such phenomena are usually associated with various extrudate distortions. The pressure decrease and flowrate increase are usually explained by wall slip.

Flow curves for HDPE 16, HDPE 12065, and LLDPE 12J1 are illustrated in Figures 5.1, 5.2 and 5.3 respectively.

Discontinuities in HDPE 16A flow curve happen near the apparent shear stress value of 0.3 MPa. The overlapping of the curve at the discontinuities was caused by pressure decreases with increasing apparent shear rate. The flow curve can be divided into three parts: 1) before, 2) during, and 3) after discontinuity.

The flow in the first part is stable and the extrudates are smooth. The curves of two channels coincide which indicates no slip.

In the second part, the extrudate begins to show roughness. We found that the pressure decreased with the increasing extruder RPM in this extrusion region. The apparent shear rate of two channels showed noticeable differences, an indication of slip as shown in Figure 5.1.

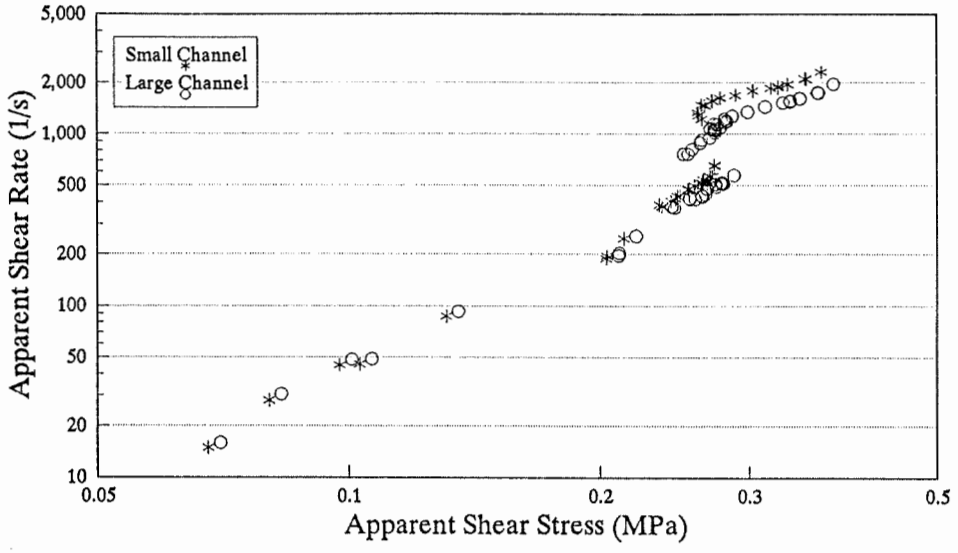

Figure 5.1. Flow curve of HDPE 16A with two-hole die.

Moreover, spurting also happened in this part. This will be elaborated later.

The third part of the flow curve is after the discontinuity. The apparent shear rates of both channels once again increase in proportion to the apparent shear stress. However, the apparent shear rate values in the small channel are larger than those in the large channel. According to Mooney's Equation, such differences indicate slip in both channels. For instance, at apparent shear stress of 0.33 MPa, the slip velocity obtained from the Mooney's Equation (poltting apparent shear rates against the reciprocals of the

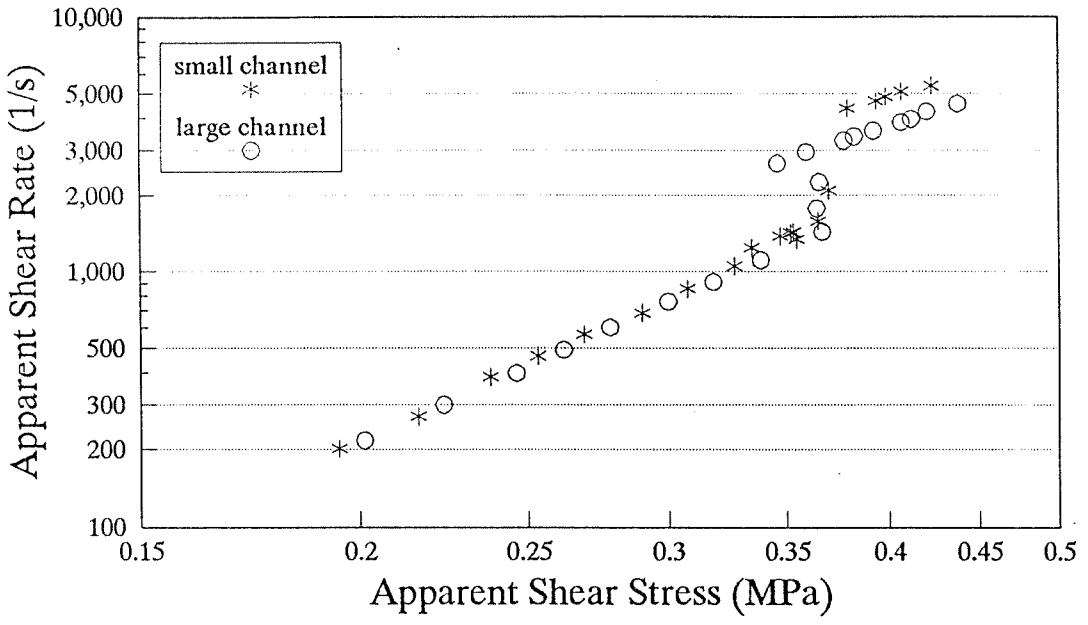

Figure 5.2. Flow curve of HDPE 12065 with two-hole die.

die radii) is 13.3 cm/s, which is 53% of the average velocity.

Figure 5.2 depicts the flow curves of HDPE 12065. There is a similar discontinuity. However this time, it starts at higher shear stress: over 0.35 MPa. One can also find three parts of the flow curves as found for HDPE 16A. Spurting is also found in large channel at the beginning of discontinuity.

Figure 5.3 shows the flow curves for LLDPE 12J1. Letters A, B, C, and D in the graph are to be used for the later

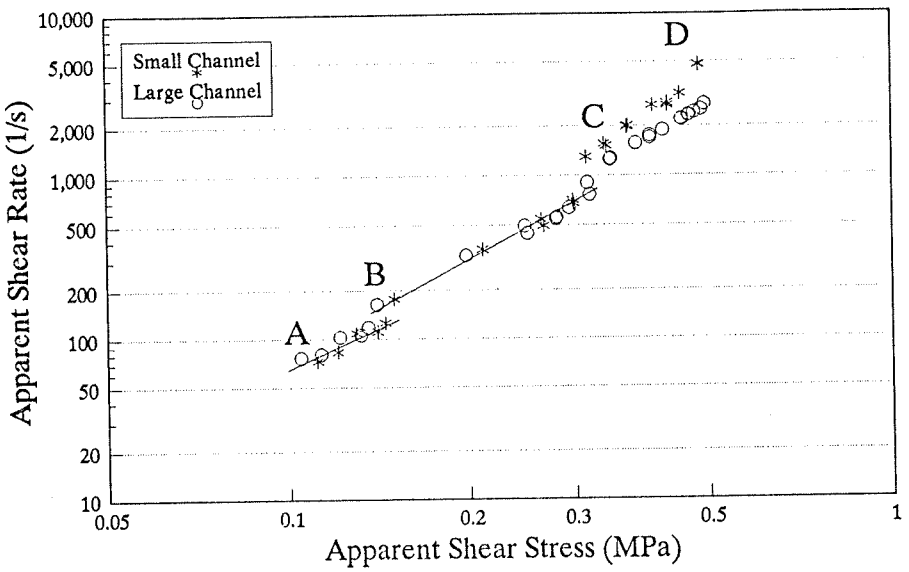

Figure 5.3. Flow curve of LLDPE 12J1 with two-hole die.

discussion. This figure shows two discontinuities: one below 0.2 MPa and the other over 0.3 MPa. Before the second discontinuity, the apparent shear rate values from the two channels coincide, and the extrudates are smooth. After the first discontinuity, we found surface roughness. Such discontinuity should be caused by wall slip, which, however, can not be detected by Mooney's equation, since the two flow curves from the two channels still concide after first discontinuity. Another possibility is that the difference of the two flow curves is too small to be detected by the two hole die because of the low slip velocity.

Further, there is no overlapping at both discontinuities that implies no significant pressure decreases at the two discontinuities. This differs from the flow curve for the two HDPE polymers. In other words, the changes in the flow curves are less abrupt than those of HDPE. Moreover, in the discussion of next section, we will see rather graduate roughness development with LLDPE.

After the second discontinuity, the apparent shear rate in the small channel is higher than that of large one. This indicates wall slip.

5.2.2 Observation of Extrudate Roughness and Associated Wall Slip

Extrudate roughness is observed at the discontinuities for the two HDPE polymers. While for the LLDPE polymer, roughness starts at a rather lower apparent shear rate: at the first discontinuity.

Since there are overlapping area at the discontinuities for HDPE polymers, a given shear stress corresponds to more than one apparent shear rate. It is because that the shear stress doesn't increase with the flowrate monotonously. Therefore higher apparent shear stress in the discontinuity

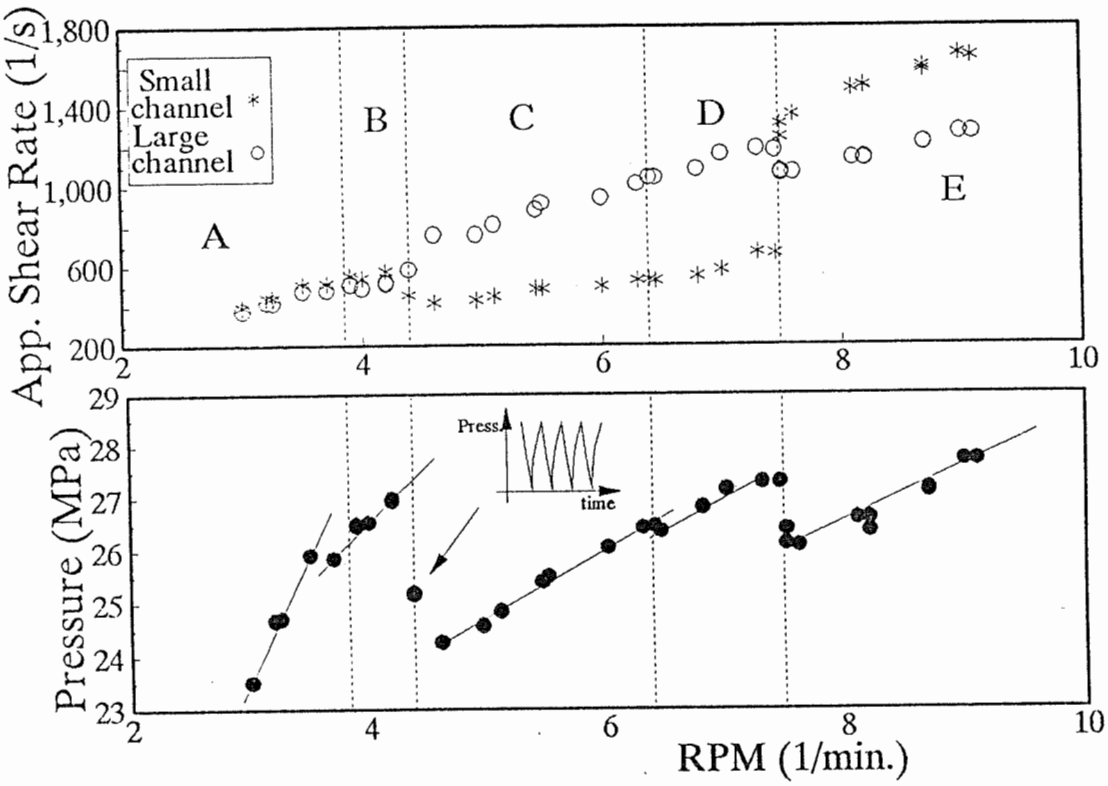

Figure 5.4. Apparent shear rate and reservoir pressure variations of HDPE 16A.

region doesn't necessarily correspond to a higher flow rate. Moreover, since there are two channels, the apparent shear rate in one channel can be higher than the other, which makes it difficult to interpret the flow situations through flow curves. In order to have a clearer picture of what happened at the discontinuity, a plot (to be called "RPM based plot") of the apparent shear rate and reservoir pressure versus the extruder RPM will be used in the following discussion.

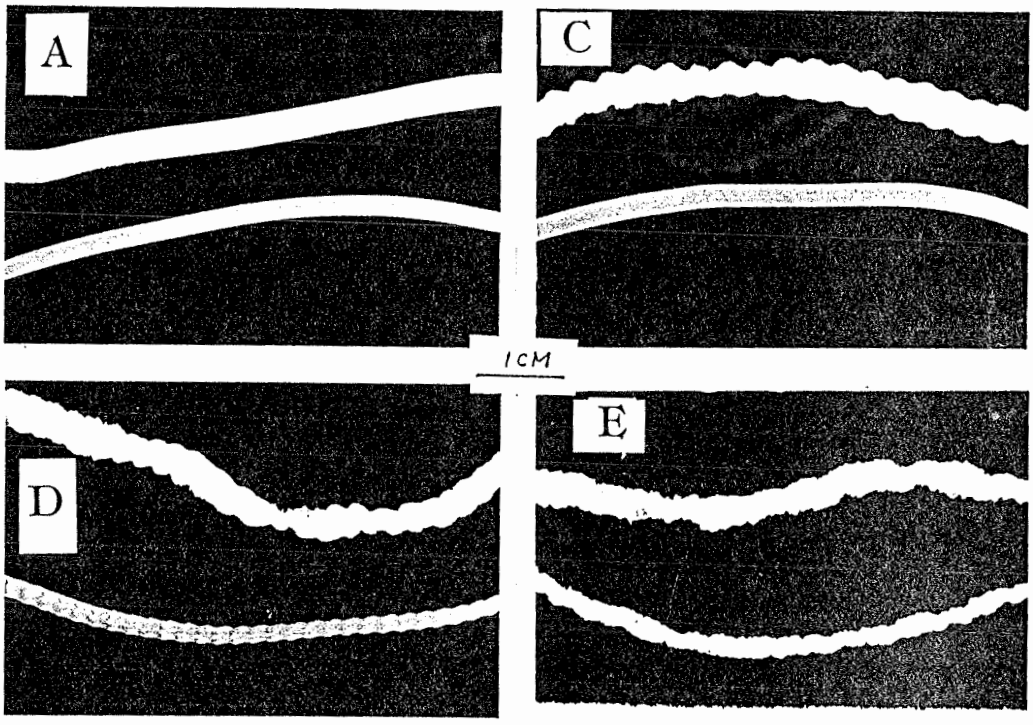

Figure 5.5. Photos of extrudates of HDPE 16A. A, C, D, and E are corresponding to the sections in Figure 5.4.

Figure 5.4 shows the RPM based plot for HDPE 16A. The upper part is the apparent shear rate; the lower part the reservoir pressure. The figure covers the apparent shear rate range of 200 to 1800 (1/s), mainly overlapping zone shown in Figure 5.1. Figure 5.4 is divided into five sections, from A to E according to extrudate appearances. The photos of extrudates A, C, D, and E are shown in Figure 5.5. The spurting sample of section B will be discussed in the next section.

Section A. The apparent shear rate from the two channels coincides and the reservoir pressure increases steadily with RPM as shown in Figure 5.4. Extrudates for this section are smooth for both channels, (A in Figure 5.5).

Section B. Very fine roughness (almost not visible) appears associated with slight apparent shear rate split. At the same time, the reservoir pressure shows a slight down shift at the beginning of the section. This indicates start of wall slip. At the end of section B, spurting phenomenon happened in large channel (to be discussed later).

Section C. After spurting, the large channel produces rough extrudates while the small one gives a smooth extrudate.

The apparent shear rate in the large channel jumps to a high value, but the reservoir pressure shows an abrupt drop (Figure 5.4). This is attributed to slip in the large channel. Note that the apparent shear rate in the small channel is even lower than that in Section B. This is because that the total flowrate (from both channels) does not change abruptly (which is controlled by RPM), the sudden decrease of flow resistance of the large channel is bond to cause a decrease of polymer melt through the small channel. Slip is closely related with extrudate roughness: the rough extrudate is from the slipping large channel. On the other hand, the larger pressure drop represents a more severe slip compared to that in section B.

Section D. As the RPM increases the small channel begins to show rough extrudate (Figure 5.5, D) and this causes a slight decrease of the reservoir pressure and a gradual increase of the apparent shear rate in the small channel (Figure 5.4). It is interesting to see that although the small channel shows roughness, it's apparent shear rate is still lower than large channel. This time, the polymer in the small channel begins to slip but with lower slip velocity than that in the large channel.

Section E. The apparent shear rate in the small channel jumps at the beginning of this section to a value even higher

than that of the large channel. It is certain that slip occurs in the small channel, which can be showed by Mooney's plot. However it is hard to say the two channels experience the same slip velocities. This section also features rough extrudates from both channels (Figure 5.5, E) but the roughness from the small channel is more severe than that in section D. The decrease of the reservoir pressure can be explained as the result of sudden decrease of resistance in the small channel.

Figure 5.6 shows a similar graph for HDPE 12065. The graph is also divided by four sections: A, B, C, and D. The corresponding photos of extrudates are shown in Figure 5.7.

Section A. This is the same as that of section A in Figure 5.4 featuring stable flow and smooth extrudates.

Section B. Spurting happens in the large channel while the smooth extrudate comes out of the small channel. The extrudate samples are shown in Figure 5.7 B. The extrudate of the large channel changes from rough to smooth. However, the roughness is not obvious.

Section C. This section is quite similar to section D of Figure 5.4. There is a pressure down shift at the beginning

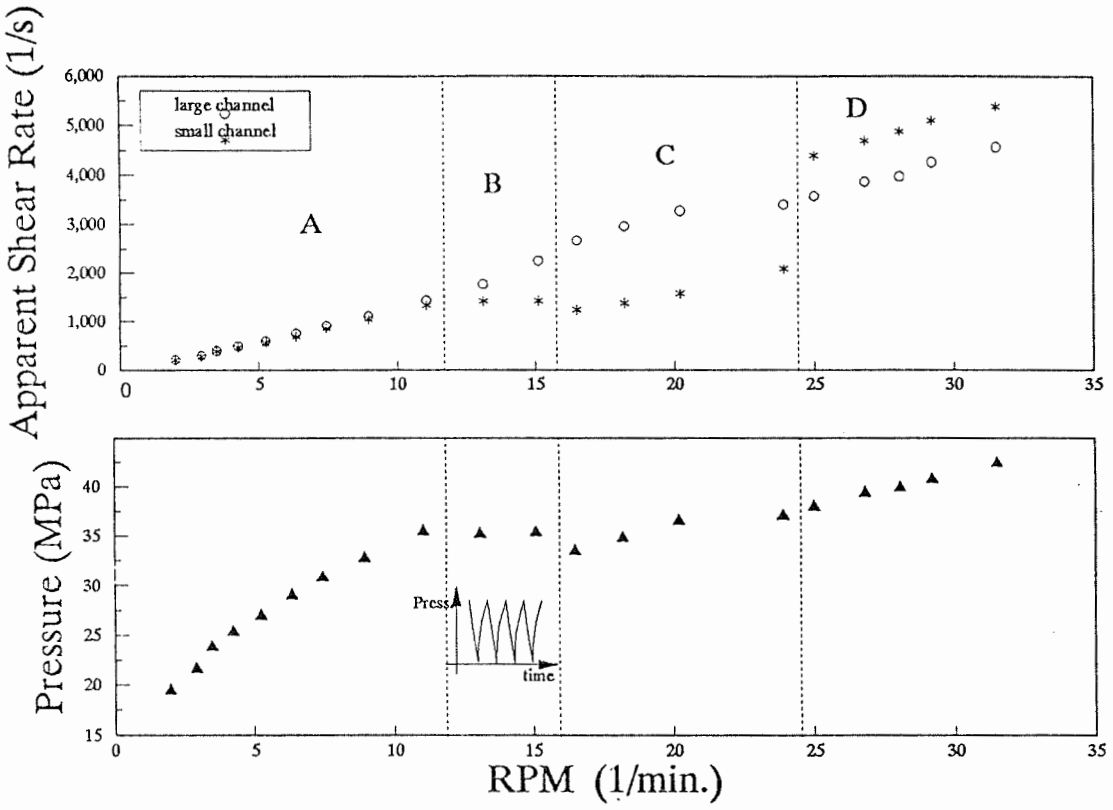

Figure 5.6. Apparent shear rate and reservoir pressure variations of HDPE 12065.

when the spurting of the large channel has changed to continuous roughness. The pressure decrease is in the same order (0.3 MPa) as that shown in section C of Figure 5.4. At the same time, the apparent shear rate in the large channel increases and that of small channel decreases. The striking difference is that the roughness of HDPE 12065 (Figure 5.7) is remarkably less severe than that of HDPE 16A (Figure 5.5) although both polymers show sign of slip. This suggests that

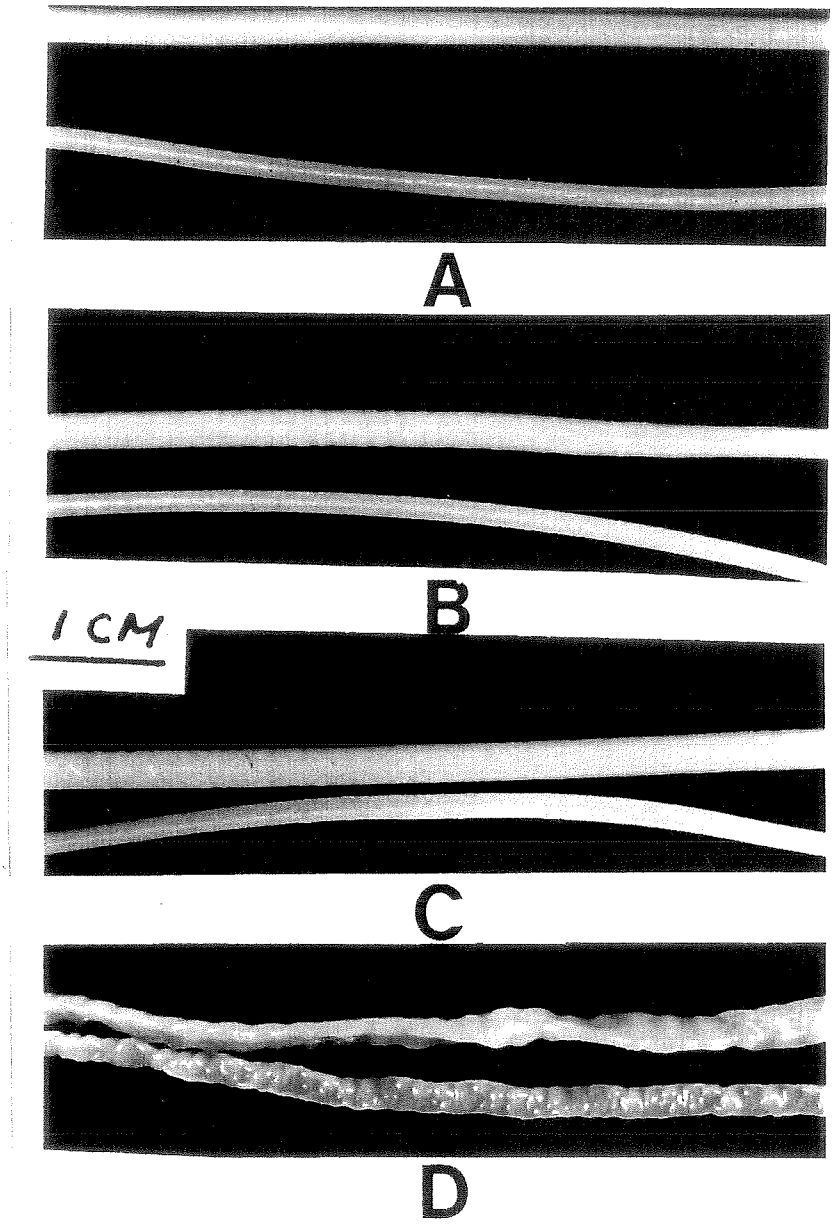

Figure 5.7. Extrudate photos of HDPE 12065. A, B, C, and D are corresponding to the sections in Figure 5.6.

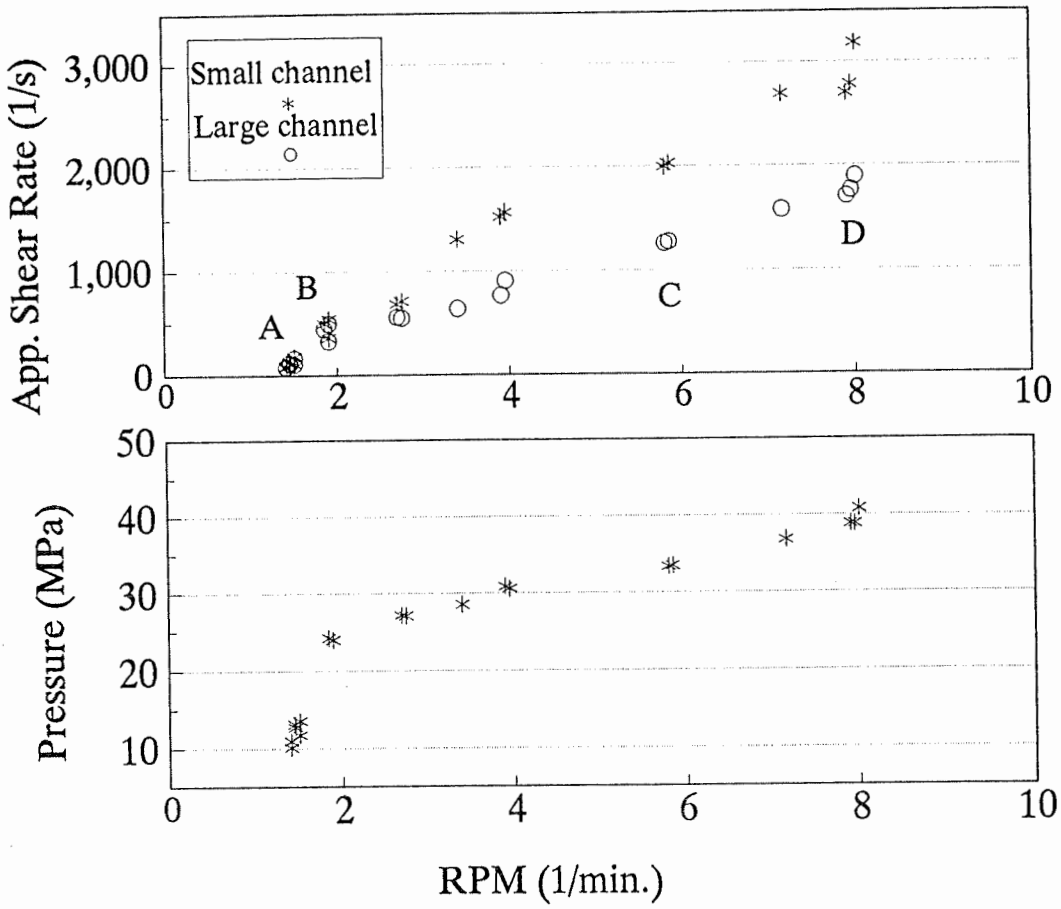

Figure 5.8. Apparent shear rate and reservoir pressure variations of LLDPE 12J1.

the extrudate distortion depends much on the molecular structure of the polymer. Figure 3.1 and 3.2 illustrates molecular distributions of the three polymers used. HDPE 16A exhibits a high molecular weight tail which is not the case for HDPE 12065. These large molecules likely cause more severe extrudate roughness. The molecular distribution of HDPE 16A is also wider (Mw/Mn=7.85) than that of HDPE 12065 (Mw/Mn=5.7). This could also contribute to extrudate roughness. Rudin (1970) has suggested that a wider distribution promoted melt elasticity.

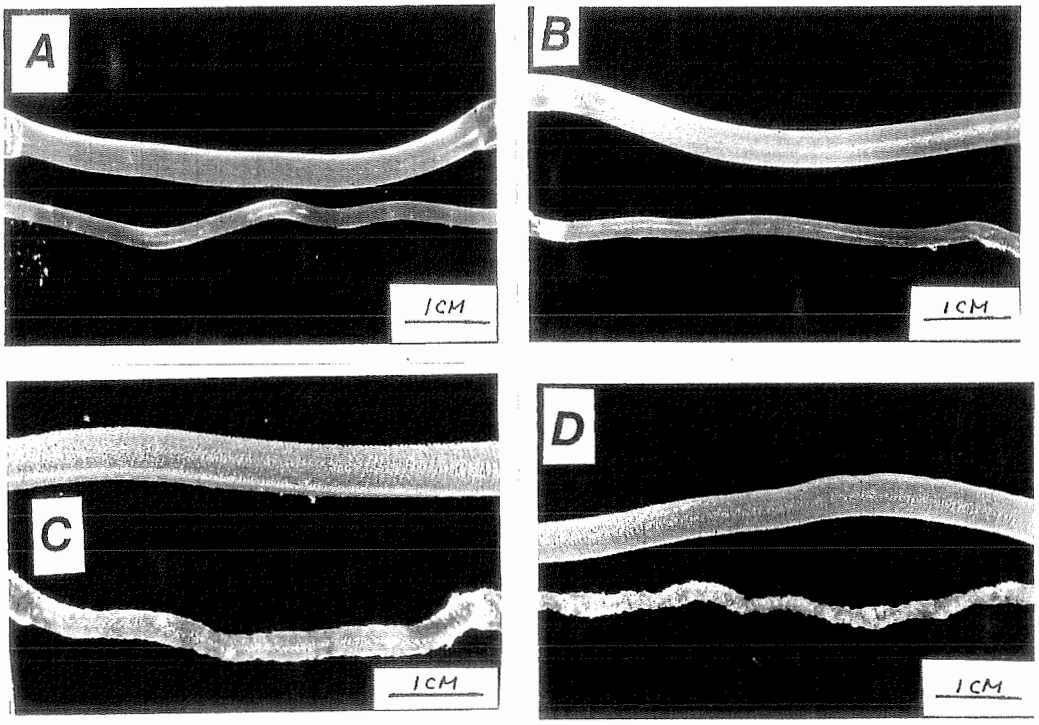

Figure 5.9. Extrudate photos of LLDPE 12J1. A, B, C, and D are corresponding to the sections in Figure 5.3.

Section D. This section is similar to that of section E for HDPE 16A (in Figure 5.4). Here the extrudates are rather flat-shape deformed, more serious fracture compared to that shown for HDPE in Figure 5.5.

RPM based plot of LLDPE 12J1 is shown in Figure 5.8. Since the extrudate roughness as observed at a lower apparent shear rate, the figure covers all the apparent shear rate range shown in Figure 5.3. Compared to the graphs for two HDPE polymers, there is no distinct apparent shear rate jump nor reservoir pressure drop.

The reservoir pressure increases rapidly at the early stage of the extrusion (where the first discontinuity occurs) and then levels off at an apparent shear rate of 1000 1/s. It is at that point that the second discontinuity occurs. Both discontinuities are not obvious in the RPM based graph here but is better shown in form of flow curve by Figure 5.3. Before this point, the apparent shear rate values for both channels coincide which demonstrates no wall slip based on Mooney's Equation. Starting from this point, the apparent shear rates in the small channel is larger than that in the large one. This suggests the beginning of wall slip. Since less energy is needed for the extrusion, the reservoir pressure doesn't increase at the same rate as before. The obvious pressure decreases observed for HDPE 16A and HDPE 12065 are not seen here. It is possible that the slip here happens between the polymer near the wall and that stick to the wall (cohesive failure) rather than between polymer and solid wall.

Since the flow curve in Figure 5.3 gives a better view of discontinuities, the extrudate distortions will be discussed in relation to the flow curve. Figure 5.9 shows the extrudate photos in the typical regions of Figure 5.3 indicated by A, B, C, and D.

Sample A represents a stable extrusion with smooth surface before the first discontinuity.

Sample B shows the extrudate at the first discontinuity. The extrudates of both channels show a very fine surface roughness (light sharkskin), even hardly visible in the photo. During extrusion, we found the emerging extrudate became opaque. This indicated fine roughness at the extrudate surface reducing the transparency of the polymer melt.

Sample C features extrudates at the second discontinuity. Here both extrudates show visible roughness. The large extrudate still shows surface roughness while the small extrudate shows signs of gross fracture. However, compared to the HDPE extrudates (Figure 5.5 E and 5.8 D), the roughness shown here is rather mild.

Sample D shows the extrudates at further higher apparent shear rates. There is no dramatic change from the sample C,

but the small extrudate shows a more severe gross fracture.

Overall, the LLDPE extrudate roughness shows a rather gradual development. The differences between HDPE and LLDPE polymers are believed to be caused by polymer structures. One reason might be that LLDPE has more branching structures than HDPE does and that branching reduces the severity of extrudate roughness as reported by some researchers (discussed in Chapter 2).

5.2.3 Spurting Phenomenon

At the beginning of their discontinuities, HDPE 16A and 12065 demonstrate spurting phenomena. When spurting happens, the reservoir pressure oscillates. Figures 5.10 and 5.11 show examples of pressure oscillations for HDPE 16A and HDPE 12065. Both figures show the same order of amplitude but higher frequency for HDPE 12065.

Figure 5.12 shows the photo of HDPE 16A extrudates during spurting. (The extrudate appearances of HDPE 12065 shows less contrast between rough and smooth. Therefore samples of HDPE 16A were chosen). "a" shows the large extrudate changing from rough to smooth, while the small extrudate remains smooth; "b"

shows the large extrudate changing from smooth to rough. The correlation between the extrudate appearance and the pressure oscillations is schematically illustrated in Figure 5.13. The extrudates from both channels are smooth until the pressure reaches the peak value. As the pressure starts to decrease, the large channel starts to produce a rough extrudate (Figure 5.12, "a"). After reaching a minimum value, the pressure starts to climb again. At the same time the extrudate of large channel returns to smooth appearance (Figure 5.12, "b"). The corresponding average flowrate in the large channel increases from 9.84 g/min to 21.1 g/min. Meanwhile, the flowrate of small channel decreases form 2.2 g/min to 1.2 g/min. More than 150% increase of flowrate in large channel suggests wall slip, especially when considering pressure decrease at the same time.

There are still two main questions to answer: 1) why does roughness appear during the slipping period, 2) why does spurting happen in large channel?

1) Regarding to whether the extrudate is smooth or rough in the period of slip, there are different opinions. Bagley et al. (1958) reported HDPE roughness of extrudate when pressure decreased (when slip happened). Kissi and Piau (1990) observed "virtually but not totally smooth" extrudate during slip

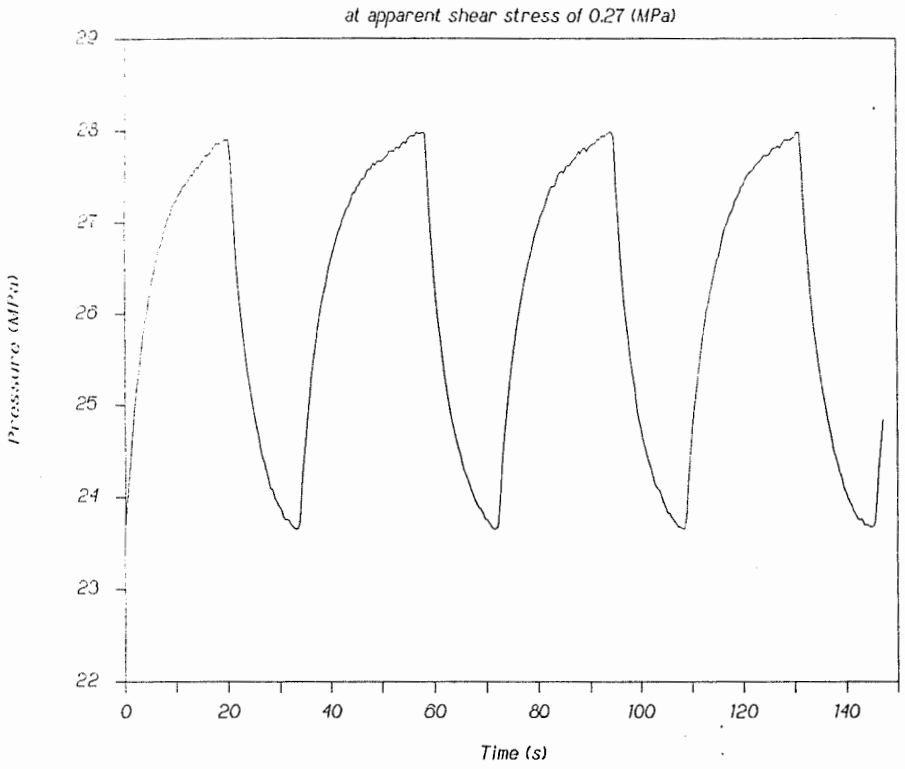

Figure 5.10. Pressure oscillation of HDPE 16A at spurting.

period but cracked surface during the stick period, for a silicon fluid at room temperature. Based on our results, (in Figure 5.13) roughness happens during the slip period. Since slip causes larger deformation of polymer melt at the die entry, hence possibly more elastic energy is accumulated. Therefore, as the polymer exits the die, the energy is released, which leads to the extrudate roughness. If such energy is large enough, it will causes gross fractures. The type and severity of roughness also depend on the nature of the polymers.

2) In two-hole die extrusion, spurting has been observed only in the large channel. The sudden slip in the large

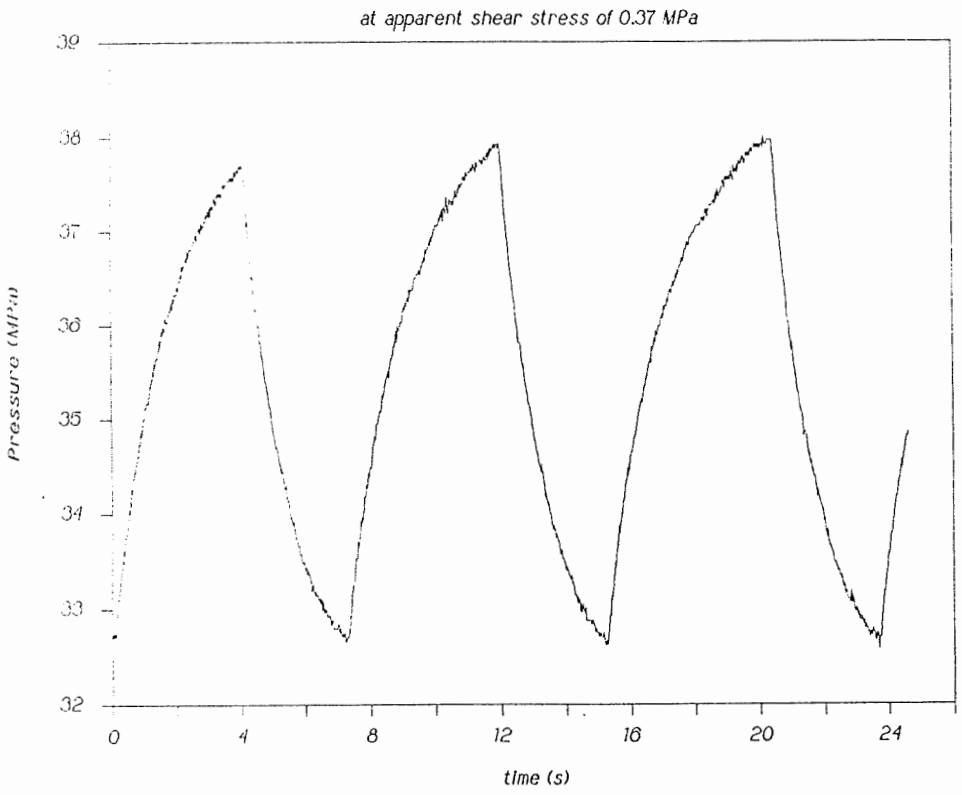

Figure 5.11. Pressure oscillation of HDPE 12065 at spurting.

channel creates a large pressure decrease in the reservoir. When there is slip in the small channel, the decrease of the overall flow resistance and increase of flowrate are not large enough to cause significant pressure variations. So there is no pressure oscillations and no spurting occurs in the small channel. Therefore, the spurting is only observed in the large channel. It is important to pointed out that it does not mean that the use of a large diameter die will favour spurting when a single channel die is used.

5.3 SUMMARY OF TWO-HOLE DIE EXTRUSION

Wall slip was clearly demonstrated by a sudden jump in

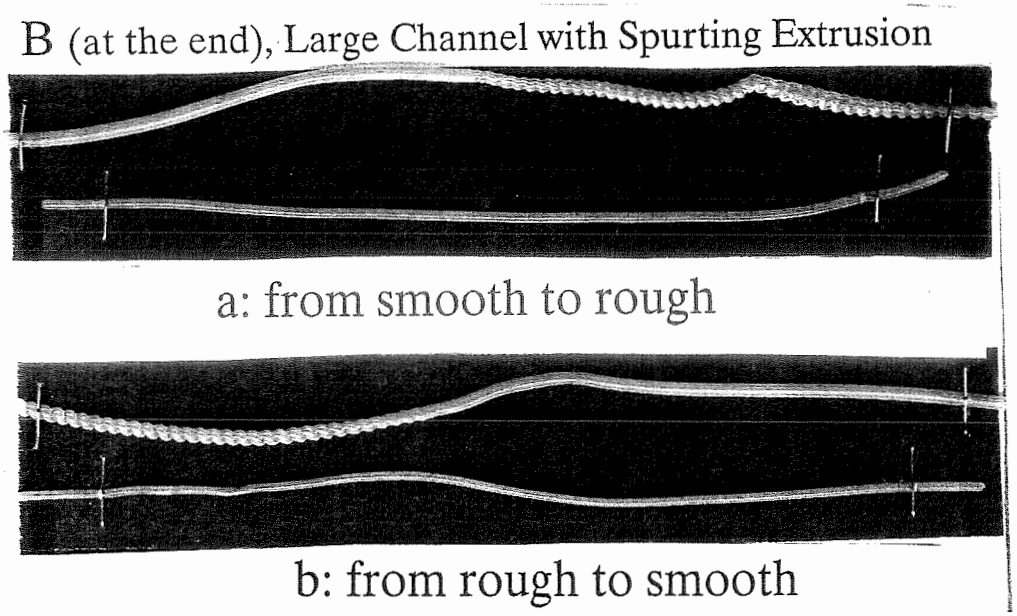

Figure 5.12. Extrudate samples of HDPE 16A during spurting.

the apparent shear rate of one channel but not in the other channel under the same reservoir pressure. Wall slip is usually associated with a reservoir pressure decrease. The magnitude of the decrease depends on the nature of the polymer. For this particular two-hole die extrusion, the pressure is affected more by the large channel than by the small channel. Wall slip is also accompanied by extrudate roughness. However, the presence of roughness does not necessarily assure the existence of wall slip. The spurting phenomenon was observed for the large channel with the HDPE polymers. It suggests that the wall slip inside the die could be the major cause of spurting. The diameter effect on the

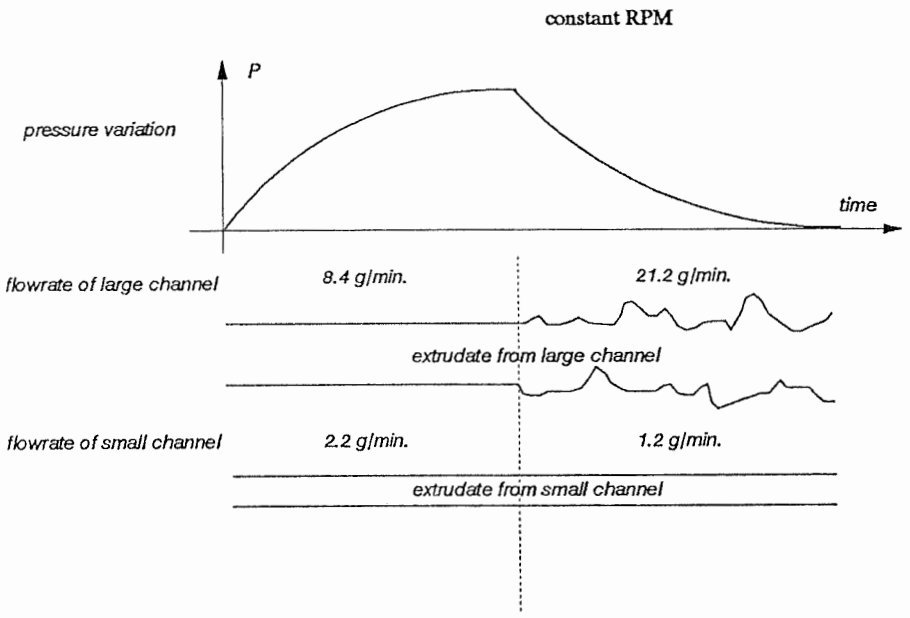

Figure 5.13. Schematic diagram of pressure change during spurting of HDPE 16A. This is under constant RPM.

severity of extrudate roughness is not so evident.

CHAPTER 6

EXTRUSION WITH SLIT DIE

6.1 INTRODUCTION AND PRINCIPLES

The two-hole die experiment (discussed in Chapter 5) shows wall slip during extrusion, especially when the extrudate roughness appears. This confirms the presence of slip proposed by many researchers (Bartos and Holomek, 1971, Ramamurthy, 1986, El Kissi and Piau, 1990, Hatzikiriakos and Dealy, 1991 and 1992). Since slip exits, the detection of where the slip is initiated along the die will help us to understand the mechanism of this phenomenon.

One of the possible approaches to obtain such information is to measure the instant pressure variations along the die. The curved surface of capillary die makes it difficult for flush mounting pressure transducers along the die. The reliability of the pressure data will be questionable. Therefore, we designed a long slit die allowing three pressure transducers to be flush installed at the surface along the die land. With the help of a rapid data acquisition system, we can obtain fast pressure responses. Since wall slip is closely related to pressure variations, the slit die enable us to determine wall slip along the die land.

According to Mooney's equation (Appendix I), if there is wall slip, the measured flowrate is a combination of slip flow (plug flow) and shear flow.

$$Q=Q_{slip}+Q_{shear}=w\cdot h\cdot u(w)+\frac{1}{4}\frac{wh^2}{\sigma_w^2}\int_0^{\sigma_w}\dot{\gamma}(\sigma,T)\,d\sigma^2 \qquad \textbf{(6.1)}$$

where Q, Q_{slip} and Q_{shear} are the total flowrate, flowrate contribution by wall slip, and flowrate contribution by shear flow. u(w) is wall slip velocity, w is the width of the die, h is the gap the die, $\dot{\gamma}(\sigma,T)$ is the shear rate, σ is the shear stress and σ_w is the shear stress at die wall. At constant total flowrate, if Q_{shear} decreases, Q_{slip} should increase, or slip velocity should increase. Q_{shear} is a function of the shear stress σ as shown in Equation 6.1 and shear stress is related to pressure gradient by $\sigma=z(dP/dx)$ (where P is the pressure , z and x are indicated in Figure 1A in appendix I). Then the decrease of Q_{shear} is indicated by a decrease of pressure gradient (dP/dx). Therefore at constant flowrate (or increase in flowrate), a decrease of dP/dx means increase of Q_{slip}. As Q_{slip} is proportional to the wall slip velocity u(w), a decrease of dP/dx demonstrates increase of slip velocity, or start of slip.

Lim and Schowalter (1989) verified the pressure-slip relationship with a slit die. They found that increase of slip

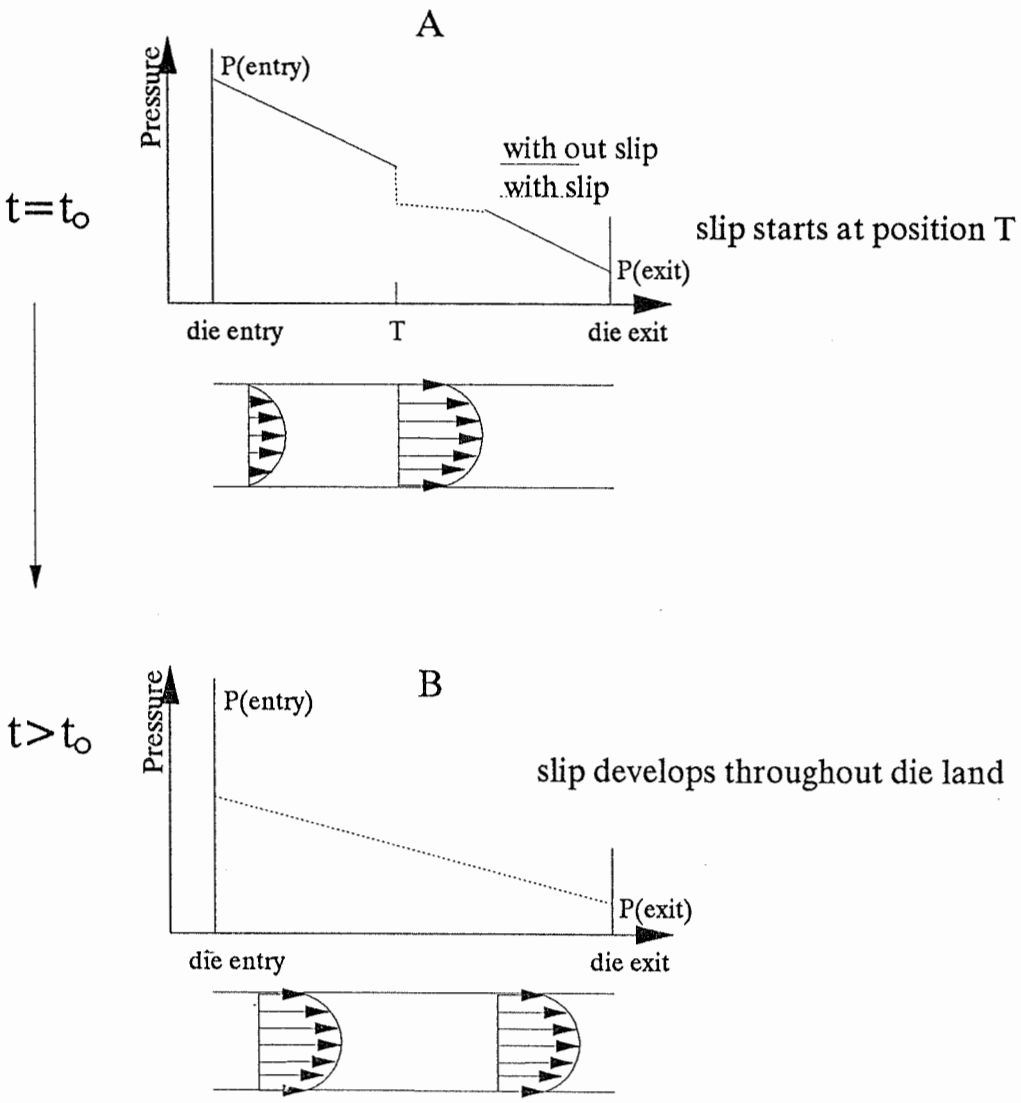

Figure 6.1. Development of wall slip and related pressure profile across the die land.

velocity leads to a decrease of wall pressure. Their result corroborates the analysis discussed so far based on Mooney's Equation. **Therefore the information of instant pressure variation along the die land can also be used to detect slip.**

Wall slip might be initiated at any position along the die land. Figure 6.1 (upper part) shows a case when slip starts at position T. At this moment, wall slip is not uniform and pressure profile is not linear. This type of slip can not be detected by measuring reservoir pressure. However the slip will propagate quickly through the die (this process happens in order of a second based on our slit results) and lead to linear pressure profile as shown in the bottom part of Figure 6.1.

It should be pointed out that this is based on the assumption that there is no sudden decrease of viscosity of the polymer melt. However, it is now fairly established that most polyethylenes slip when the wall stress is greater than 0.1 MPa (Hatzikiriakos and Dealy, 1992). Therefore the pressure decrease under shear stress higher than that critical value is mainly attributed to wall slip but not the viscosity decrease.

If we assume the polymer material obeys a power law

relationship, under isothermal conditions, the slip velocity can be calculated from Mooney's Equation (Appendix I)

$$\frac{6u(w)}{h} = \dot{\gamma}_a - \frac{3n}{2n+1}\left(\frac{\sigma_w}{m}\right)^{(1/n)} \qquad (6.2)$$

since $\sigma_w=(h/2)(\Delta P/L)$, ($\Delta P$ is pressure drop through die length without end effect, L is the length of the die, m and n are the power law parameters) then Equation (6.2) becomes

$$\frac{6u(w)}{h} = \dot{\gamma}_a - \frac{3n}{2n+1}\left[\frac{h\Delta P}{2Lm}\right]^{(1/n)} \qquad (6.3)$$

Equation 6.3 allows us to calculate the slip velocity if the real pressure drop can be measured.

If slip velocity is different along the die (Hatzikiriakos and Dealy, 1992), this calculation provides us only an approximation of slip velocity since it assumes that the slip velocity is identical across die land.

For the beginning moment of slip (as shown in upper part of Figure 6.1), assuming that the flowrate is constant for the short period of time, we can obtain the local slip acceleration by deviation of Equation 6.3.

$$\frac{\partial u(w)}{\partial t} = -\frac{h}{6}\frac{3}{2n+1}\cdot\left(\frac{1}{m}\right)^{\frac{1}{n}}\sigma_w^{\frac{1}{n}-1}\frac{\partial \sigma_w}{\partial t} \qquad (6.4)$$

6.2 FLOW CURVE AND EXTRUDATE ROUGHNESS

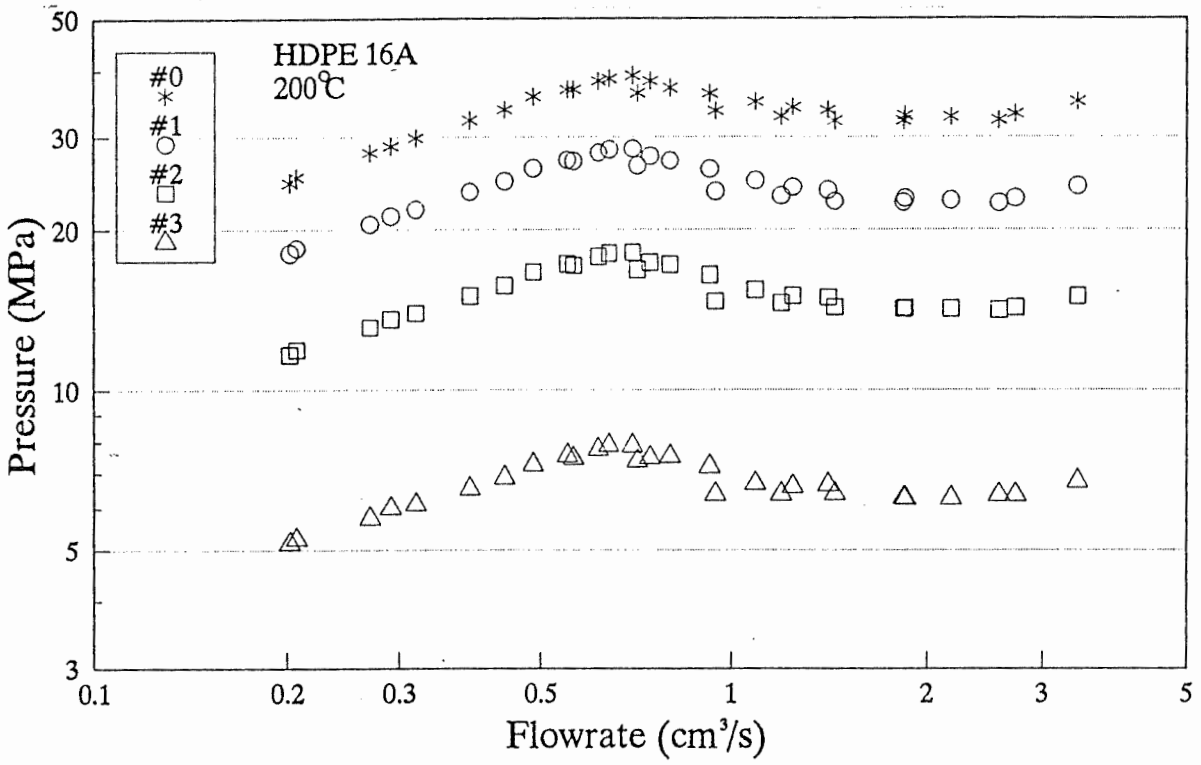

Figure 6.2. Pressure variations of HDPE 16A at 200 °C from slit die extrusion. #0, #1, #2, and #3 represent four positions depicted in Figure 3.8.

The extrusions were conducted at 200 °C, except for HDPE 12065, which was also run at 150 °C. The reason for the low-temperature extrusion is due to pressure limitations of extruder. Since spurting of HDPE 12065 happens at the pressure

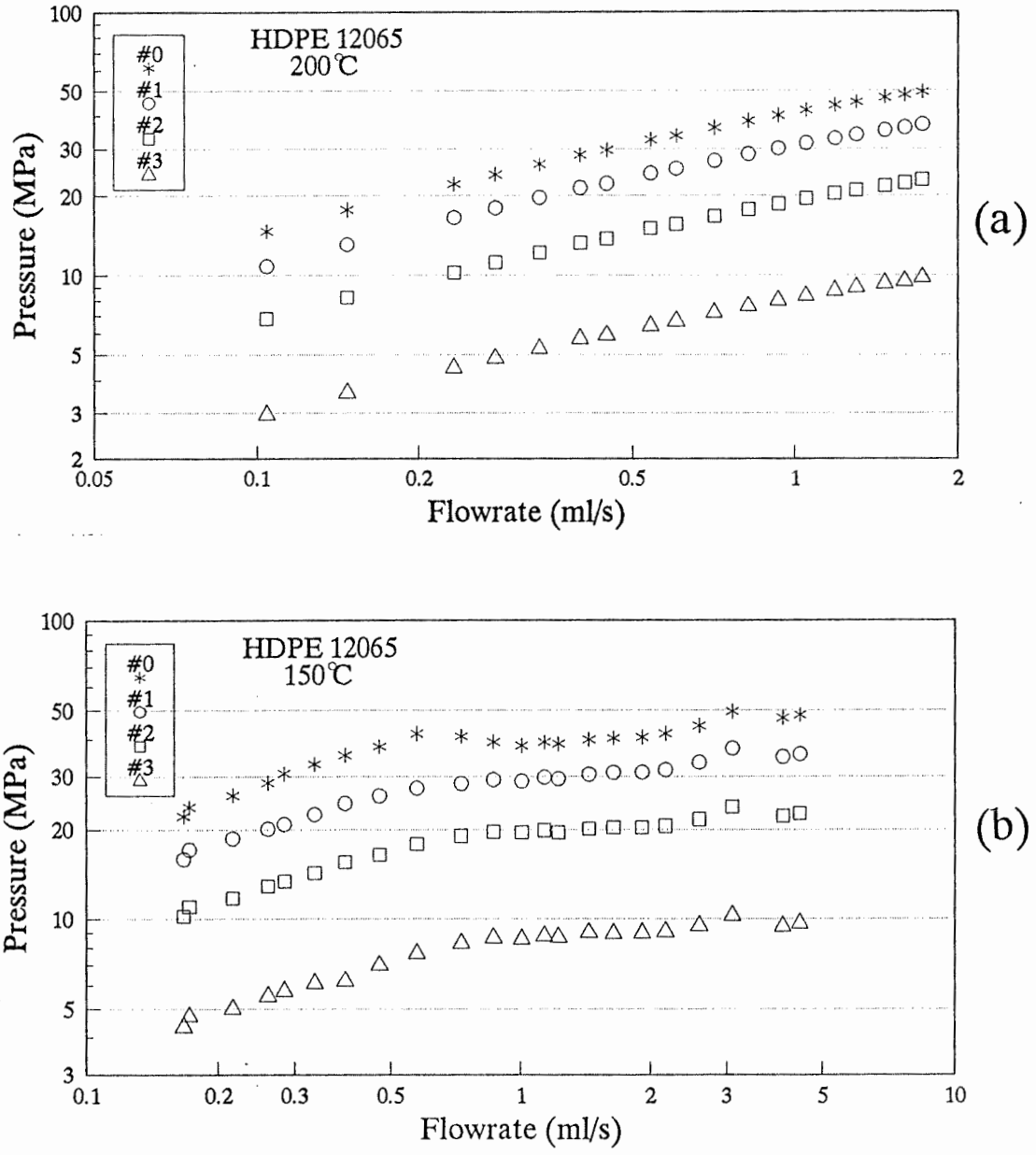

Figure 6.3. Pressure variations of HDPE 12065 from slit die extrusion at 200 °C (a) and at 150 °C (b). #0, #1, #2, and #3 represent four positions depicted in Figure 3.8.

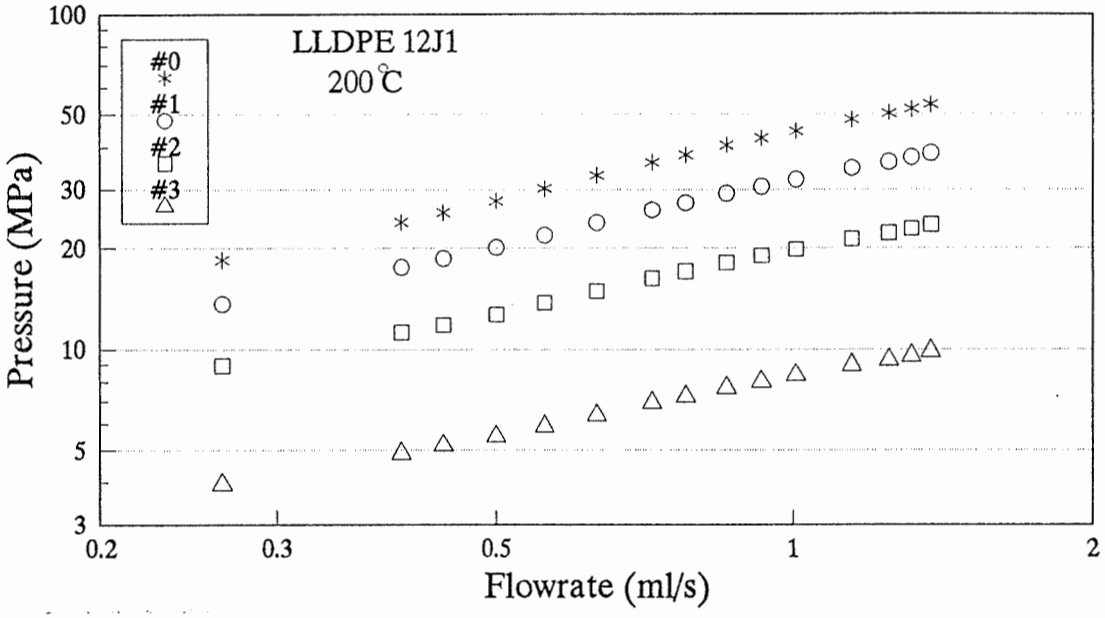

Figure 6.4. Pressure variations of LLDPE 12J1 at 200 °C from slit die extrusion. #0, #1, #2, and #3 represent four positions depicted in Figure 3.6.

exceeding the limit, we had to extrude it at 150 °C to bring down the onset pressure of spurting.

Figures 6.2, 6.3, and 6.4 show the pressure variations with flow rate at positions #0, #1, #2, and #3 (see Figure 3.8 for details of these positions) for HDPE 16A, HDPE 12065, and LLDPE 12J1.

For HDPE 16A (Figure 6.2), the pressures at the four

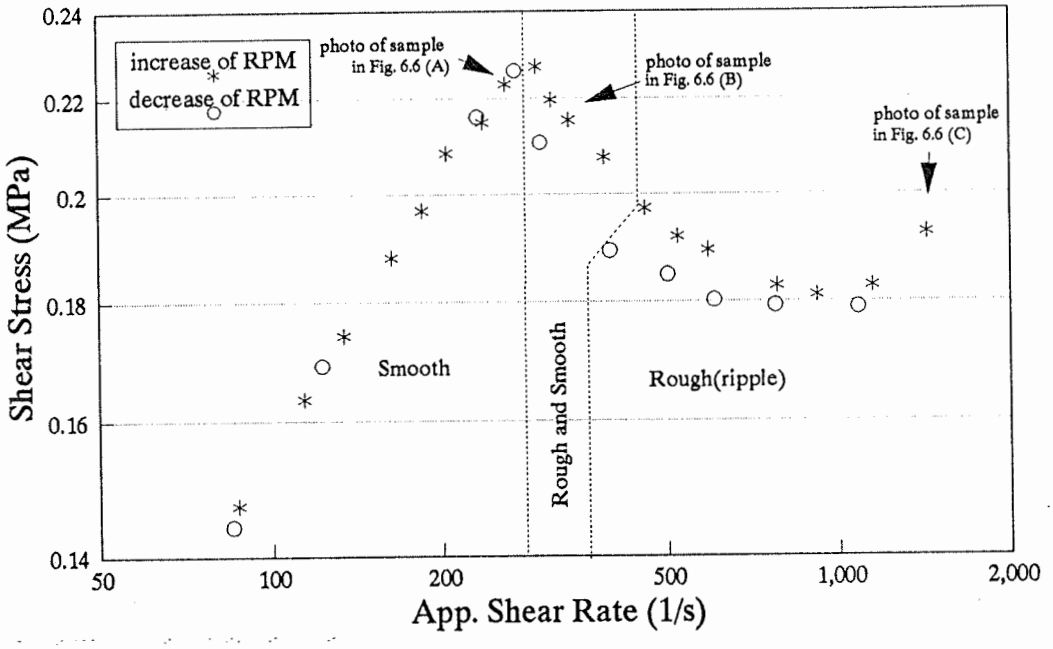

Figure 6.5. Flow curve of HDPE 16A through the slit die at 200 °C.

positions increase lineally with flowrate until the flowrate reaches 0.6 (mL/s). After that, the pressure begins to fall and eventually increases again.

Figure 6.3,(a) gives the situation for HDPE 12065 at 200 °C. The pressures of four positions increase continuously without discontinuity. Figure 6.3,(b) shows the curves at 150°C. A pressure decrease was found at position #0 at flow rate of 0.6 mL/s. At the same time, the pressures level off at #1, #2, and #3 positions.

LLDPE 12J1 (Figure 6.4) shows only linear pressure increases for all the four positions.

From the pressure measured along the die (shown from Figures 6.2 to 6.4), plots of the shear stress versus the apparent shear rate (flow curves) were obtained. Since pressures along the die were measured, the shear stress at wall was calculated by

$$\sigma_w = \left(\frac{h}{2}\right)\left(\frac{dp}{dl}\right) \qquad (6.5)$$

where h is the thickness of the slit die. The pressure gradient, dp/dl, is determined by linear regression of the pressure values at #1, #2 and #3 positions. The apparent shear rate was calculated by

$$\dot{\gamma}_a = \frac{6Q}{wh^2} \qquad (6.6)$$

where Q is the volume flowrate, w, h, the width and thickness of the slit die.

Figure 6.5 is the flow curve for HDPE 16A. Comparing the data from increasing and decreasing RPM, one could find hysteresis in the early part of the nonlinear curve which shows the fluid to be apparently thixotropic. The flow curves can be divided into three parts according to the extrudate

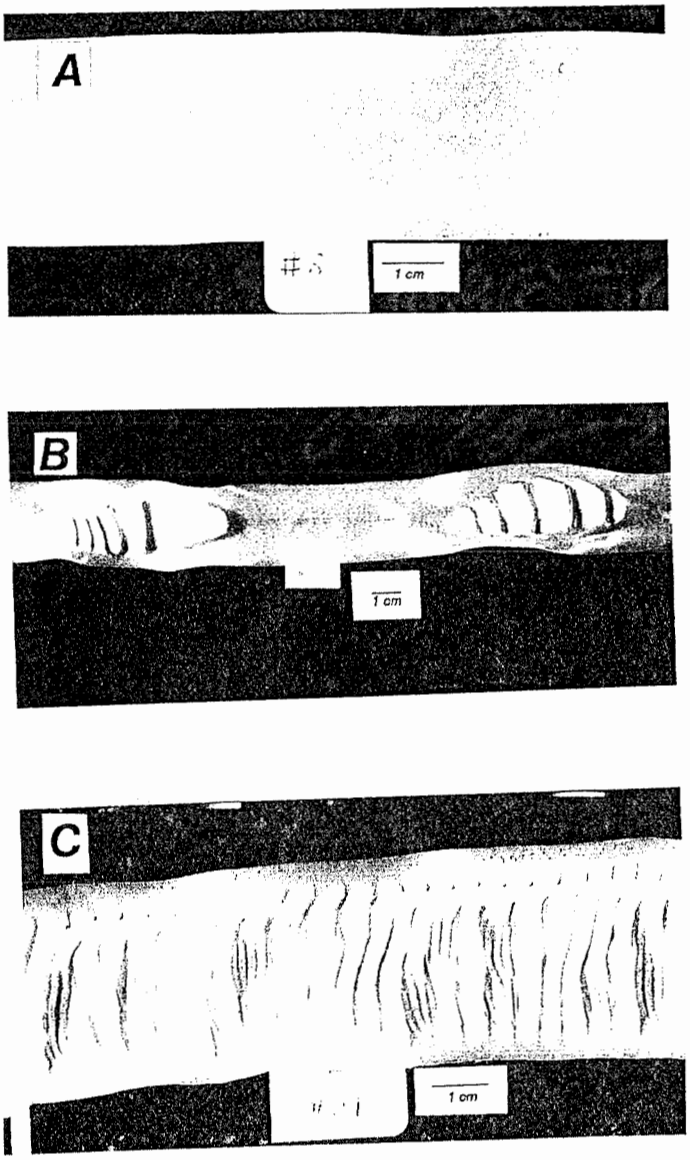

Figure 6.6. Extrudates of HDPE 16A from slit die extrusions as indicated in Figure 6.5.

appearances. The first part features a linear flow curve and smooth extrudate. The photo of a smooth extrudate at apparent shear rate of 260 (1/s) is shown in Figure 6.6 (A). The second part is associated with spurting extrusion. Stick and slip leads to rough and smooth extrudate. One such extrudate is

shown in Figure 6.6 (B). The roughness appears in the center part of the extrudate. As flowrate increases, the frequency of

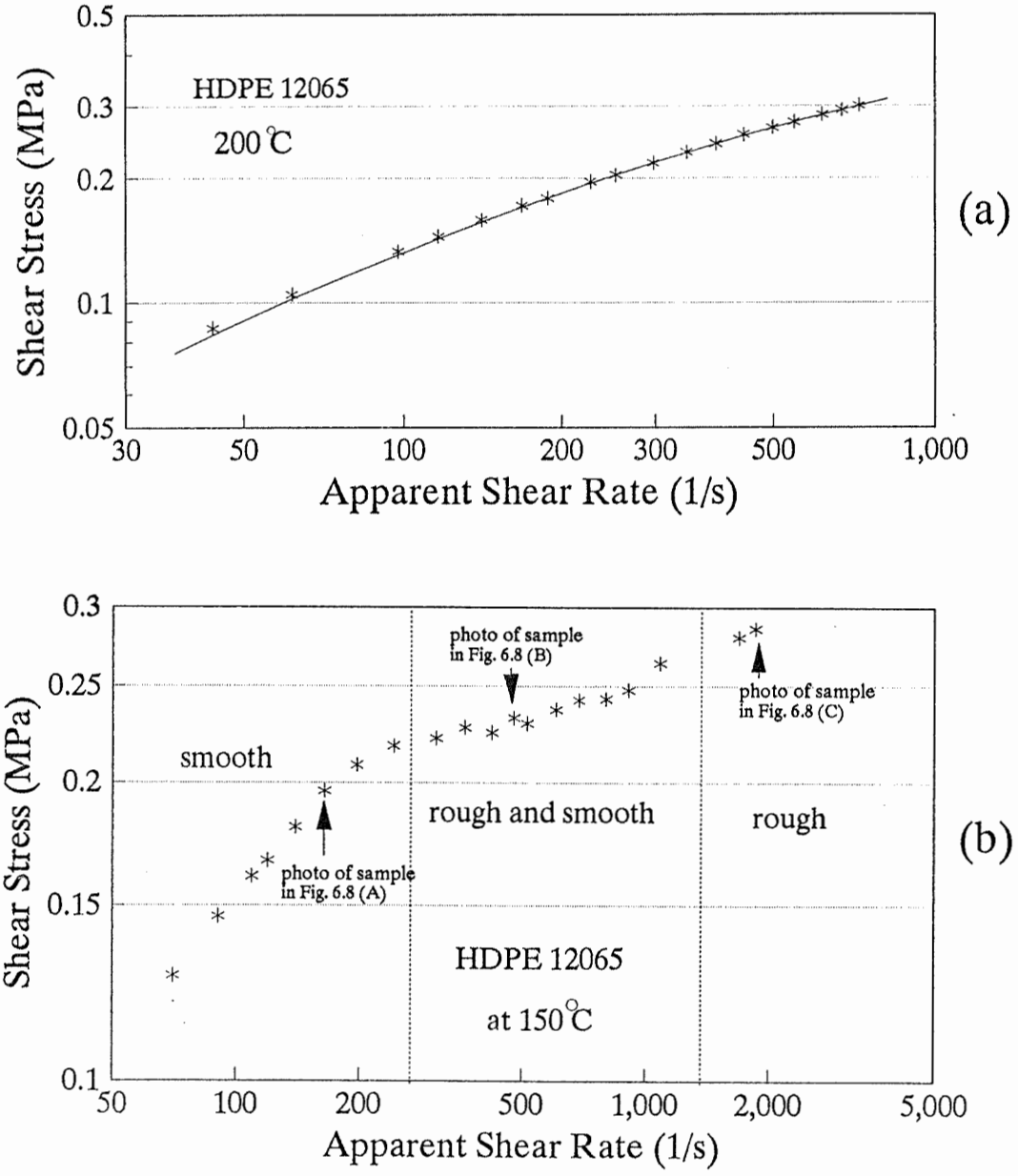

Figure 6.7. Flow curves of HDPE 12065 from the slit die at 200 °C (a) and 150 °C (b).

rough/smooth interchange increases too. The third part of the flow curve is the end of spurting and the shear stress stops falling. At the same time, the extrudate becomes continuously rough. One extrudate is shown in Figure 6.6 (C). As shown in the figure, most part of the extrudate are in ripple form, except at two edges.

Since slip flow (plug flow) requires lower energy, the pressure in the reservoir decreases as slip increases. Therefore, shear stress values calculated by Equation (6.5) is lower, which confers decreasing trend of the second part in Figure 6.5. As flowrate increases, the roughness area expends from extrudate center towards the two edges. This implies that larger portion of the polymer/solid interface begins to experience slip. As a result, the total pressure drop keeps falling, denoted as shear stress decrease in the second part of the flow curve.

The third part of the flow curve represents continuous slip in most part of the die, except at the two edges. The extrudate shows continuous roughness. The shear stress stop falling and begins to climb. This manifests end of changing from laminar flow into slip (plug) flow. Thereafter, further increase of flowrate needs more energy input, so the pressure head increases. Note as long as slip happens, σ_w obtained by

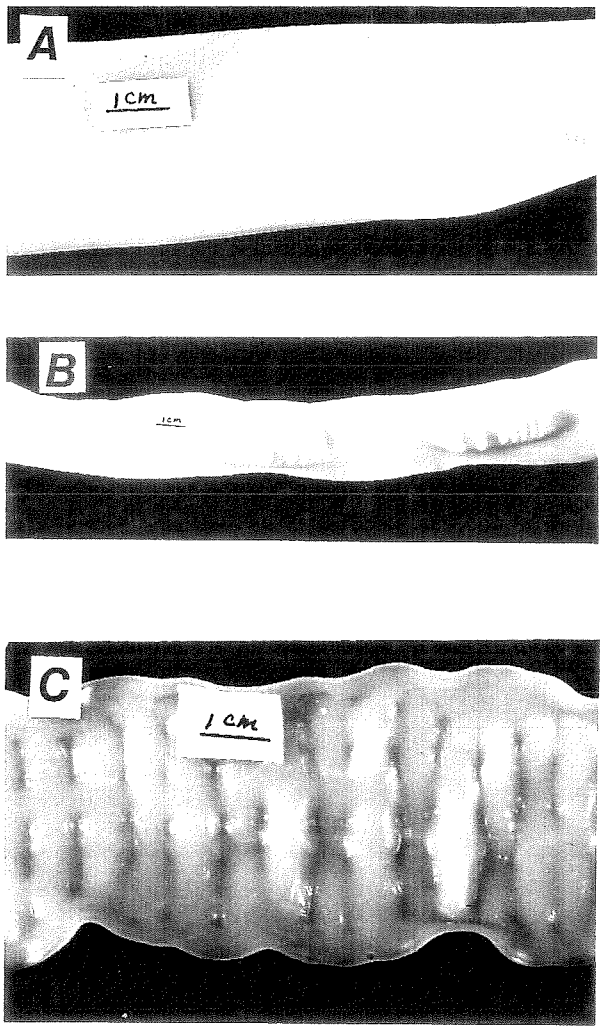

Figure 6.8. Extrudates of HDPE 12065 at 150 °C as indicated in Figure 6.7.

Equation 6.5 (which is based on non slip situation) should not be considered as the shear stress any more. It rather indicates energy consumption.

Figure 6.7 (a) shows the flow curve for HDPE 12065 at 200

°C. The curve features a continuous increase of shear stress without obvious discontinuity. The curve is not linear, showing deviation from power-law fluid. No extrudate roughness of any kind was found from the beginning to the end of the extrusion.

The flow curve at 150 °C is shown in Figure 6.6,(b). It has also three parts similar to those shown in Figure 6.5, but with no pronounced shear stress decreases. The extrudates from the three parts are shown in Figure 6.8 (A), (B), and (C) respectively. The second part has lower increasing rate of shear stress than first part. The extrudate (shown in Figure 6.8 (B)) begins to show rough and smooth surfaces: spurting begins. At the end of the second part, the extrudate becomes continuously rough (Figure 6.8 (C)). Compared to the continuous rough extrudate of HDPE 16A (Figure 6.6 (C)), the severity of the extrudate roughness of HDPE 12065 is noticeably lower, although the extrudate is under a higher apparent shear rate (1860 1/s) than that of HDPE 16A (1500 1/s).

It is noted that there is no similar shear stress decreases in the second part as those in Figure 6.5 (for HDPE 16A). This similar to the results from two-hole die extrusion. There are two possible reasons that cause the different

behaviors between the two polymers. Firstly, the extrusion of HDPE 12065 was conducted at lower temperature (150 °C). Low temperature usually causes lower slip velocity (Hatzikiriakos and Dealy, 1992). If slip velocity is low, as a result, pressure decrease is less remarkable. Secondly, differences in molecular structures between two polymers might be the more important reason. This has been discussed in Chapter 5.

The extrudate of the third part is shown in Figure 6.8 (C). It is less rough than that of HDPE 16A, (shown in Figure 6.6 (C)). Once again, it can be attributed to difference in the polymer properties.

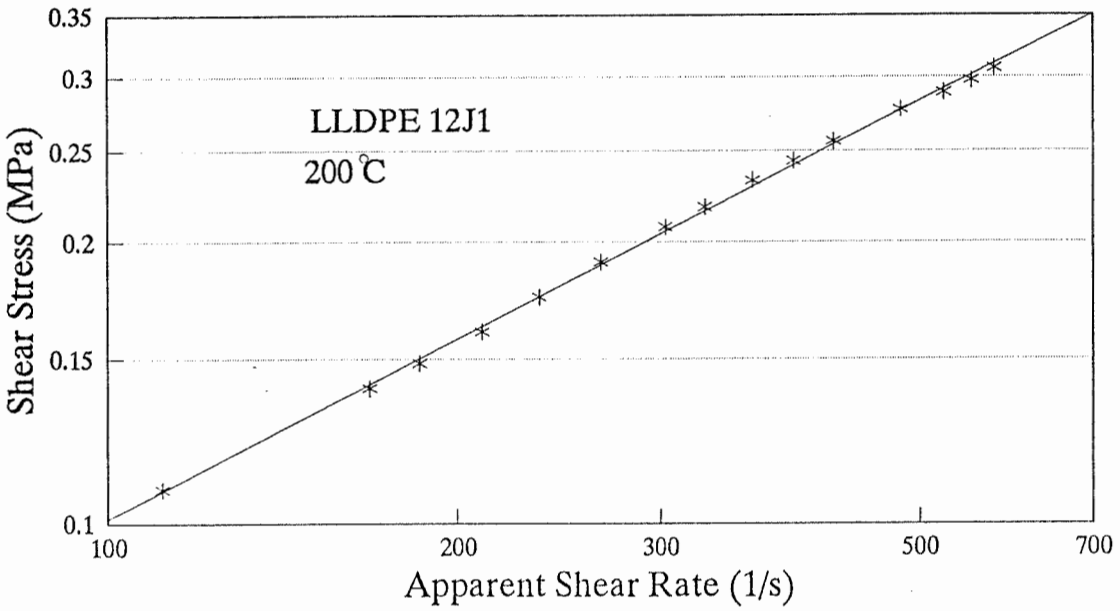

Figure 6.9. Flow curve of LLDPE 12J1 from the slit die at 200 °C.

Figure 6.9 gives the flow curve of LLDPE 12J1. It shows a very straight line throughout the extrusion range. There is no obvious slope changes or other discontinuity. Further, no extrudate roughness was observed. This is in line with the two-hole die result discussed in last chapter. However, the slit die extrudate shows even smoother surface than those of two-hole die with LLDPE 12J1. This is quite likely attributed to geometrical difference between the two dies. The slit die has L/h (length/gap) value of 81; while the two capillary channels of two-hole die have a L/D value of 24. The use of larger L/D die reduces surface roughness.

With longer die (slit die) extrudate roughness has not been found to be diminished with HDPE polymers. This again suggests different mechanisms of extrudate roughness appearances for HDPE and LLDPE polymers. Spurting and continuous roughness found for HDPE polymers are believed mainly caused by entrance flow, which is not very sensitive to the die length.

6.3 PRESSURE OSCILLATIONS DURING SPURTING

One of our goals in using a slit die is to verify where the slip starts. It is very hard to detect initiation of slip, since one cannot precisely predict the starting time of slip.

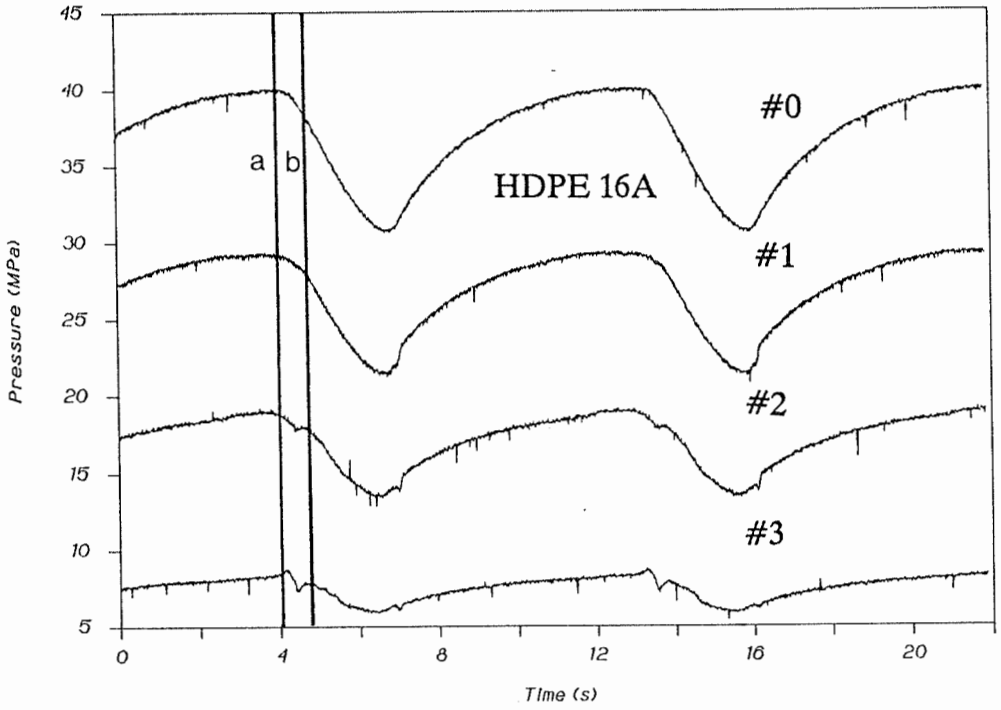

Figure 6.10. The pressure oscillations of HDPE 16A at apparent shear rate of 340 1/s. The extrudate is shown in Figure 6.7 (B).

It is more difficult to generate slip at the identical pressure conditions, so as to repeat the measurements. However, spurting provides us the best opportunity.

Figure 6.10 shows the pressure oscillations for HDPE 16A at spurting extrusion. The corresponding extrudate with this oscillation is in Figure 6.6 (B). The period of the pressure increase is associated with smooth extrudate, while the decreasing pressure is with the rough part. Four curves in

Figure 6.10 (from top to the bottom) represent the pressure variations at positions #0, #1, #2, and #3. The average

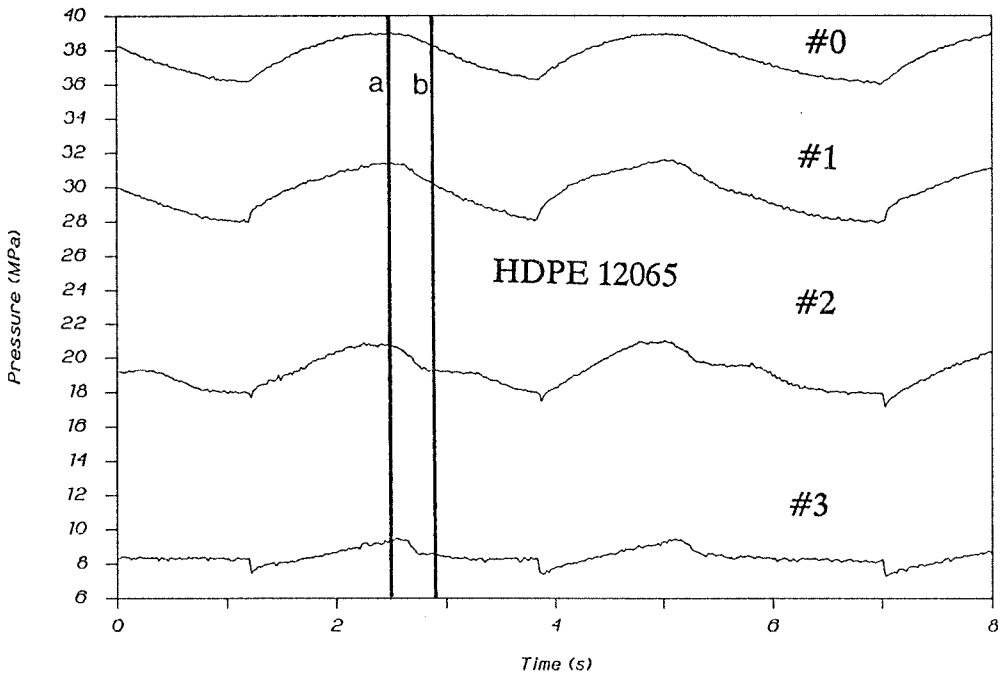

Figure 6.11. The pressure oscillation of HDPE 12065 at apparent shear rate of 480 (1/s). The extrudate is shown in Figure 6.9 (B).

apparent shear rate is 340 1/s. The period and amplitude of the oscillations are respectively 9.3 seconds and 8.7 MPa.

As shown in Figure 6.10, four pressure curves show synchronous oscillations for the most part of the cycle. However, it is not true for the time period at beginning of the pressure decreases: between ''a'' and ''b''. At time ''a'', the pressure at position #0 is relatively stable

(plateau), while the pressure values at positions #1 and #2 show trend of falling. On the contrary, the pressure at position #3 still increases at the moment. This implies that there is slippage at positions #1 and #2, while at position #3 there has been no slip yet. The stable pressure at the reservoir indicates constant pressure head at that moment. About 0.4 second later, there is a sudden drop of pressure at position #3, which is an obvious sign of local slip. This slip happens at a faster rate than that of slip happened at positions #1 and #2. At time ''b'', the pressures start to fall synchronously (which will be verified by the following discussion of the shear stress variations at different positions inside die).

The previous analysis suggests that slip originates upstream, possibly from the entrance area where there is a highly concentrated shear stress and and large deformation in the polymer (Tordella, 1973). On the other hand, we found that the most pronounced instant pressure drop happens at #3 position near the exit. This can be explained by the assumption of the normal pressure effect on the wall slip proposed by Hatzikiriakos and Dealy (1992): lower pressure near die exit facilitates wall slip.

Spurting was also found for HDPE 12065. Figure 6.11 shows

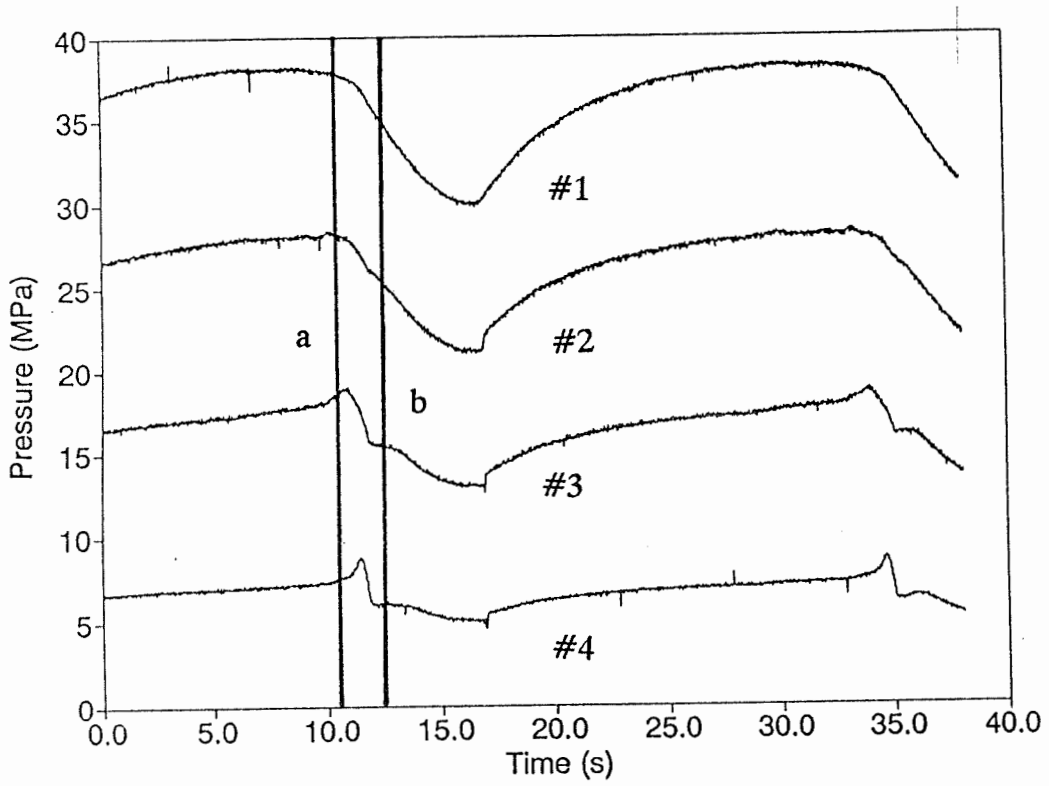

Figure 6.12. The pressure oscillation of HDPE 16A at 200 °C, with #1 and #3 pressure transducers interchanged. This is recorded at apparent shear rate of 300 1/s.

the pressure variations when spurting extrusion happened. The corresponding extrudate is shown in Figure 6.8 (B). Compared to HDPE 16A, HDPE 12065 showed smaller amplitude of pressure variations. As illustrated in Figure 6.11, the slip velocity at spurting is lower for HDPE 12065. Once again, let us look at the beginning of the pressure falling (at time ''a''). The pressure at position #2 falls first, when the pressure at other three positions have not. Therefore, slip happens at further downstream from the entrance. This hypothesis is

corroborated by lower entrance pressure loss observed (which will be discussed later on). Similar to the results for HDPE 16A, the pressure decrease at #3 happens last, but it is the most abrupt one.

Observations of spurting for two HDPE polymers suggest the slip doesn't originate at the die exit, but further upstream.

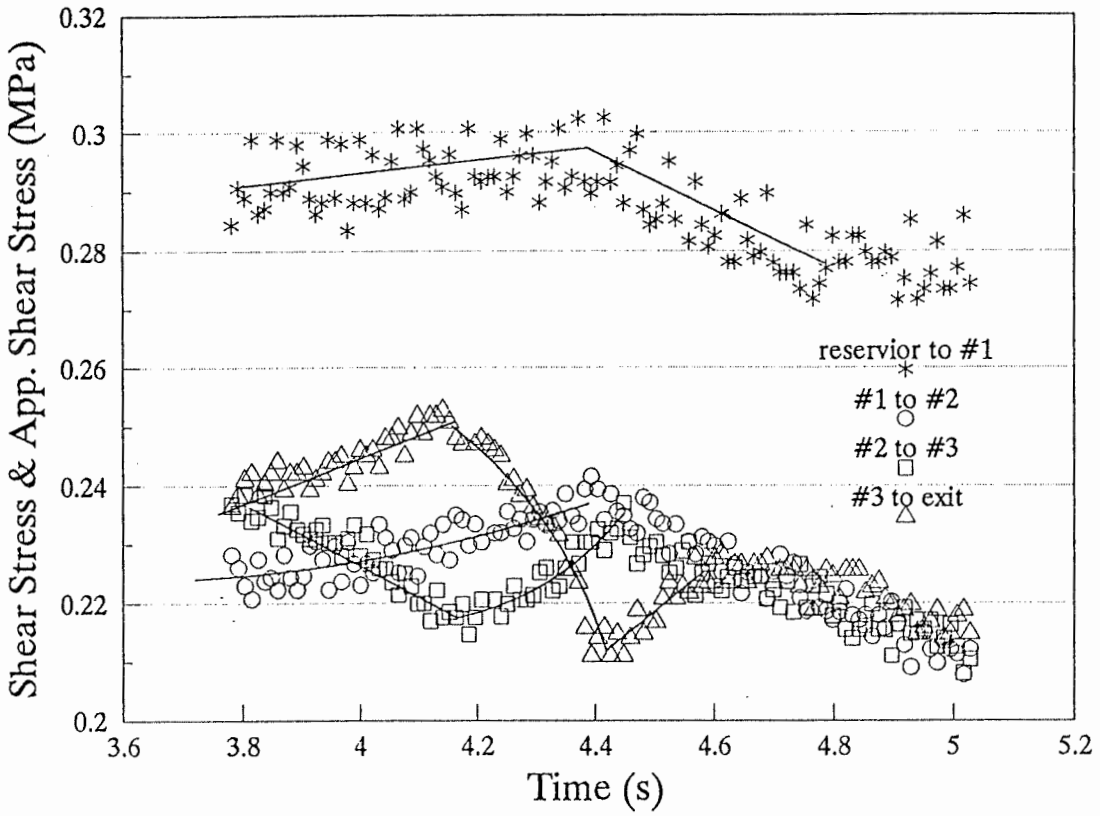

Figure 6.13. Shear stress variations of HDPE 16A at 200 °C, calculated from four sections between the time period of ''a'' and ''b'' in Figure 6.10.

Caution should be exercised when considering the time differences of the pressure decreases at different positions, since it may be caused by the delay in responses of the pressure transducers. According to the manufacture, the pressure transducers used can detect pressure variations in 0.013 s. In Figure 6.10, the time difference between positions #1 and #3) at the start of pressure falling is in order of 0.2 s. Therefore the delay of the pressure falling should not be the error caused by pressure transducer. On the other hand, we interchanged the pressure transducers at position #3 and #1, to observe spurting of HDPE 16A again. The spurting of reversed transducer arrangement is shown in Figure 6.12. Once again the pressure at position #3 falls last (between ''a'' and ''b''). It corroborates the results shown in Figure 6.10: slip begins upstream.

The slit die extrusion shows that slip does not occur simultaneously. In other words, slip is not uniform at the moment of initiation. Therefore shear stresses at the wall along the die land is not uniform. Let us consider the period between ''a'' and ''b'' in Figure 6.10. Four shear stress curves were generated and presented in Figure 6.13. They are corresponding to four sections along the die (Figure 6.13), which are: from #0 to #1, from #1 to #2, from #2 to #3 and from #3 to the exit. For example, the shear stress of section

#1 to #2 is calculated by $\sigma_w=(h/2l_{12})(P_1 - P_2)$. P_1 and P_2 are the pressure values measured at positions #1 and #2 and l_{12} is the distance between positions #1 and #2.

The figure shows higher values calculated from #0 (reservoir) to #1. This is due to the entrance effect (since the slip was not uniform at that moment, entrance correction was not applied here). Therefore, those values are apparent shear stresses. However the other three are shear stresses without end effects.

There is an early decrease of shear stress between #2 and #3 and then followed by that between #3 to the exit. Assuming the overall flowrate is constant during the short period, then slip acceleration can be calculated by Equation 6.3.

Consider the power law parameters m=22770 Pa.s^n, and n=0.38 (obtained from capillary rheometer) for HDPE 16A. From Figure 6.13, we found the shear stress decreases by 0.02 MPa during 0.4 s for the section between #2 and #3, and 0.03 MPa during 0.3 s for the section between #3 and the exit. Therefore, slip accelerations calculated from Equation 6.3 are 0.020 m/s^2 and 0.053 m/s^2 respectively. If there is no slip at the beginning of the sudden shear stress drop, the slip velocities by the ends of these sudden pressure decreases (0.4

and 0.3 second at positions #2 and #3 respectively) will be 0.008 m/s and 0.015 m/s at the two positions. Those values are about 21% and 40% of the average velocity.

The data of Bartos and Holomek (1971) for the extrusion of polybutadiene suggested that the slip velocity was about 62% of the average flow velocity when oscillations in flowrate happened. Our values are lower because the slip velocities continue to increase after the sudden pressure drop. So the slip velocity will eventually reach higher values.

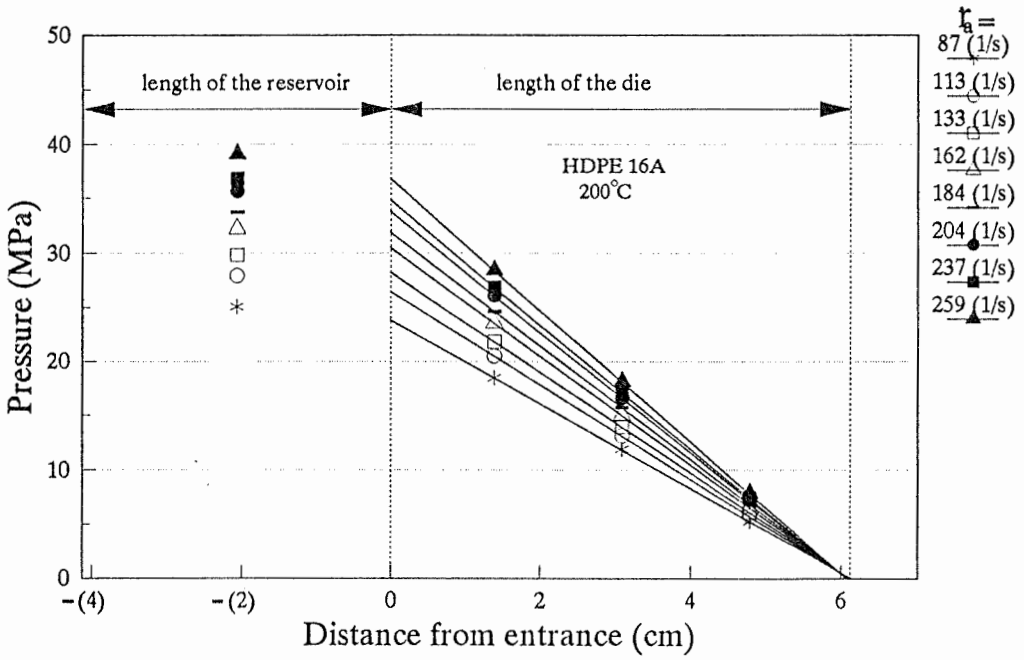

Figure 6.14. Pressure profiles of HDPE 16A along the slit die for stable extrusion, "smooth" part of Figure 6.5.

6.4 PRESSURE PROFILE

With slit die, one can observe the pressure gradient across the die and obtain the true entrance pressure loss (Bagley correction comprises both entrance and exit pressure losses)

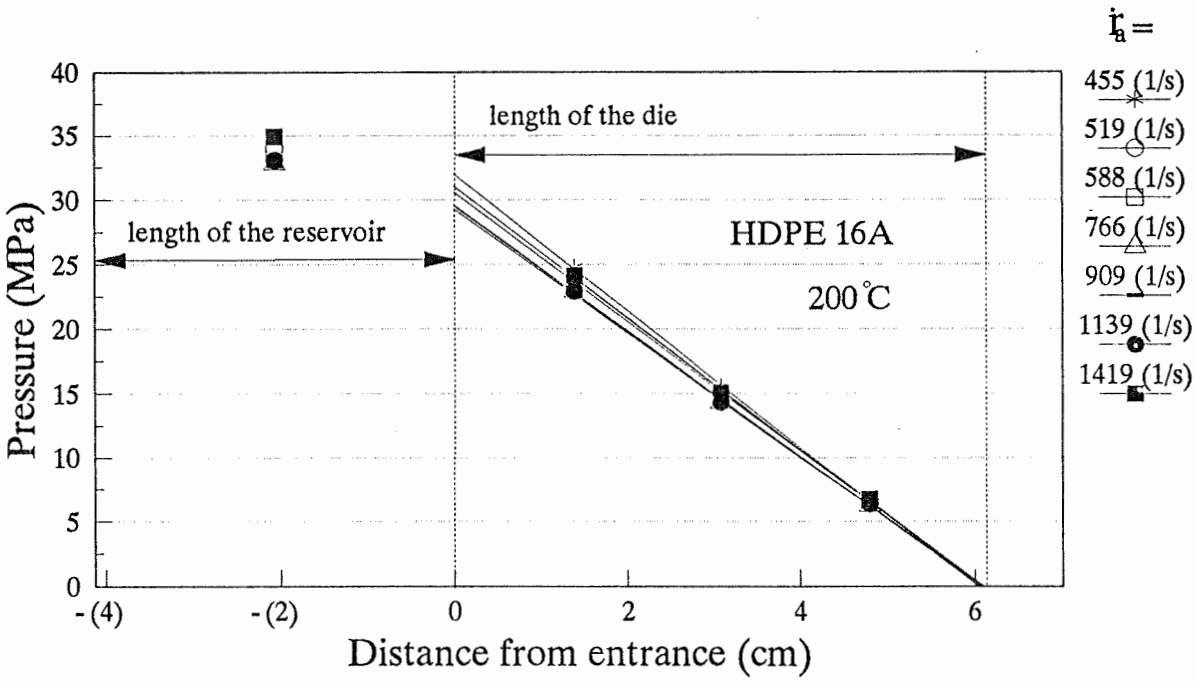

Figure 6.15. Pressure profiles of HDPE 16A along the slit die at higher apparent shear rates: "rough and smooth" and "rough" parts in Figure 6.5.

Figure 6.14 shows the pressure profile of HDPE 16A at 200 °C. The apparent shear rate ranges from 87 1/s to 259 1/s, which covers stable extrusion (first part of Figure 6.5). The figure shows perfect straight lines indicating linear pressure

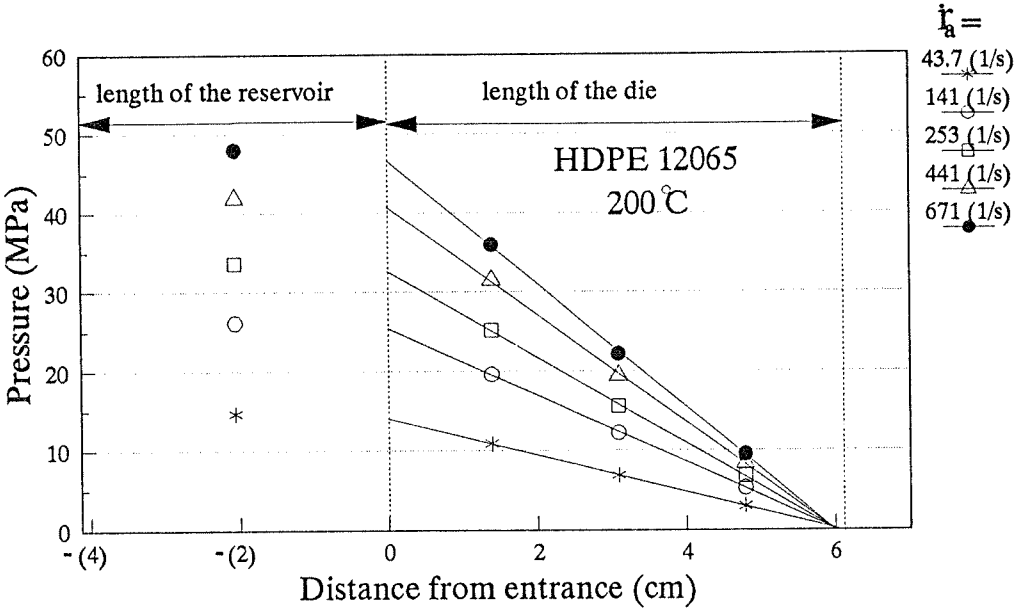

Figure 6.16. Pressure profiles of HDPE 12065 along the slit die at 200 °C.

gradient inside the die land. There are obvious entrance pressure loss; but no exit pressure loss.

Figure 6.15 shows the pressure profiles at higher apparent shear rates (the second and third parts of Figure 6.5) with rough/smooth and continuous roughness extrudates. Although there is wall slip for this extrusion range, the pressure gradients are still linear. That suggests constant slip velocity across the die land. However, if the slip acceleration happens between the pressure transducer #3 and die exit, it would not be detected. Hatzikiriakos and Dealy

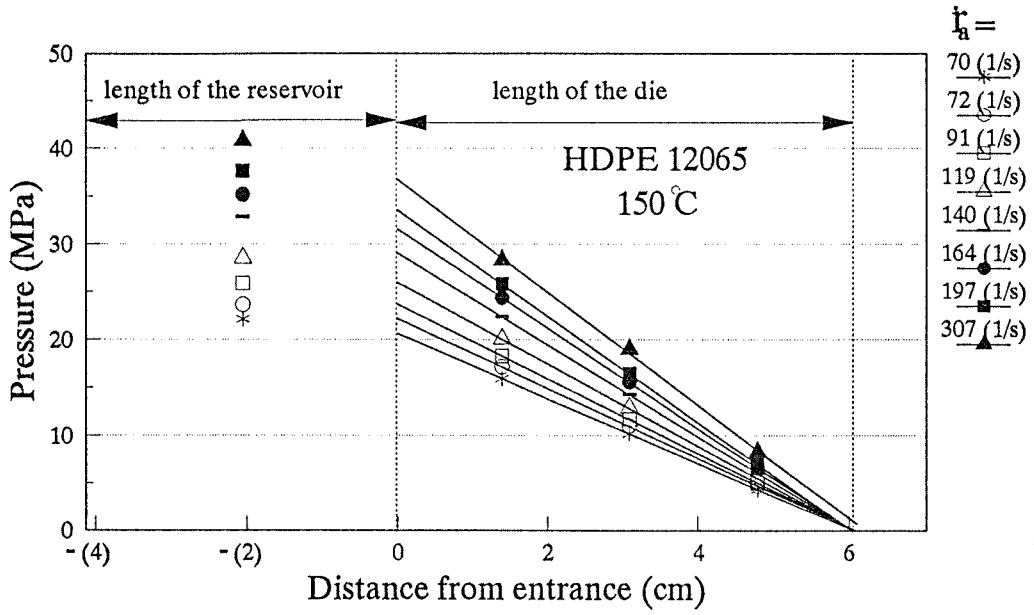

Figure 6.17. Pressure profiles of HDPE 12065 along the slit die at 150 °C, before spurting occurs.

(1992) predict that slip acceleration happens at about 80% of the die length from the entry, and it is where pressure transducer #3 is installed. Therefore, it is quite possible the slit die is unable to detect the slip acceleration near die exit.

The pressure profile of HDPE 12065 at 200 °C is shown in Figure 6.16. Pressure gradients are linear through the extrusion range. The exit pressure losses are negligible.

Figure 6.17 shows the pressure profile of HDPE 12065 at 150 °C with stable flow. Exit pressure at apparent shear rate of 307 1/s is higher than the others, which is found just before spurting. This indicates noticeable elastic energy in

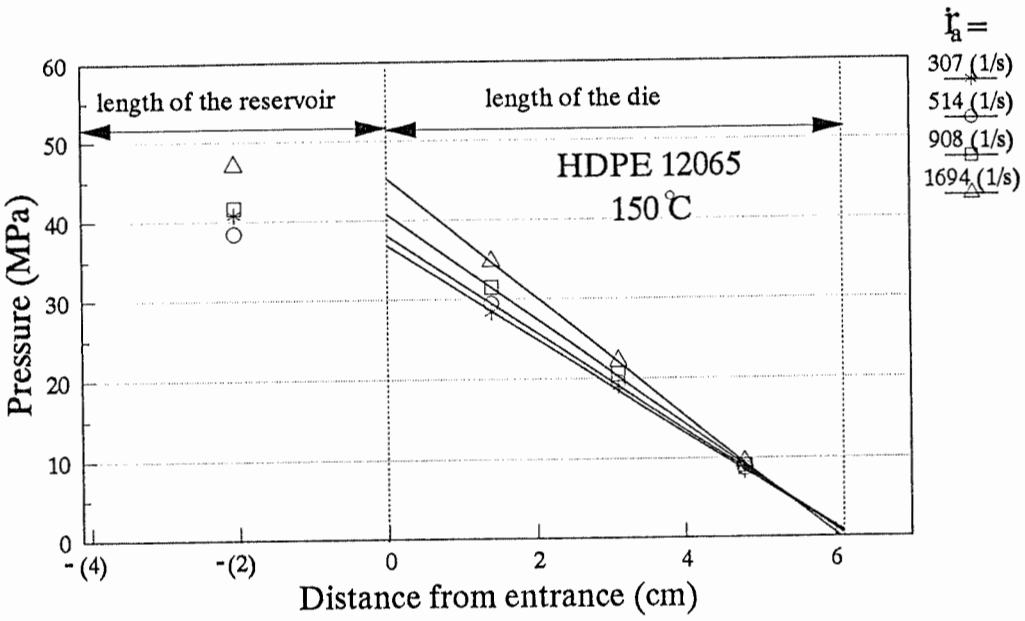

Figure 6.18. Pressure profiles of HDPE 12065 along the slit die at 150 °C, after spurting occurs.

the polymer melt prior to the die exit. Figure 6.18 gives the pressure profiles after spurting happened (parts 2 and 3 in Figure 6.7,(b)). It shows linear pressure gradients inside die land, although slip has already started. This is similar to what was obtained for HDPE 16A after spurting.

The pressure profiles of LLDPE 12J1 are shown in Figure 6.19. There are no surface roughness and abnormal pressure variations. Once again, the pressure gradients are linear throughout the extrusion range.

In short, the pressure profiles of three different polymers show linear pressure gradients under both slip or non

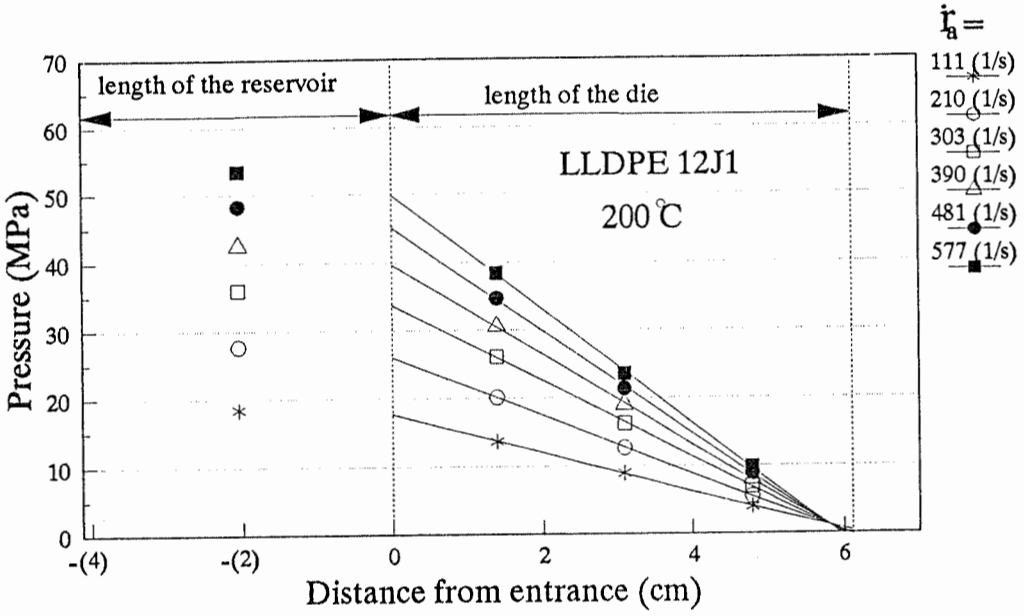

Figure 6.19. Pressure profiles of LLDPE 12J1 along the slit die at 200 °C.

slip conditions. Linear pressure gradients under slip condition implies constant slip velocity. Due to the limited number of pressure transducers, slip acceleration between #3 transducer and die exit could not be observed. On the other hand, good linearity of pressure along the die confirms the three pressure transducers are free of entrance and exit effect. This ensures those calculated shear stress values used in the flow curve of last section are reliable. Generally speaking, the exit pressure losses are quite low. That might be due to a high L/h (length/thickness) value for the slit die.

Since entrance pressure loss is an important factor, it will be discussed in a separatesection.

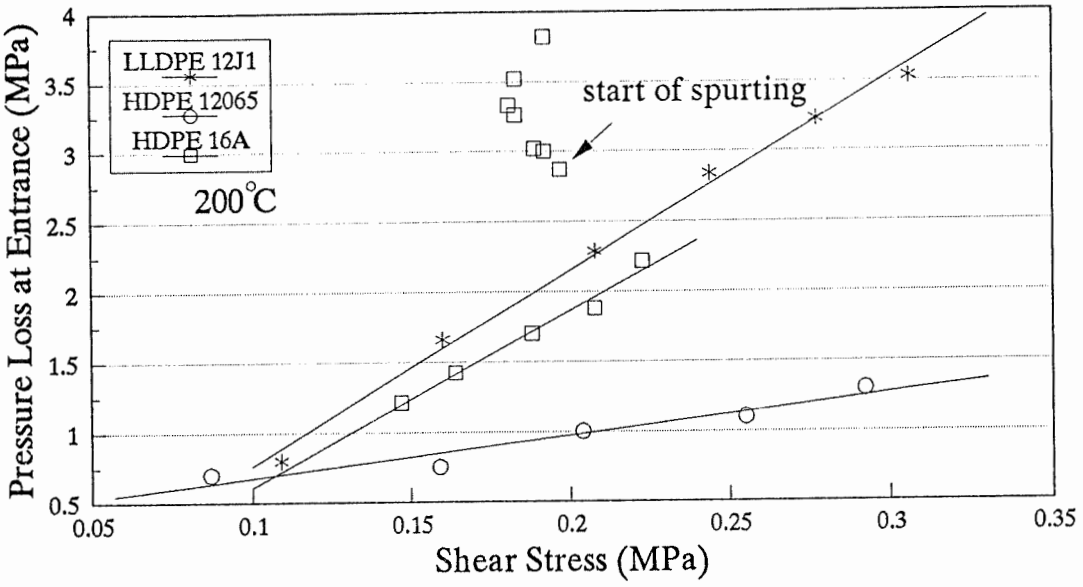

Figure 6.20. Entrance pressure losses versus shear stress of three polymers at 200 °C.

6.5 ENTRANCE PRESSURE LOSSES

Entrance pressure loss is important when extrusion roughness appears. While with capillary dies (usually a group of dies) it is very hard to obtain entrance pressure loss, especially at the onset of gross fracture. As a result, pressure curve versus L/D will not be a straight line. With the slit die, we can obtain the true entrance pressure loss, free of exit effect, by extrapolating the linear pressure profiles obtained from the three transducers installed along the die.

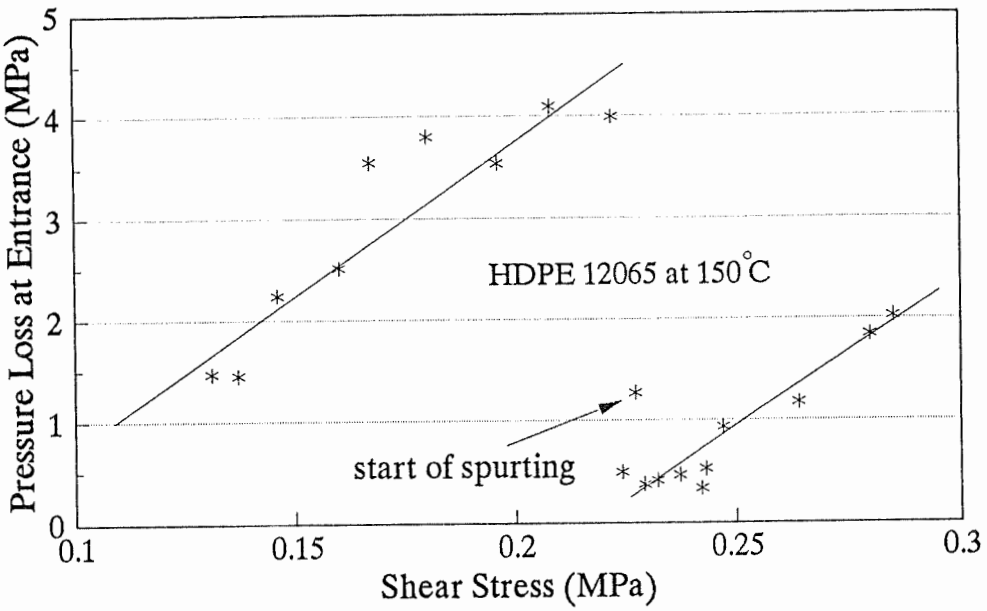

Figure 6.21. Entrance pressure loss versus shear stress of HDPE 12065 at 150 °C.

The entrance pressure losses of both HDPE 16A, HDPE 12065 and LLDPE at 200 °C are shown in Figure 6.20. HDPE 16A shows higher entrance pressure loss than HDPE 12065. The sudden increase of entrance pressure loss for HDPE 16A at about 0.2 MPa is related with the onset of spurting. In other words, for HDPE 16A, when spurting happens (slip is believed to occur at that time) the entrance pressure increases sharply. LLDPE 12J1 shows a continuous increase of entrance pressure loss. Its values are higher than HDPE 12065 and higher than the values of HDPE 16A during extrusion before spurting happens.

Figure 6.21 shows entrance pressure loss of HDPE 12065 at 150 °C. In contrary to what happened to HDPE 16A, entrance

pressure loss falls sharply at onset of spurting.

For viscoelastic fluids, like polymer melt, the total entrance loss can be divided into two parts: the viscous loss and elastic loss. For several polymers (Han, 1973), 90% and more of the total entrance pressure loss is attributed to the elastic energy. In that sense, entrance pressure loss is a manifestation of elastic energy accumulated at the entry.

Higher entrance pressure loss in the case of HDPE 16A compared to HDPE 12065 at 200 °C suggests more elastic energy is stored at the entry. This explains why the roughness of HDPE 16A in both two-hole die and slit die extrusions is more serious than that of HDPE 12065. Elastic energy is directly related to extrudate roughness (Rudin, 1970). Hutton (1965) pointed out that there is a limit to the amount of elastic shear energy that can be held in a shear field. If this limit is exceeded, a fraction of the elastic energy is converted into free surface energy, yielding a distorted extrudate. Although the situation is much more complex than simple shear flow the rougher surface of HDPE 16A with higher entrance pressure loss (compared to HDPE 12065) confirms this theory.

The roughness of the extrudate is also largely dependent on properties of the polymer. Figure 6.20 shows even higher

entrance pressure loss for LLDPE 12J1 than for HDPE 16A before spurting. The LLDPE undergoes a different slip history: there is no catastrophic failure of wall adhesion but a rather gradual change from stick to slip. Therefore spurting is not found for LLDPE 12J1. As we discussed before on surface roughness, the wider molecular distribution of HDPE polymers could be one of the reasons.

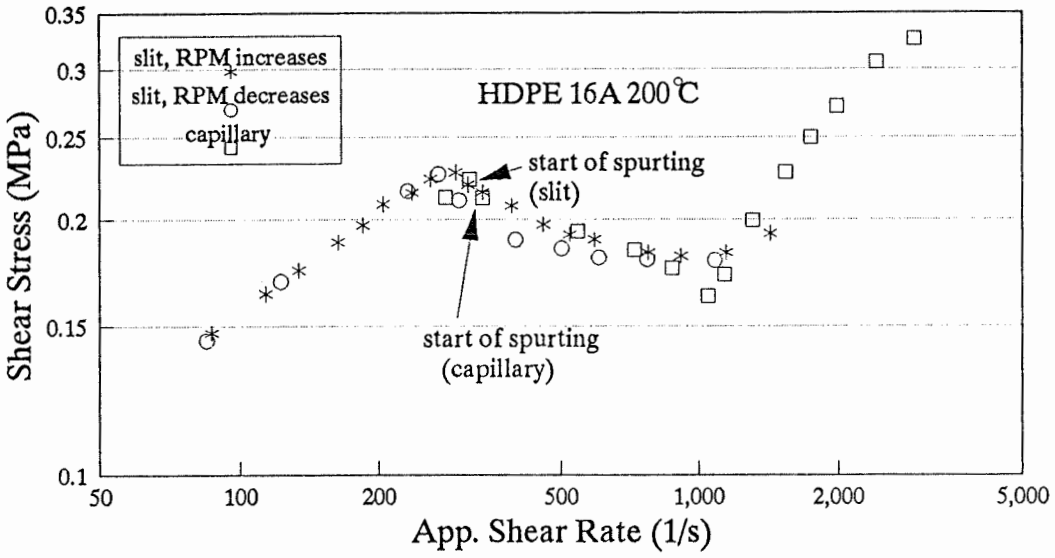

Figure 6.22. Comparison between the flow curves from capillary and slit dies.

6.6 COMPARISON BETWEEN SLIT DIE AND CAPILLARY DIE RESULTS

A comparison between the slit die and regular capillary die results have been made to ensure the reliability of the

results.

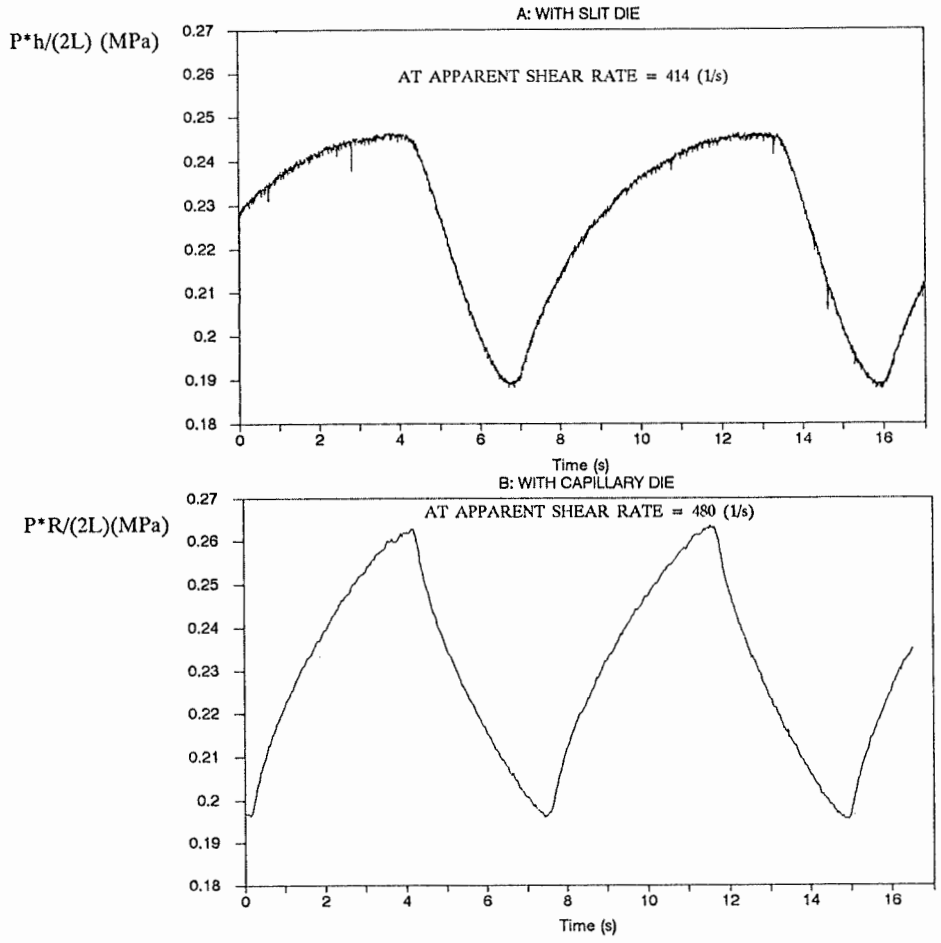

Figure 6.23. Pressure oscillations during spurting extrusion of HDPE 16A from slit and capillary dies.

A capillary die of diameter equal to 1.59 mm and L/D of 24 with a flat (180°) entry was used to extrude HDPE 16A at 200 °C. The flow curves from this capillary die and the slit die are shown in Figure 6.22. The two curves show a reasonable agreement. The spurting phenomenon is observed at a similar

shear stress and apparent shear rate.

Using the same polymer, we compared the pressure oscillations during spurting between the slit and capillary dies as shown in Figure 6.23. At a similar apparent shear rate, both curves show quite similar oscillation amplitude and period. The shorter period shown for the capillary die is due to the slightly higher flow rate.

The slit die and the capillary die confer the same flow curves. More important, in both dies spurting occurs at the same shear stress and apparent shear rate. Hence both sets of data are reliable.

6.7 SUMMARY OF SLIT DIE EXTRUSIONS

Spurting was observed for two HDPE polymers. The pressure data suggest that slip is initiated upstream, which supports the contention that slip is associated to entrance flow. Since entrance pressure reflects elastic energy created at die entry, higher entrance pressure loss can be associated to more severe extrudate roughness. Slit die result also suggests different mechanisms for the extrudate roughness of HDPE and LLDPE polymers. The former features sudden changes in flow pattern observed as spurting; the latter shows a rather

gradual development of roughness. The pressure profiles are linear through slit die, even when slip happens. It indicates that the slip velocity is independent of the axial positions, except those near the die entry and exit where the pressures could not be measured by this slit die.

CHAPTER 7

CORRELATION OF THREE EXPERIMENTS

Three experiments, capillary extrusions using screening design, two-hole die extrusions and slit die extrusions, were conducted to understand the extrudate roughness. Hereby, we summarize the results.

7.1 ENTRANCE EFFECT ON EXTRUDATE ROUGHNESS

As discussed in Chapter 2, large deformation at die entry causes gross fracture or melt fracture (Tordella, 1950, 1957, and 1958). The converging flow at the entry generates elastic energy. Such energy might be released through wall slip or at the die exit, which causes extrudate roughness. The screening design (Chapter 4) and two-hole die (Chapter 5) experiments support the evidence of entrance effect.

The screening design (three level design results) suggests that the entrance angle is important for HDPE polymers: 180° entry caused more severe extrudate roughness than 60° entry, because the former led higher degree of elastic deformation when polymer flow from reservoir into the channel. That indicates strong entrance effect on the extrudate roughness. On the other hand, slit die experiment shows higher entrance pressure loss for HDPE 16A than for HDPE

12065. The extrudate roughness of the former is more severe than that of the latter. Higher entrance loss indicates more elastic energy has been generated.

7.2 DEPENDENCE OF EXTRUDATE ROUGHNESS ON PROPERTIES OF POLYMERS

The screening design results indicate strong molecular weight effect on extrudate roughness. The results also suggest different mechanisms for HDPE and LLDPE polymers. For HDPE polymers, shear stress, molecular weight and entrance angle are the dominating parameters while the others have negligible effects. For LLDPE polymers, the extrudate roughness is affected by many parameters.

Two-hole die results show an abrupt appearance of extrudate roughness for HDPEs. Spurting phenomena were found for both HDPE polymers, but not for LLDPE polymers. For HDPE, we found extrudates of one channel rough and that of the other smooth, although both channels were under same pressure head. While for LLDPE, the roughness happened simultaneously and developed for the two channels. This suggests that HDPE extrudate roughness is mainly caused by an important overall slip. This type of slip often leads to spurting and sudden pressure decrease or flow rate increase. In the two-hole die

extrusion of HDPE polymers, we found sudden increase of flow rate in one channel while the other channel remained unchanged. Usually, it is accompanied by marked extrudate roughness from the channel where the flow rate increased. That demonstrates typical wall slip related roughness. On the other hand, LLDPE shows that the roughness starts from surface roughness and gradually develops into gross fracture. The surface roughness (sometimes called as sharkskin) is believed to be caused by exit disturbance. There might be slip acceleration and release of residual energy at the exit.

The screening design results show that the roughness of HDPE polymers is mainly affected by shear stress, molecular weight and die entrance angle. Die entrance angle is directly related to entrance converging flow which causes sudden slip, shown by spurting and gross fracture. For HDPEs, in both two-hole die and slit die experiments, spurting phenomena were observed. For LLDPE, the screening design results show that many parameters affect roughness, due to different mechanisms compared to HDPE. Since the surface roughness of LLDPE is an exit phenomenon, it is not only affected by entrance flow, but also by other parameters, such as temperature, L/D values, etc.

7.3 WALL SLIP AND ACCOMPANIED EXTRUDATE ROUGHNESS

Wall slip has been clearly demonstrated by the two-hole die experiments. When slip occurs in one individual channel, the flow rate of that channel jumps, while it remains constant or decreases in the other channel. The two-hole die experiment also shows that extrudate roughness is accompanied with slip. When there is slip in one channel and no slip in the other, the extrudate roughness appears from the channel with slip. The severity of roughness is dependent on nature of polymer as well as the wall slip. The three polymers used (two HDPEs and one LLDPE) showed different extrudate roughness.

Wall slip was also confirmed by slit die extrusion (with HDPE polymers): there are marked slope changes of the pressure profile across the die. At the same time, the extrudate begins to show rough surface although the severity depends the polymers. For LLDPE, due to equipment limitation, we did not observe slope change nor obvious extrudate roughness during slit die extrusions.

In short, three sets of experiments described the extrudate roughness phenomena from different respects. For a summary, the conclusions and the evidences from each of the experiments are listed in Table 7.1.

Table 7.1. Summary of three experimental approaches.

conclusions drawn	Evidences from Individual Experiment		
	screening design	two-hole die	slit die
gross fracture relates to entrance flow	die entrance angle is the dominating parameter		slip starts upstream, entrance pressure affects roughness
polymer property affects extrudate roughness	molecular weight is second most important factor	different rough extrudates & slip patterns for three polymers used	entrance pressures different for two HDPEs at spurting
wall slip exists and relates to extrudate roughness		flowrate jumps in one channel only, with rough extrudate	slope of pressure profile changes abruptly

CHAPTER 8

CONCLUSIONS

8.1 CONCLUSIONS

Using a statistical method called screening design, we studied the effects of number of factors on extrudate roughness of HDPE and LLDPE polymers. It is found that shear stress and polymer molecular weight are the most important ones.

A long slit die was used to observe local slip when extrudate roughness happened. During spurting extrusion, slip was found to originate upstream, far from the exit. Slit die experiments show entrance pressure loss is closely related to extrudate roughness: higher entrance pressure loss relates to more severe roughness.

The two-hole die experiment has shown that the extrudate from one channel could be smooth while the other extrudate was rough due to slip. During the two-hole die extrusion, we found spurting in one channel while the flow remained stable in the other channel. The one-channel spurting suggests that this phenomenon is not driven by pressure oscillations in the reservoir, but by slip and stick inside the die land. On the other hand, during some spurting extrusion, the reservoir

pressure was observed to fall down after changes along the die land in slit die extrusions. This also shows that spurting can be caused by wall slip, but not by oscillations in the reservoir.

Based on two-hole and slit die experiments, HDPE 16A and 12065 showed abrupt developments of the extrudate roughness; while LLDPE 12J1 showed rather a gradual one. HDPE 16A was proved to be a unique polymer demonstrating extrudate roughness at the lower shear stress than HDPE 12065 and LLDPE 12J1 and in the more severe form.

For the first time using a slit die, we report that wall slip originates from upstream.

8.2 RECOMMENDATIONS

The effect of the precessing aid (additives) could be further studied by using the additive coated dies, possibly with screening design.

The effect of polymer compressibility should be further studied by using various sizes of reservoirs. If the compressibility plays an important role, the period and magnitude of spurting would be affected.

A die with tapered exit (diverging) could be used for two-hole die setup (for instance, one with straight and one with tapered exit) to examine the exit effect. Since surface roughness is an exit effect, tapered die exit should diminish the surface roughness and give a comparison between the two streams.

A tapered-entry slit die could be used to confirm the effect of the die entry since the screening design showed strong entrance effect for HDPE polymers.

The pure effects of the molecular weight and molecular weight distribution should be further studied. The polymer samples could be made by blending those with narrow molecular weight distributions. Further, the effect of the molecular branching should be also considered in the future studies, since molecular branching of commercial products varies from one producer to another.

REFERENCES

AGASSANT, J. F., P. AVENAS, J.-PH. SERGENT, and P. J. CARREAU, Polymer Processing, Hanser Publishers, Munich, Vienna, New York, page 307 (1991).

AJJI, A, S. VARENNES and H. P. SCHREIBER, ''Flow Defects in LLDPE Processing: Instrumental Detection and Molecular Weight Dependence'', to be published, (1992).

ATWOOD, B. T., and W. R. SCHOWALTER, ''Measurements of Slip at the Wall During Flow of High Density Polyethylene through a Rectangular Conduit'', Rheol. Acta, **28**, 134 (1989).

BAGLEY, E. B. ''End Corrections in the Capillary Flow of Polyethylene''. J. Appl. Phys. Chem., **28**, 624 (1957).

BAGLEY, E. B., I. M. CABBOT, and D. C. WEST, ''Discontinuity in the Flow Curve of Polyethylene'', J. Appl. Phys., **29**, 109 (1958).

BAGLEY, E. B. and M. BIRKS, ''Flow of Polyethylene into a Capillary'', J. Appl. Phys., **31**. 556 (1960).

BAGLEY, E. B., ''The Separation of Elastic and Viscous Effects in Polymer Flow'', Trans. Soc. Rheol., **5**, 355 (1961).

BAGLEY, E. B., ''Unstable Flow of Molten Polymers: A Second Site of Melt Fracture'', J. Appl. Polym. Sci. **7**, 215 (1963).

BAGLEY, E. B. and H. B. SCHREIBER, In Rheology, Vol. 5, Acadimic, New York, Chap.3, 1969.

BALLENGER, T. F. and J. L. WHITE, ''Experimental Study of Flow Pattern in Polymer fluid in Reservoir of a Capillary Rheometer'', Chem. Eng. Sci., **25**, 1191 (1970).

BALLENGER, T. F., I. J. CHEN, J. W. CROWDER, G. E. HAGLER, D. C. BOGUE, and J. L. WHITE, ''Polymer Melt Flow Instabilities in Extrusion: Mechanism, Material and Geometric Variables'', Trans. Soc. Rheol., **15**, 195 (1971).

BARTOS, O., ''Fracture of Polymer Melts at High Shear Stress'', J. Appl. Phys., **28**, 624 (1964).

BARTOS, O., ''A Note on the Discontinuity in Flow Curves of Melton Polyethylene'', J. Polym. Sci. Letter. **3**, 1025 (1965).

BARTOS, O. and J. HOLOMEK, ''Unstable Flow of Amorphous

Polymers Through Capillaries I, Velocity Profiles of Polymer Having Discontinuous Flow Curve'', Polym. Eng. Sci., **11**, 324 (1971).

- BEAUFILS, P. B. VERGNES and J. F. AGASSANT, ''Characterization of the Sharkskin Defect and its Development with the Flow Conditions'', Inten. Polymer Processing, **4**, 78 (1989).

- BECKER, J. P. BENGTSSON, C. KLASON, J. KUBAT and P. SAHA, ''Pressure Oscillations during Capillary Extrusion of High Density Polyethylene'', Intern. Polymer Processing, **VI(4)**, 318 (1991).

BENBOW, J. J., R. V. CHARLEY, and P. LAMB, ''Unstable Flow of Molten Polymers'', Nature, **192**, 223 (1961).

BENBOW, J. J. and P. LAMB, ''Melt Fracture in Molten Polymers''. SPE Trans., **3**, 7 (1963).

BOND, W. N., ''Viscous Flow through Wide Angle Cones'', Pilos. Mag., **50**, 1058 (1925).

- BOUDREAUX, E. and J. A. CUCULO, ''Polymer Flow Instability: A Review and Analysis'', J. Macromol. Sci., **16C**, 39 (1977-1978).

BUDINSKI, K. G., Engineering Materials, Prentice Hall, New Jersey, Ch. 1, (1992).

CLEGG, P. L. in Rheology of Elastomers, (Mason and Wookey, eds.), Pergamon, New York, 1957.

COGSWELL, F. N., J. Rheol., **37**, 407 (1993).

COOK, D. G., R. COOKE, and A. RUDIN, ''Use of Chilled Die Lips to Improve Production Rates in Extrusion of PE'', Intern. Polym. Processing, **4**, 73 (1989).

DEN OTTER, J. L. ''Mechanism of Melt Fracture'', Plast. Polym., **38**, 155 (1970).

DEN OTTER, J. L. ''Some Investigation of Melt Fracture'', Rheol. Acta, **10**, 200 (1971).

DENN, M. M., ''Issue in Viscoelastic Fluid Mechanics'', Annu. Rev. Fluid Mech., **22**, 18 (1990).

EL KISSI, N. EL and J. M. PIAU, ''The Different Capillary Flow Regimes of Entangled Polydimethylsiloxane Polymers: Macroscopic Slip at the Wall, Hysteresis and Cork Flow'', J. Non-Newtonian Fluid Mech., **37**, 55 (1990).

EL KISSI, N. EL and J. M. PIAU, ''Adherence of LLDPE on the Wall for Flow Regimes with Sharkskin'', (1992), to be published.

HAN, C. D., "Influence of the Die Entry Angle on the Entrance Pressure Drop, Recoverable Elastic Energy, and Onset of Flow Instability in Polymer Melt Flow", J. App. Polym. Sci., **17**, 1403 (1973).

HATZIKIRIAKOS, S. G., and J. M. DEALY, ''Wall Slip of Molten High Density Polyethylene I, Sliding Plate Rheometer Studies'', J. Rheol., **35,** 497 (1991).

HATZIKIRIAKOS, S. G., and J. M. DEALY, ''Wall Slip of Molten High Density Polyethylene II, Capillary Rheometer Studies'', J. Rheol., **36**, 703 (1992).

HUTTON, J. F., Modern Plat., **41,** 133 (1964).

HOWELLS, E. R. and J. J. BENBOW, ''Flow Defects in Polymer Melts'', Trans, J. Plast. Inst., **30**, 240 (1962).

KALIKA D. S., and M. M. DENN, ''Wall Slip and Extrudate Distortion in Linear Low-Density Polyethylene'', J. Rheol., **31**, 815 (1987).

KARBASHEWSKI, E., A. RUDIN, L. KALE, W. J. TCHIR and H. P. SCHREIBER, ''Effects of Polymer Structure on the Onset of Processing Defects in Linear Low Density Polyethylenes'', Polym. Eng. Sci. **31**, 1581 (1991).

LEONOV, A. I., ''A Linear Model of the Stick-Slip Phenomena on Polymer Flow in Rheometers'', Rheol. Acta, **23**, 591 (1984).

LIM, F. J. and SCHOWALTER, W. R., ''Wall Slip of Narrow Molecular Weight Distribution Polybutadienes'', J. Rheol., **33**, 1359 (1989).

LIN, Y.-H., ''Explanation for Slip-Stick Melt Fracture in Terms of Molecular Dynamics in Polymer Melts'', J. Rheol., **29(6)**, 605 (1985).Metzger, A. P. and C. W. Hamilton, ''The Oscillation Shear Phenomenon in High Density Polyethylenes'', SPE Transactions, April, 107 (1964).

METZGER, A. P. and C. W. HAMILTON, ''The Oscillating Shear Phenomenon in High Density Polyethylenes'', SPE Trans. **4**, 107 (1964).

METZNER, A. B., J. L. WHITE and M. M. DENN, ''Behavior of Viscoelastic Materials in Short-Time Process'', Chem. Eng. Progr., **62**, 81 (1966).

MOURNIAC, P., ''The Wall Slip Problem in Flow of Elastomer Blend'', Ph.D thesis, Ecole Nationale Superieure des Mines de Paris, 1991.

NASON, H. K., ''High Temperatue, High Pressure Rheometer for Plastics'', J. App. Phys., **16**, 338 (1945).

PETRIE, C. J. S., and M. M. DENN, ''Instabilities in Polymer Processing'', AIChE. J., **22**, 209 (1976).

PHILIPPOFF, W., and F. H. GASKINS, ''Normal Stresses; Flow Curves, Flow Birefringence, and Normal Stress of Polyisobutylene Solutions, (I) Principles'', Ibid. **2**, 263 (1958).

PIAU, J. M., N. EL KISSI and B. TREMBLAY, ''Influence of Upstream Instabilities and Wall Slip on Melt Fracture and Sharkskin Phenomena during Silicones Extrusion through Orifice Dies'', J. Non-Newtonian Fluid Mechanics, **34**, 145 (1990).

RAMAMURTHY, A. V., ''Wall Slip in Viscous Fluids and Influence of Materials of Construction'', J. Rheol., **30**, 337 (1986).

RAMAMURTHY, A. V., ''Extrudate Irregularities and the Polymer-Metal Interface Connection'', Proceeding of 10th Intern.

Congr. Rheol. Sydney, 1988.

REINER, M., ''The Deborah Number'', Phys. Today, **12**, 64 (1964).

RUDIN, A., ''Effect of Processing History on Melt Flow Defects'', Polym. Eng. Sci., **10**, 94 (1970).

SABIA, R. and M. E. MULLIER, ''Discontinuity in the Flow Curve of Polyethylene'', J. Appl. Polym. Sci., **6**, 542 (1962).

SCHOTT, H. and W. S. KAGHAN, ''Flow Irregularities in the Extrusion of Polyethylene Melts'', Ind. Eng. Chem., **51**, 844 (1959).

SCHOTT, H. ''Elastic Effect and Extrudate Distortions in Capillary Flow of Molten Polyethylene Resins'', J. Polym. Sci. **A2**, 3791 (1964).

SCHREIBER, H. P., E. B. BAGLEY, and A. M. BIRKS, ''Filament Distortion and Die Entry Angle Effects in Polyethylene Extrusion'', J. Appl. Polym. Sci. **4**, 362 (1960).

SCHREIBER, H. P., A. RUDIN, and E. B. BAGLEY, ''Separation of Elastic and Viscous Effects in Polymer Melt Extrusion'', J.

Appl. Polym. Sci. **9**, 887 (1965).

SCHREIBER, H. P., ''Molecular Dependence of Flow Instability in Polyethylene'', J. Polym. Sci., Part B, Polymer Letter, **7**, 851 (1969).

SCHUT, J. H., ''Lots of New Polyolefins on Tap'', Plastics Technology, Jan. 146 (1992).

SPENCER, R. S and R. E. DILLON, ''Viscous Flow of Molten Polystyrene'', J. Colloid Sci., **4**, 241 (1949).

TORDELLA, J. P., ''Fracture in Extrusion of Amorphous Polymers Through Capillaries'', J. Appl. Phys., **27**, 454 (1956).

TORDELLA, J. P., ''Occurrence of Melt Fracture in Extrusion of Molten Plastics'', Trans. Soc. Rheol., **1**, 203 (1957).

Tordella, J. P., ''An instability in the Flow of Molten Polymers'', Rheol. Acta, Babnd 1, Nr. 2-3, 216 (1958).

TORDELLA, J. P., ''Unstable Flow of Molten Polymers: A Second Site of Melt Fracture'', J. Appl. Polym. Sci., **7**, 215 (1963).

TORDELLA, J. P., in Rheology, Vol. 5 (F. R. Eirich, ed.),

Academic, New York, Chap. 2 (1969).

TREMBLAY, B.,''Sharkskin Defects of Polymer Melts: The Role of Cohesion and Adhesion'', J. Rheol., **35**, 985 (1991).

UHLAND, E, ''Model for Describing the Flow of Wall Slipping Substances through Dies'', Rheol. Acta, **15**, 30 (1976).

UTRACKI, L. A. and R. GENDRON, ''Pressure Oscillation During Extrusion of Polymers. II'', J. Rheol., **28(5)**, 601 (1984).

VALEZA, A. and F. P. LA MANTIA, ''Extrusion Characteristics of Lubricated LLDPE'', Intern. Polymer Processing, **2**, 220 (1988).

VINOGRADOV, G. V. and V. N. MANIN, ''Experimental Study of Elastic Turbulence'', Kolloid Z. -Z. Polym., **201**, 93 (1965).

VINOGRADOV, G. V., ''Critical Regimes of Shear in Linear Polymers'', J. Polym. Eng. Sci., Sept. **12**, 323 (1972).

VINOGRADOV, G. V., ''Limiting Regimes of Deformation of Polymer'', Polym. Eng. Sci., April, **21**, 339 (1981).

VINOGRADOV, G. V., V. P. PROTASOV, and V. E. DREVAL, ''The

Rheological Behavior of Flexible-chain Polymers in the Region of Spurting, and Supercritical Conditions of their Movement at $T > T_g$'', Rheol. Acta, **23**, 46 (1984).

WEILL, A., ''About the Origin of Sharkskin'', Rheol. Acta, **9**, 623 (1980).

WHEELER, D. J. ''Tables of Screening Designs'', SPC Press, Inc., Tennessee, (1989).

WHITE, J. L., ''Critique of Flow Pattern in Polymers Fluids at the Entrance of a Die and Instabilities Leading to Extrudate Distortion'', Appl. Polym. Sci. Symp. , 20, 155 (1973).

APPENDIX I

MOONEY EQUATION FOR SLIT DIE

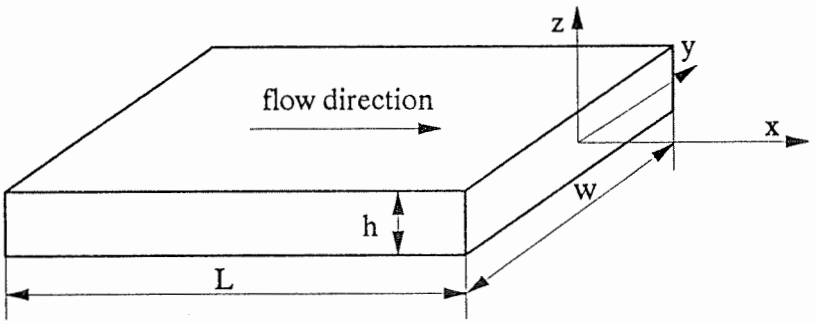

Figure A1: Sketch of slit die channel.

For a flow through a slit die (shown in Figure A1), we define shear rate $\dot{\gamma}$ as $\dot{\gamma}(\sigma,T)=-du/dz$, where σ is shear stress, T is temperature, u is the velocity of the fluid in x direction. The negative sign is used because the velocity has opposite sense to the pressure gradient along the channel. Assuming isothermal flow, integration between the outermost layer of liquid in the channel, that laying at the die wall and some inner layer at z gives the velocity increment arising through shear flow (Lupton and Regester, 1965)

$$u(z)-u(w)=\int_{u(w)}^{u(z)} du=\int_{u(w)}^{u(z)} \frac{du}{dz}\,dz=\int_{z}^{1/2h} \dot{\gamma}\,dz \qquad \text{A(1)}$$

where u(w) is the velocity at die wall (slip velocity), u(z) is the velocity at the position z.

If the pressure, P(x) varies only in x direction, shear stress $\sigma=z[dP(x)/dx]$. Therefore the shear stress at the die wall, $\sigma_w=(h/2)(dP/dx)$, where h is the gap of the die. If P(x) is a liner function of x, $dP/dx=P_{total}/L$, where P_{total} is total pressure drop across the channel in length of L. Therefore there is relation

$$\frac{\sigma}{\sigma_w}=\frac{z}{h/2} \qquad \text{A(2)}$$

$$dz=\left(\frac{h}{2\sigma_w}\right)d\sigma \qquad \text{A(3)}$$

Combination of Equations A(1), A(2) and A(3) yields

$$u(z)=u(w)+\frac{h}{2\sigma_w}\int_{\sigma}^{\sigma_w}\dot{\gamma}(\sigma,T)\,d\sigma \qquad \text{A(4)}$$

Since volumetric rate of flow Q through the slit die is:

$$Q=2w\int_0^{h/2}u(z)\,dz \qquad \text{A(5)}$$

substituting u(z) by Equation A(4) and dz by Equation A(3),

$$Q=2w\int_0^{\sigma_w}\left[u(w)+\frac{h}{2\sigma_w}\int_\sigma^{\sigma_w}\dot{\gamma}(\sigma,T)\,d\sigma\right]\frac{h}{2\sigma_w}d\sigma \qquad \text{A(6)}$$

integration by parts

$$Q=w\cdot h\cdot u(w)+\frac{1}{4}\frac{wh^2}{\sigma_w^2}\int_0^{\sigma_w}\dot{\gamma}(\sigma,T)\,d\sigma^2 \qquad \text{A(7)}$$

The above Equation can be rewritten by multiplying both sides by $6/(wh^2)$

$$\dot{\gamma}_a=\frac{6Q}{wh^2}=\frac{6u(w)}{h}+\frac{3}{2\sigma_w^2}\int_0^{\sigma_w}\dot{\gamma}(\sigma,T)\,d\sigma^2 \qquad \text{A(8)}$$

This is the Mooney equation for slit die channel. The equation indicates the apparent shear rate $\dot{\gamma}_a$ (which can be measured through extrusion) includes two parts: the contribution by shear flow and the contribution by wall slip. Therefore, Equation A(8) can be simplified as

$$\dot{\gamma}_a=\dot{\gamma}_s+\dot{\gamma}_t \qquad \text{A(9)}$$

where $\dot{\gamma}_s$ is the contribution to the apparent shear rate $\dot{\gamma}_a$ from slip flow, $\dot{\gamma}_t$ is the contribution from shear flow.

For power law fluids ($\dot{\gamma}(\sigma,T)=(\sigma/m)^{(1/n)}$, where m and n are power law constants), then equation A(8) becomes

$$\dot{\gamma}_a=\frac{6u(w)}{h}+\frac{3n}{2n+1}\left(\frac{\sigma_w}{m}\right)^{\frac{1}{n}} \qquad \text{A(10)}$$